

**Follicular targeted drug delivery via nanocarriers
in the treatment of
(auto)inflammatory skin diseases**

Dissertation

zur Erlangung des Grades

der Doktorin der Naturwissenschaften

der Naturwissenschaftlich-Technischen Fakultäten

der Universität des Saarlandes

von

Rebekka Christmann

Saarbrücken

2021

Tag des Kolloquiums:	01.02.2022
Dekan:	Prof. Dr. Jörn Walter
Berichterstatter:	Prof. Dr. Claus-Michael Lehr Prof. Dr. Markus R. Meyer
Vorsitz:	Prof. Dr. Marc Schneider
Akademische Mitarbeiterin:	Dr. Agnes-Valencia Weiß

Die vorliegende Arbeit wurde von Februar 2017 bis Juli 2020 unter der Leitung von Herrn Prof. Dr. Claus-Michael Lehr, Herrn Prof. Dr. Thomas Vogt, Herrn Prof. Dr. Ulrich Schäfer und Frau Dr. Brigitta Loretz am Institut für Pharmazeutische Technologie der Universität des Saarlandes, am Helmholtz-Institut für Pharmazeutische Forschung Saarland (HIPS) in der Abteilung Drug Delivery und in der Klinik für Dermatologie, Venerologie und Allergologie des Universitätsklinikums des Saarlandes und der Medizinischen Fakultät der Universität des Saarlandes angefertigt.

To my beloved family

TABLE OF CONTENTS

I. SUMMARY	V
II. ZUSAMMENFASSUNG	VI
III. ABBREVIATIONS	VII
1. INTRODUCTION	08
1.1. HAIR FOLLICLE – THE TARGET SITE	08
1.1.1. HAIR FOLLICLE TYPES	08
1.1.2. HISTOLOGY & ANATOMY	09
1.1.3. GROWTH CYCLE	10
1.1.4. IMMUNE PRIVILEGE OF ANAGEN HAIR FOLLICLE	12
1.2. ALOPECIA AREATA PATHOGENESIS & PATHOMECHANISM	12
1.3. JANUS KINASES	14
1.4. NANOPARTICULATE DRUG DELIVERY SYSTEMS	16
1.5. FOLLICULAR DRUG DELIVERY	17
1.5.1. IMPACT OF FOLLICULAR PATHWAY ON (TRANS)DERMAL DELIVERY	17
1.5.2. FOLLICULAR RESERVOIR	17
1.5.3. TARGETED FOLLICULAR DELIVERY VIA NANOPARTICLES	18
1.5.4. DETERMINATION METHODS OF FOLLICULAR DELIVERY	19
2. GOAL OF THESIS	22
2.1. CHAPTER 1	22
NANOPARTICLE UPTAKE INTO HUMAN SCALP HAIR FOLLICLES WITH AND WITHOUT A HAIR SHAFT	
2.2. CHAPTER 2	33
CHOICE OF AN APPROPRIATE NANOPARTICULATE DRUG DELIVERY SYSTEM FOR TARGETED FOLLICULAR DRUG DELIVERY OF TOFACITINIB – CHARACTERIZATION AND DEVELOPMENT OF VERSATILE AMPHIPHILIC SQUALENYL DERIVATIVE NANOPARTICULATE DRUG DELIVERY SYSTEM PLATFORMS	
2.3. CHAPTER 3	49
DEVELOPMENT OF TOFACITINIB LOADED SQUALENYL DERIVATIVE NANOPARTICULATE DRUG DELIVERY SYSTEM AND CHARACTERIZATION OF ITS ABILITY FOR TARGETED FOLLICULAR DRUG DELIVERY AND BIOLOGICAL RESPONSE – <i>EX VIVO</i> AND <i>IN VIVO</i>	
3. DISCUSSION	68
4. CONCLUSION & OUTLOOK	70
5. REFERENCES	71
6. SCIENTIFIC OUTPUT	84
6.1. AWARD	84
6.2. PUBLICATIONS	84
6.3. ORAL PRESENTATIONS	85
6.4. POSTER PRESENTATIONS	85
7. ACKNOWLEDGEMENTS	87

SUMMARY

Today, it is widely known that nanoparticles (NPs) maximize follicular and minimize interfollicular drug delivery, thereby reducing systemic drug levels and severe side effects.

Non-life-threatening skin diseases, like Alopecia Areata (AA), a reversible hair loss disorder associated with major negative effect on quality of life, lack of sufficient treatment, among other things caused by negative risk-benefit profiles of potent drugs such as Janus Kinase inhibitors, e.g., tofacitinib (TFB). Therefore, NPs are predestined to enable a targeted drug delivery into hair follicles (HFs) for a safer treatment against skin diseases like AA.

As proof of concept, the NP deposition inside human scalp HFs was studied by adjustment of a quantification method for human forearm HFs. Investigations on healthy human, AA-affected hairless and hairy body donor scalp HFs showed that NP uptake into HFs depends on follicular density but is independent of hair shaft presence and hair type. Accordingly, TFB-loaded NPs were developed. Previously-synthesized squalenyl derivative NPs exceeded other approaches, demonstrating high drug loading capacity, biocompatibility, colloidal stability, and enhanced follicular delivery in an *ex vivo* pig ear model, which was supported by a biological effect in an *in vivo* dermatitis mouse model.

Further investigations on follicular targeted delivery via NPs for a safe and potent treatment of skin diseases, leading to translation into the clinics, are highly desired.

ZUSAMMENFASSUNG

Nanopartikel (NP) maximieren den follikulären und minimieren den interfollikulären Arzneistofftransport. Sie reduzieren dabei systemische Wirkstoffspiegel und schwere Nebenwirkungen.

Für nicht lebensbedrohliche Hauterkrankungen wie Alopecia Areata (AA) gibt es keine zufriedenstellende Behandlung, da unter anderem für potente Arzneistoffe wie Janus Kinase Inhibitor Tofacitinib (TFB) negative Nutzen-Risiko-Verhältnisse existieren.

Daher ist ein gezielter Arzneistofftransport durch NP in Haarfollikeln (HF) prädestiniert, um eine sichere und effiziente Behandlung von AA zu ermöglichen.

Die Machbarkeitsstudie untersuchte die NP-Deposition in menschlichen Kopfhaut-HF unter Zuhilfenahme einer Quantifizierungsmethode für menschliche Unterarm-HF. Sowohl Untersuchungen an gesunden, an AA-befallenen haarlosen als auch an Körperspenden Kopfhaut-HF zeigten, dass die NP-Aufnahme in HF abhängig ist von der Follikeldichte, jedoch nicht vom Haarschaft-Vorhandensein oder dem Haartyp.

TFB beladene Squalen-Derivat-NP überzeugten durch hohe Arzneistoffbeladung, Biokompatibilität, kolloidale Stabilität und verbesserten follikulären Arzneistofftransport – gezeigt im Ex-vivo-Schweineohrmodell und unterstützt durch eine biologische Antwort im In-vivo-Dermatitis-Mausmodell.

Weitere Untersuchungen des follikulären gezielten Arzneistofftransports mit NP zur Erreichung einer sicheren und effizienten Behandlung von Hauterkrankungen, welche zu einer Translation in die Klinik führen, sind sehnlichst erwünscht.

ABBREVIATIONS

ABBREVIATIONS

Alopecia Areata	AA
Antigen presenting cells	APC
Hair follicle	HF
Immune privilege	IP
Interferon γ	IFN- γ
Interleukin 15	IL-15
Janus Kinase	JAK
Major histocompatibility complex	MHC
Nanoparticle	NP
Nanoparticulate drug delivery system	NDDS
Natural killer cells	NK cells
Polycaprolactone	PCL
Poly-lactic-co-glycolic acid	PLGA
Signal transducer and activator of transcription	STAT
Squalenyl derivative	SqD
Transforming growth factor	TGF
Tyrosine-kinase 2	TYK2
U.S. Food and Drug Administration	FDA

1. INTRODUCTION

Humans possess approximately 5 million hair follicles (HFs) ¹. The HF is a mini-organ, which is important for thermoregulation, protection from harmful environmental influences, and social interactions. For example, eyebrows and eyelashes strengthen facial expressions and protect the eyes from external influences ². Due to social standards, disorders, such as hair loss and hirsutism, can diminish quality of life ².

Alopecia Areata (AA) is a non-scarring, reversible hair loss disorder ³. It most commonly starts with patchy hair loss and can progress to total loss of all body hair (Alopecia Universalis). Even though AA is a non-life-threatening disease, it can have a major negative effect on quality of life and lead to depression and anxiety disorders ³. Unfortunately, until now there has been no agency-approved treatment available ³, due to the unfavorable risk-benefit profile of potent drugs like Janus Kinase (JAK) inhibitors.

Therefore, the following thesis focuses on the development of a method for targeted and safe delivery of potent drugs into HFs to treat AA.

1.1. HAIR FOLLICLE – THE TARGET SITE

1.1.1. HAIR FOLLICLE TYPES

With exception of the lips, the palms of the hands, the soles of the feet and part of the genitals, the human body is covered by HFs, which develop congenitally ^{1,2}. Around 100,000 to 150,000 of these 5 million HFs are found on the human scalp ¹. HFs can be divided into different types ¹. The two main types are called terminal and vellus HFs and are characterized as follows by their body location, hair shaft, and hair bulb embedment ¹:

- i) Terminal HFs ¹
 - a. Body areas e.g., human scalp; pubic area
 - b. Hair shaft strongly pigmented, visible
diameter > 0.06 mm
length > 2 mm
 - c. Hair bulb location subcutaneous fatty tissue
- ii) Vellus HFs ¹
 - a. Body areas most parts of the human body e.g., cheek, forehead ⁴
 - b. Hair shaft fine, poorly pigmented
diameter < 0.03 mm
length < 2 mm ¹

c. Hair bulb location viable dermis

The HF can be seen as an invagination of the skin and interruption of the main skin barrier – the epidermis with the overlaying stratum corneum ¹. However, barrier mechanisms are still present inside the HF. The upper part is covered by stratum corneum transitioning into tight junctions in deeper parts ⁵. Moreover, the HF is a mini-organ, with over 20 different cell populations ⁶. It constitutes the pilosebaceous unit together with an associated sebaceous gland and arrector pili muscle, which is attached to 4 to 5 HFs ^{6,7}.

1.1.2. HISTOLOGY & ANATOMY

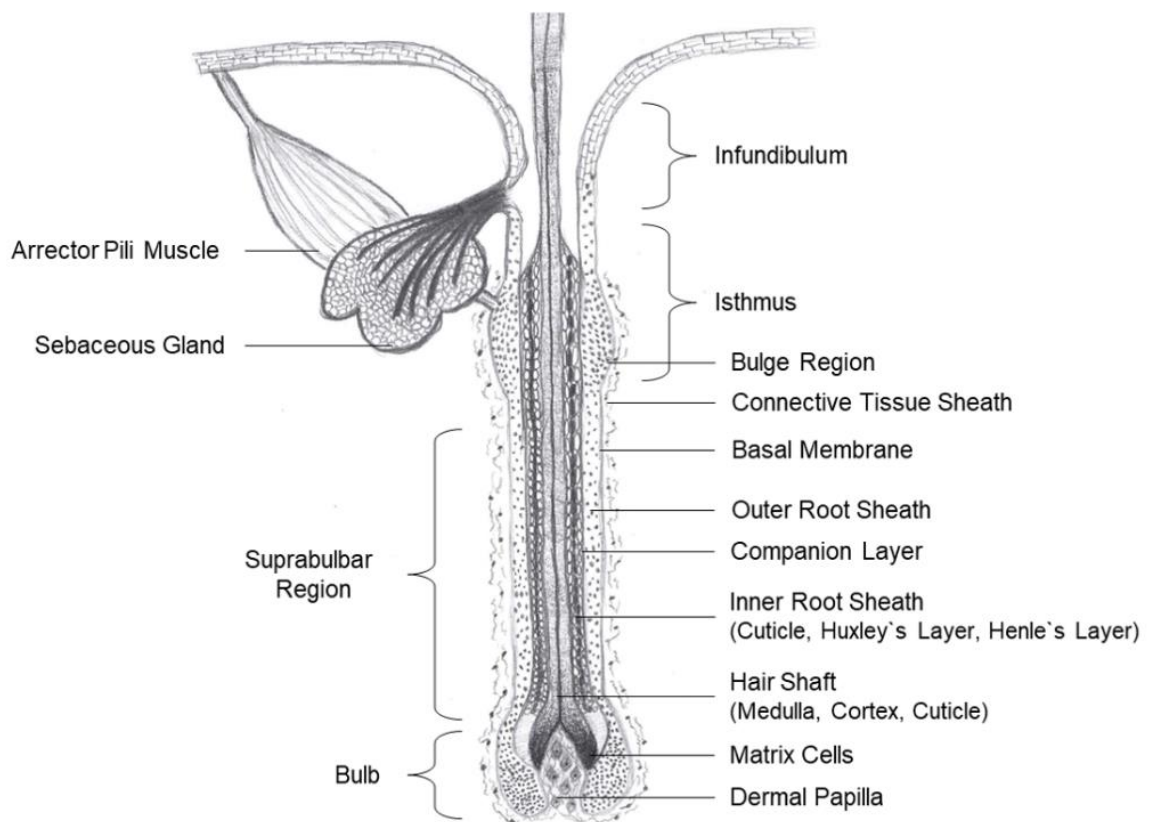


Figure 1. Scheme of longitudinal section of terminal anagen HF according to Ref ^{2,8,9}.

Important anatomical and histological parts of a healthy anagen HF are depicted in Figure 1 and elucidated in the following section ^{1,2,6,10,11}:

- i) **Infundibulum:**
 ranges from skin surface to sebaceous gland duct opening and is initially still lined with epidermis ^{1,10}.

- ii) **Isthmus:**
 ranges down to the end of the bulge region, where epithelial stem cells are accommodated and the arrector pili muscle is located ¹⁰.
- iii) **Suprabulbar and bulb region:**
 contains the dermal papilla (specialized fibroblasts) and undifferentiated matrix cells ^{1,6,10,11}.

Further, the HF consists of concentric sheets of epithelial and mesenchymal components, which are separated by a basal membrane (Figure 1) ¹⁰. The main mesenchymal component comprises the outermost **connective tissue sheath** ¹⁰. It surrounds the HF and the dermal papilla ¹⁰. The **dermal papilla** controls the number of the undifferentiated matrix cells, and thereby the size of the hair shaft – they are separated by a **thickened basal membrane** ¹¹. The **outer root sheath**, part of the epithelial regions, surrounds the HF and connects to the basal membrane ¹⁰. In the bulge region the outer root sheath accommodates undifferentiated multipotent stem cells ¹. Another part of the epithelial regions is the **inner root sheath**. It consists of three partly keratinized layers (Henle's layer, Huxley's layer, and cuticle) and is separated by a **companion layer** from the outer root sheath, therefore a free movement during hair growth is possible ¹⁰. In the middle of the isthmus part, the inner root sheath vanishes and the outer root sheath continues until it migrates into the epidermally-lined infundibulum ¹. The **keratinized hair shaft** is the innermost part of the HF, guarded by the outer parts and evolves from the hair bulb matrix cells by growing upwards ¹⁰. The hair shaft comprises different layers: terminal HFs have an innermost medulla, which is not present in vellus HFs, followed by the hair cortex and the hair shaft cuticle ¹⁰. The hair shaft cuticle consists of keratinized stacked cells interlocking with the cuticle cells of the inner root sheath ¹⁰. This fact plays an important role in targeted drug delivery into HFs via nanoparticles (NPs). A postulated mechanism hypothesizes that the cuticle cells act as a gear pump and push the NPs down into the HFs (see section 1.5.3.) ¹².

1.1.3. GROWTH CYCLE

HFs undergo a lifelong hair growth cycle ^{1,13}. Relying on these hair cycling abilities, the HF can be divided into two major parts: a permanent and a cycling part ¹. The upper permanent part includes the infundibulum down to the bulge region (Figure 1) ¹. The lower part comprises the cycling one ¹.

The cycle is divided into three different main stages ^{1,11}:

1. Growth phase = anagen

The hair shaft is produced by matrix cells located in the hair bulb near the dermal papilla. All HF cells are highly proliferative during this phase. Around 85 % of all human HFs are in this stage and the phase can last around 2-6 years for terminal scalp HFs (Figure 2 A) ^{1,2,11}.

2. Regression phase = catagen

This phase is affected by stop of hair shaft growth, massive destruction and involution of the HF by programmed cell deaths leading to apoptosis. A “club-hair shaft” is formed. For terminal scalp HFs, this phase takes approximately 2 to 3 weeks (Figure 2 B) ^{1,2,11}.

3. Resting phase = telogen

After the HF shrinks to almost half of its size, consisting only of an epithelial sac surrounding the club hair, the resting phase starts. Here, the rest of the dermal papilla is only a small cluster of quiescent dermal fibroblasts in close association with the remaining HF. For terminal scalp HFs this phase can take ~ 3 months. Fifteen percent of the HFs are in this phase (Figure 2 C) ^{1,2,11}.

Before a new growth phase can start, the hair shaft is shed. Since new insights into the physiological mechanism lead to the suggestion of an active and highly controlled shedding process, this additional phase is called “exogen” ^{1,2}.

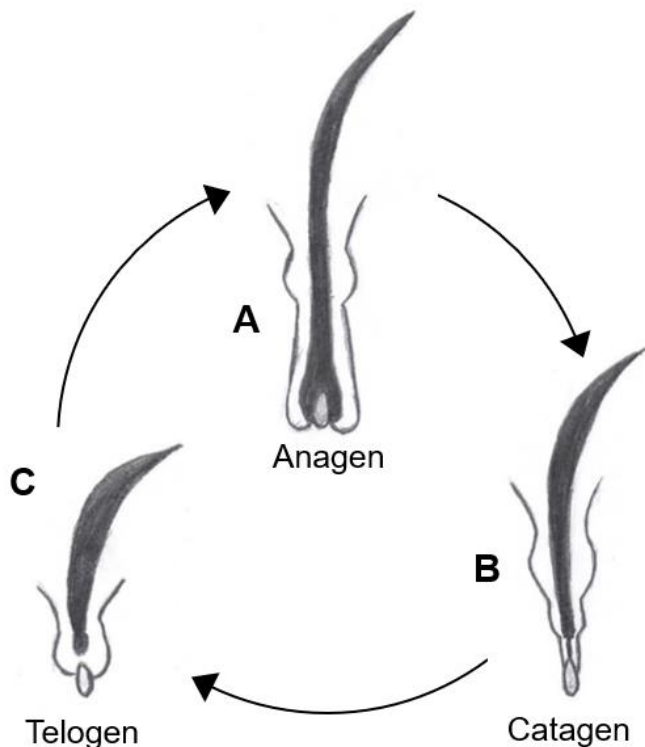


Figure 2. Hair growth cycle.

A) Anagen – growth phase of the HF and hair shaft;

B) Catagen – regression phase – stop of hair shaft growth and deformation of HF;

C) Telogen – resting phase – epithelial sac with a club hair according to Ref. ^{14,15}

1.1.4. IMMUNE PRIVILEGE OF ANAGEN HAIR FOLLICLE

In addition to the lifelong growth cycling ability, the HF exhibits a relative immune privilege (IP) during the anagen HF phase^{9,16,17}. IP is a dynamic and functional state of an organ or tissue (e.g., placenta, corneal tissue, and testes) to protect itself against an undesired immune response triggered by autoantigens¹⁶. The relative IP in anagen HFs is limited to the lower cycling part of the HF, reaching from the bulge to the bulb region¹⁶. It is suggested that the IP protects the HF during the growth phase from an undesired immune response against possible autoantigens, emerging e.g., from melanogenesis and/or hair shaft growth¹⁶. Therefore, during the IP state of the anagen HF, immune cells are absent and immune suppressors are present^{3,16}.

The connective tissue sheath surrounding the HF is suggested to have a special function by preventing the migration of immune cells into the HF epithelium¹⁶. Moreover, immune suppressors and immunosuppressive neuropeptides and -hormones (e.g., transforming growth factor β 1 and 2 (TGF- β 1 and 2)) modulate immune cells in close proximity of the HF¹⁶.

Furthermore, the IP status is mostly characterized by the absence of major histocompatibility complex (MHC) class I and II molecules¹⁶.

MHC class I molecules are normally expressed by all nucleated cells, presenting antigen epitopes to CD8⁺ T-cells¹⁶. Cells lacking MHC class I molecules are normally eliminated by natural killer (NK) cells¹⁶. However, the expression of TGF- β 1 and 2 prevent the attack of NK cells¹⁶. In addition, NK cells lack of the receptor NKG2D for cell activation^{16,18}.

MHC class II molecules, normally expressed by antigen presenting cells (APCs), e.g., dendritic cells, macrophages and Langerhans cells, are either absent, isolated or have altered and limited activity during IP in anagen HF¹⁶.

1.2. ALOPECIA AREATA PATHOGENESIS & PATHOMECHANISM

Unfortunately, the specialized ability of anagen HF to express relative IP is closely associated with the development of AA¹⁶. The breakdown of the IP in anagen HFs is suggested to be one of the key factors of the AA pathomechanism¹⁶.

Following androgenetic alopecia, AA is the second most non-scarring hair loss disorder³ with a lifetime prevalence of ~ 2.5 %¹⁹. The disease onset can occur in each period of life and has no gender preference³.

AA is a reversible hair loss disorder, where the hair shaft gets lost, but the HF is still preserved^{3,16}. It is characterized by either widespread or sharply defined bald lesion patterns, exclamation mark hair shafts and a possible exacerbation to a total loss of all scalp hair (Alopecia Totalis) or even all body hair (Alopecia Universalis)^{3,16}. However, a spontaneous remission can occur^{3,16}. The disease is often associated with co-morbidities like depression, anxiety, auto-immune diseases (e.g., psoriasis, rheumatoid arthritis, vitiligo and inflammatory bowel syndrome), and has a major negative effect on the quality of life^{3,20}. In addition to the psycho-social burden, the body is exposed to environmental influences without hair, e.g., missing nasal hair leads to a dripping nose, missing eyebrows and -lashes to eye irritations, and missing body hair to a poor thermoregulation²⁰.

AA is hypothesized to be a complex poly-genetic auto-immune disease²¹. Autoreactive CD8⁺NKG2D⁺ T-cells against autoantigens, originated from hair growth, infiltrate peri- and intrafollicular sites in the bulb region²¹. A positive feedback loop between these CD8⁺NKG2D⁺ T-cells and the epithelial HF cells, which employ MHC class I molecules and NKG2D ligands, is hypothesized to cause the major inflammatory event in AA^{21,22}. In short, epithelial HF cells express MHC class I molecules and NKG2D ligands, and therefore they interact with CD8⁺NKG2D⁺ T-cells, which then secrete interferon γ (IFN- γ)^{21,22}.

The epithelial HF cells, on the other hand produce interleukin 15 (IL-15), upon stimulation by IFN- γ ^{21,22}. IL-15 in turn activates CD8⁺NKG2D⁺ T-cells and the IFN- γ production^{21,22}. These cytokines signal downstream through the JAK/STAT (signal transducer and activator of transcription) pathway^{21,22}. This hypothesis, regarding the major role for IL-15 in the IP collapse of the anagen HF, was discussed controversially, since IL-15 is also known to act as apoptosis suppressor in different tissues¹⁶. However, to live up to the heterogeneity of the disease, previously the pathomechanism hypothesis was expanded and an additional possible non-autoimmune-caused AA onset was postulated, leading to the same "stereotypic HF response pattern"^{16,21}. The non-autoimmune-induced AA can be caused by a dysbiosis of the HF microbiome, neurogenic HF inflammation (caused by IFN- γ or Substance P), or upregulated immune cell activities¹⁶. Both pathomechanisms lead to an IFN- γ induced IP collapse. Hereupon, MHC class I and II molecules, as well as NKG2D ligands are extensively expressed by the HF epithelium, the peri-follicular mast cells become pro-inflammatory mast cells and extensively interact with T-cells¹⁶. Moreover, the lower HF is exposed to a peri- and intrafollicular immune cell infiltration, e.g., CD8⁺ cells (intrafollicular), CD4⁺ cells (peri-follicular), APCs, pro-inflammatory mast cells, and NK cells¹⁶.

Interestingly, this heterogeneity of the disease evolution is also reflected in the responses to treatment regimens, leading to non-responders or inconsistent treatment responses¹⁶. This might be one of the reasons that AA lacks an agency approved medicine.

A study of international expert opinions regarding the treatment of AA was published in 2020²³. Consensus was found on the importance of intralesionally applied glucocorticoids as first line treatment. However, the patient's age, as well as disease severity, were factors leading to a preferred systemic or topical application of glucocorticoids²³⁻²⁵. Furthermore, topical applications including calcineurin inhibitors, minoxidil and contact immunotherapy, as well as methotrexate and JAK inhibitors applied systemically, were agreed to be effective^{23,24}. Additionally, the newly-approved JAK inhibitors were deemed appropriate second-line therapy. The expert consensus states: "If all treatments were equally reimbursed, JAK inhibitors would be the ideal choice of systemic therapy in adults"²³.

The application of JAK inhibitors against AA arose from the downstream signaling via JAK/STAT pathways of various cytokines included in AA development and IP collapse. These pathways were suggested to be an important interventional target to modulate the immune response^{16,21,22}. First case reports in mice as well as in human diseased skin with JAK inhibitors demonstrated very promising results^{22,26,27}. Further case reports and clinical trials followed supporting the results, but even here non-responders were detected²⁷⁻⁴⁷.

1.3. JANUS KINASES

JAKs, intracellular tyrosine-kinases, are responsible for downstream signaling by (auto)phosphorylation and activation of their associated receptors, belonging to type I and II cytokine receptor family, and of STAT (Figure 3)⁴⁸. JAKs can be divided into four different subtypes: JAK1, JAK2, JAK3 and Tyrosine-kinase 2 (TYK2)^{48,49}. The cytokines, activating the type I and II cytokine receptor family, have a broad range of effects in the human body, e.g., immune response, inflammatory reduction and hematopoiesis^{48,49}. It is therefore not surprising that JAK inhibitors lead to a broad range of adverse effects, when applied systemically. For example, Tofacitinib (TFB) citrate, a JAK inhibitor mainly inhibiting JAK1 and -3, agency-approved to treat rheumatoid arthritis, psoriatic arthritis and ulcerative colitis⁵⁰, received in 2019 a U.S. Food and Drug Administration (FDA) boxed warning concerning an "increased risk of blood clots and death with higher dose"⁵¹. Additionally, in 2021 the FDA published a drug safety communication of TFB regarding results of a TFB safety trial, which showed "increased risk of serious heart-related problems and cancer"⁵². Therefore, the drug and the pending final results of the safety

study are under close monitoring⁵². Moreover, in the case of AA, a continuous long-term treatment seems to be necessary to gain a sustained hair regrowth^{53–55}. Such a broad and severe side effects profile of JAK inhibitors like TFB result in an unfavorable risk-benefit profile when using JAK inhibitors against a non-life-threatening disease like AA. Therefore, the establishment of a targeted and safe delivery of TFB to the site of action is highly desirable to overcome these problems.

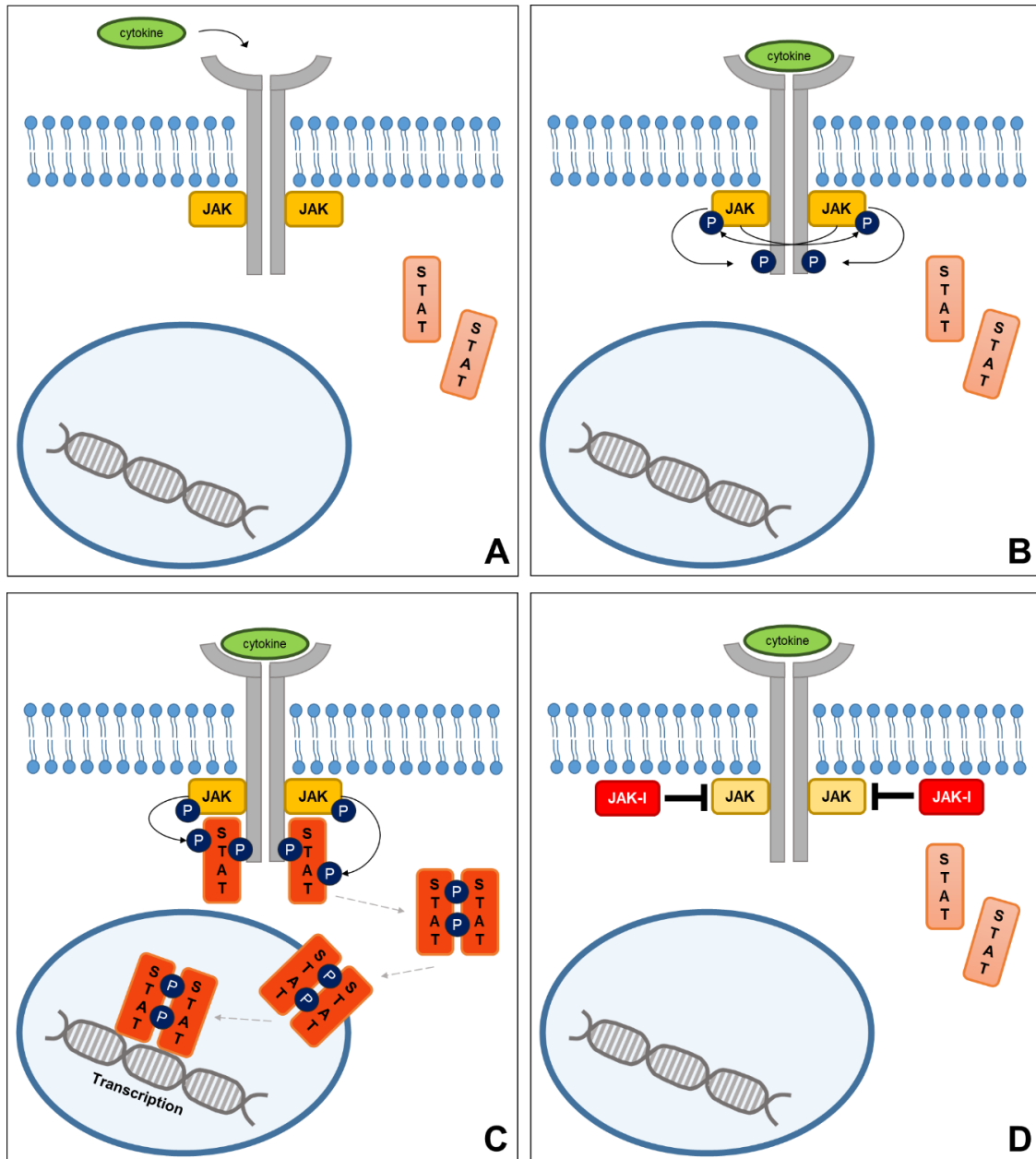


Figure 3. JAK/STAT (*Janus Kinase/Signal Transducers and Activators of Transcription*) signalling pathway. A) Cytokine is docking to the extracellular site of the transmembrane receptor. B) The receptor activates the adjacent JAKs on the intracellular site. JAKs auto-phosphorylate themselves and phosphorylate the receptor. C) STAT molecules attach to the phosphorylated receptor and get phosphorylated and thereby activated by JAKs. The phosphorylated STATs dimerize and

translocate into the nucleus. Here, the dimerized STAT molecules act as activators of transcription. D) JAK inhibitors (JAK-I) inhibit their kinase function and thereby the phosphorylation and activation of the receptor and the JAKs after the extracellular cytokine docking ^{48,56}.

1.4. NANOPARTICULATE DRUG DELIVERY SYSTEMS

Nanoparticulate drug delivery systems (NDDS) comprise delivery systems in the size range of ~ 10 to 1000 nm. They have been widely investigated and shown to improve the efficiency and efficacy of treatments in a broad variety of diseases by targeting delivery to the site of action ⁵⁷⁻⁶¹. The desired properties of NDDS express following aspects: i) high drug loading capacity ⁵⁸, ii) solubility enhancement of hardly soluble drugs ⁶², iii) drug protection from degradation due to environmental influences e.g., light ⁶³, and iv) drug release in a controlled manner ⁶⁴. Polymeric NDDS are mostly composed of biodegradable, biocompatible polymers e.g., poly-lactic-co-glycolic acid (PLGA), which is a FDA approved excipient ^{65,66}. Additional excipients like surfactants are often needed for stabilization of the NP suspension. This can result in drug loading capacities of below 5 % (w/w) ^{58,67}. However, since the HF is a delimited reservoir, high loading capacity is highly desired in NDDS. Couvreur et al. invented the squalenylation technique to circumvent this drawback ⁶⁸. The squalenylation technique comprises bioconjugation of a squalenyl moiety to a drug molecule by an easily accessible and straightforward chemical reaction, forming a prodrug. These prodrugs are able to form NDDS upon nanoprecipitation into aqueous solution without further necessary stabilization by additional surfactants ⁶⁹. This technique did not only lead to very high drug loading capacities of ~ 30 % (w/w), but also enhanced the biological effect of the drugs ⁶⁸⁻⁷³. However, the bioconjugation is not easily facilitated on all drug molecules. Drugs with missing reactive groups (e.g., TFB) ⁷⁴ or with multiple reactive groups cannot be easily covalently linked to the squalenyl moiety ^{75,76}.

To overcome this drawback and make the benefits of this technique – high drug loading capacity, surfactant free NP suspension – for NDDS formation accessible to a broader audience of drugs, Ho et al. synthesized an amphiphilic squalenyl derivative (SqD) by coupling the hydrophobic squalenyl moiety to an anionic hydrophilic head group – hydrogen sulfate ⁷⁶. The resulting amphiphilic SqDs are able to form stable NPs upon nanoprecipitation in an aqueous solution. The stabilization of the NPs by charge repulsion makes the addition of surfactant unnecessary ⁷⁶. Drug loading is enabled by charge and/or hydrophobic interactions. It was suggested that the NPs are shaped in a core-shell structure: the core consisting of the hydrophobic squalenyl moieties and the shell of the hydrophilic negatively charged head groups. So, positively charged drugs can be loaded to

the outer shell of the NPs by charge interactions and hydrophobic drugs are loaded by hydrophobic interactions to the NP core⁷⁶. This approach was successfully demonstrated by co-loading tobramycin and a hydrophobic quorum sensing inhibitor to the negatively charged SqD NPs⁷⁶.

A further point to establish the approach of SqD-based NDDS in follicular delivery is the fact that squalene, a natural lipid and precursor of the cholesterol biosynthesis⁷⁷, is one of the major components (~ 12 %) of human sebum^{78,79}. Sebum is the squalene richest region in the human body, because for some reasons squalene is not further processed in the sebaceous glands^{78,79}. Therefore, NDDS for follicular delivery composed only of SqD and the active substance would be desirable to preserve the natural environment of the HF as much as possible.

1.5. FOLLICULAR DRUG DELIVERY

1.5.1. IMPACT OF FOLLICULAR PATHWAY ON (TRANS)DERMAL DELIVERY

Today, the impact of the follicular pathway for trans- and intrafollicular delivery is widely known – the HF is thought of as an invagination in the skin barrier, enlarging the accessible skin surface and creating the possibility of a long-term reservoir for topical skin applications^{80–83}. Early investigations demonstrate a significant increase in systemic drug absorption with follicular pathway involvement^{84–87}. For example, a study investigating the follicular pathway influence on *in vivo* transdermal caffeine solution absorption in humans showed impressive results. With follicular pathway involvement, caffeine blood levels were detectable after 5 minutes, versus 20 minutes when the follicular pathway was excluded by artificially closed HFs^{88,89}. Another study demonstrated that the impact of the HF pathway on substance permeation through pig skin is associated with the substance's lipophilicity. For hydrophilic substances a greater reduction in permeation was observed after HF plugging than for lipophilic ones⁹⁰. However, inside the HF biological barriers are still present, the upper part being lined by stratum corneum and replaced by tight junctions in the lower parts⁵.

1.5.2. FOLLICULAR RESERVOIR

In comparison to stratum corneum, HFs can be seen as a long-term reservoir⁹¹. Only by permeation into deeper tissues and/or with slow outward sebum-flow can a substance reduction occur⁹¹, whereas substances deposited in a stratum corneum reservoir are exposed to influences like textile contact and desquamation⁸². Differences in HF density and size of follicular orifice lead to different follicular reservoirs on different body sites. A

previous study in humans demonstrated the highest follicular density, of the tested sites, on the forehead and the largest follicular orifice on the calf, leading to a high infundibular volume for both regions, and to follicular reservoirs comparable to the estimated stratum corneum reservoir in these body regions. The follicular reservoir on the human forearm was the smallest^{92,93}. Further important findings about the follicular pathway were that HFs can reside in an “open/active” and “closed/inactive” status for follicular delivery. HFs with an active sebum production and hair growth are accessible for follicular penetration. In contrast, inactive HFs, coated by a “plug” composed of cell debris, dandruffs and old sebum, are not available for follicular penetration. Application of pretreatments, e.g., peeling or washing, can make the inactive HFs accessible for follicular penetration^{94–97}.

1.5.3. TARGETED FOLLICULAR DELIVERY VIA NANOPARTICLES

In addition to the important follicular pathway for transdermal and dermal absorption, investigations illuminated that solid particle-containing formulations, especially NPs, are superior in penetrating into and residing inside HFs⁹⁸. The behavior of other nanosystems such as flexible liquid vesicles (e.g., liposomes) on dermal delivery, which do not favor the follicular delivery route, is beyond the scope of this thesis. The subject is covered by several reviews like Ref.^{99,100}.

Toxicology studies demonstrated that titanium dioxide microparticles in sunscreen do not penetrate over and through the stratum corneum into the viable dermis; instead, they accumulate inside the HFs¹⁰¹. Intensive investigations of the safe and targeted delivery into HFs via NPs followed.

After the application of a massage to enhance the penetration of the formulation *in vitro* by simulating the natural body movements, NP-containing formulations (size ~ 300 nm) penetrated deeper (~ 1500 µm) into HFs in comparison to a plain substance formulation (~ 500 µm)^{91,102,103}. Furthermore, in comparison to the stratum corneum reservoir where the formulation was depleted by textile contact and washing within one day, the follicular reservoir was found to exhibit long-term storage^{91,102,104}, retaining plain substance formulations for ~ 4 days and particle-containing formulations for up to 10 days^{91,102}. Formulation removal from the follicular reservoir is a rather slow process of sebum flow and hair growth^{91,102}.

A so-called gear pump mechanism was postulated for the penetration of NPs inside the HF. The mechanism relies on the outer cuticle structure of the hair shaft, which is formed by overlapping cuticle cells. These cells have a thickness of 530 nm for humans and 320 nm for pig ears and demonstrate a zig-zag structure¹². NPs of similar sizes are moved into the HFs upon the movement of the hair shaft, simulated *in vitro* by massage

^{89,91,102}. In addition, *in silico* modeling supported this hypothesis ¹⁰⁵. Comparing the follicular penetration depth of NPs with different sizes (122 to 1000 nm) revealed that particles in a size range of ~ 600 nm penetrated deepest, supporting the gear pump mechanism hypothesis ¹⁰⁶. Therefore, NPs with a size of 400 to 700 nm are superior in deep follicular penetration ^{12,106}. Further investigations supported the findings, that NPs maximize the follicular penetration and minimize the interfollicular permeation in comparison to plain substance formulations ^{64,107}. Moreover, the HF is still covered by different barrier mechanisms to inhibit the penetration of NPs into the living tissue. The upper part is lined by stratum corneum, with adjacent tight junctions in deeper parts ⁵. Therefore, NPs can be used as drug depots, penetrating into the HF as a long-term storage, releasing the drug in a controlled manner over time ¹². A maximized targeted drug delivery inside the HF by NDDS can reduce adverse effects and minimize interfollicular permeation. Not only can HF associated diseases be treated, but immune cells ^{108,109} residing in the upper part of the HF as well as stem cells in the bulge region may also be targeted ⁸⁵.

1.5.4. DETERMINATION METHODS OF FOLLICULAR DELIVERY

For *in vitro* investigations of follicular penetration, excised human skin cannot be used, thus pig ear skin is the gold standard: Human excised skin demonstrated a follicular reservoir of just ~ 9.5 % *in vitro* compared to *in vivo* ¹¹⁰. This is caused by contraction of the elastic fibers surrounding the HF upon excision; even re-stretching the human skin to its actual size cannot reopen the HFs ^{110,111}. In contrast, pig ear skin stays on the cartilage, therefore the HFs remain open ^{110,111}. Similar physiological characterizations for pig ear skin and human skin were found ^{111,112}.

For the *in vivo* investigations, non-invasive methods had to be developed to determine the follicular penetration without the application of skin punch biopsies. It was desirable to distinguish between the amount of formulation residing on the skin surface and the amount penetrating inside the HFs (Figure 4) ¹¹³. Therefore, the differential stripping method was developed. This method combines the skin surface cleaning tape stripping technique with the cyanoacrylate biopsy technique, to subsequently remove the follicular content (Figure 4) ¹¹³. The tape stripping method was developed previously and used to determine concentration-depth profiles of formulation in the stratum corneum ^{114–117}. The cyanoacrylate biopsy was introduced by Marks and Dawber in 1971 to remove stratum corneum and follicular content ¹¹⁸. One drop of superglue was applied to the skin and covered by a glass slide. After the polymerization of the superglue the glass slide was removed together with stratum corneum and the follicular content ¹¹⁸. By combining both

techniques, a distinct differentiation between the amount of formulation left on the skin surface and the amount that penetrated into the HFs can be made: Tape stripping is used to clean the skin surface by applying several subsequent tape strips (Figure 4 A-D), then a cyanoacrylate biopsy is applied to the cleaned skin surface to remove the follicular content (Figure 4 E-G) ¹¹³. By using a paint roller to press the tape strips onto the skin surface (Figure 4 B), the influence of the furrows and wrinkles on the skin can be neglected ⁹⁴. Raber et al. further enhanced the quantitative determination method by performing mass balance, after the formulation was extracted from each item in contact with it (glove for massage, tape strips, cyanoacrylate biopsies, and a cotton ball to clean the application area and surrounding area) and analyzed (Figure 4 A-G) ¹¹⁹. Furthermore, they compared the *in vivo* method on the human forearm to the pig ear model and demonstrated an excellent *in vivo/in vitro* correlation, highlighting the impact of the pig ear model on the investigation of new NDDS for follicular penetration ¹¹⁹.

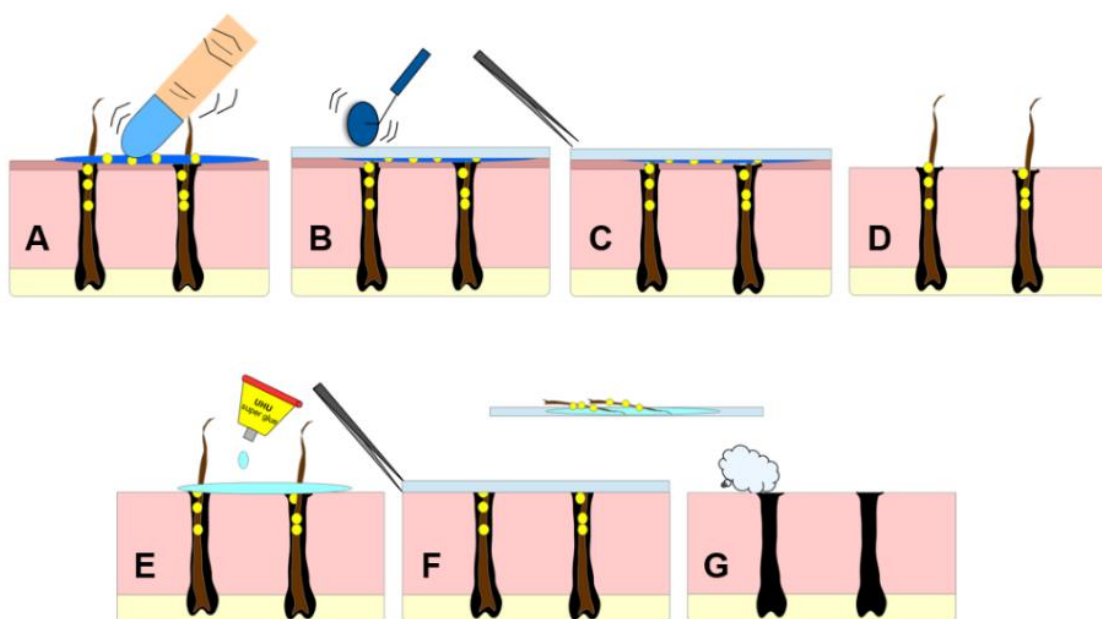


Figure 4. Differential stripping to determine nanoparticle (NP) uptake into human hair follicles *in vivo*. A) Application of NP suspension and a three minutes massage; B-D) surface cleaning by tape stripping: B) polishing wrinkles and furrows by a roller; C) removing tape strips with forceps; D) cleaned skin surface after several tape strips; E-F) cyanoacrylate biopsy – removal of follicular cast: E) covering the application area with one drop of superglue and a tape strip; F) after polymerization of superglue – removal of the tape strip with forceps; G) mass balance – cleaning of skin surface with a cotton ball according to ¹¹⁹.

Other methods investigated the follicular penetration on pig skin by “single HF harvesting”. It involves the extraction of single HFs by 1 mm diameter punch biopsies and the comparison to 1 mm diameter interfollicular skin punches, without prior skin surface cleaning⁶³. This method was developed for the investigation of acne treatments with the benefit, in comparison to cyanoacrylate biopsy, being that by punching, not only was the HF extracted but the whole pilosebaceous unit including the sebaceous gland. However, in this method pig skin detached from the cartilage was used⁶³. Another method combined the skin surface cleaning by tape stripping with a total extraction of punch biopsies of the application area, compared to punch biopsies of untreated areas¹²⁰.

In conclusion, NDDS are able to i) maximize follicular delivery^{64,91}, ii) minimize interfollicular delivery^{64,107}, iii) build up a drug depot inside the HF for up to 10 days^{91,102}, iv) protect the drug inside the HF from textile contact and washing^{91,102}, v) penetrate, depending on size, to different target sites inside the HF¹⁰⁶, thereby reducing systemic drug delivery, severe side effects, and possibly the application frequency, thus enhancing the patient's compliance¹²¹. The topical application of TFB-loaded NDDS for a safer and targeted drug delivery into the HF to treat AA seems predestined.

2. GOAL OF THESIS

This thesis focused on the development of a safe and effective therapy of AA by targeted follicular drug delivery via NDDS.

Several open questions remain and different approaches are yet to be investigated. These are addressed in the following three chapters:

2.1. CHAPTER 1 – NANOPARTICLE UPTAKE INTO HUMAN SCALP HAIR FOLLICLES WITH AND WITHOUT A HAIR SHAFT

Chapter 1 deals with the following investigations:

Are NDDS able to deposit into AA-affected human scalp skin HFs¹²²? This was one of the most urgent questions, since the postulated gear pump mechanism for the NP uptake into HFs involves the cuticle cells of the hair shaft^{91,102}, which are absent in AA-affected HFs³. **Moreover, data for healthy hair shaft-bearing human scalp skin were also still missing.** Therefore, these questions were investigated in an *in vivo* study, employing the previously developed quantitative determination method of NP uptake into HFs in pig ear and human forearm¹¹⁹. **This method was adjusted and transferred to human scalp skin, with and without a hair shaft¹²²:** First, the experimenter was trained on pig ear skin, demonstrating an excellent reproducibility of the original method. After the approval of the study by the Ärztekammer des Saarlandes ethical committee, including informed written consent of participants, the quantification method based on differential stripping was applied to human scalp skin HFs¹²². Differential stripping consists of two main steps: skin surface cleaning via successive tape stripping, and subsequent HF harvesting by cyanoacrylate biopsy. Thus, a differentiation between the formulation left on the skin surface and that deposited into the HFs is possible^{113,119}. The method transfer included an adjustment of the skin surface cleaning step¹²². Instead of 10 successive tape strips 12 were used. Additional important factors were determined: the hair shaft length had to be shortened to 1 mm and the usage of the paint roller seemed essential to ensure adherence of the tape strips¹²². For comparison, not only was the healthy human scalp skin treated with the adjusted method, but also human forearm skin, then AA-affected human scalp skin, and hairy scalp skin of human body donors followed subsequently¹²². **Body donors were used to investigate the possible model character for further investigations of NP uptake into human scalp skin HFs.** Comparing the healthy scalp HFs to HFs of body donors, similar results were found and no significant differences were shown¹²².

Furthermore, to elucidate the influence of the HF density and hair type on the NP uptake into HFs, the NP uptake into HFs per application area was normalized to the number of HF orifices on the application area¹²². For this reason, every application area was photographically documented and the HF orifices were counted. Hence, the NP uptake into one single HF could be determined and compared¹²². No significant differences between the NP uptake into human forearm or human scalp HFs were detected, regardless of hair shaft presence or absence¹²².

These findings are further addressed by the publication: “***Nanoparticle targeting to scalp hair follicles: New perspectives for a topical therapy for Alopecia Areata***”.

Rebekka Christmann, Carla Thomas, Nadine Jager, Anne S. Raber, Brigitta Loretz, Ulrich F. Schaefer, Thomas Tschernig, Thomas Vogt, Claus-Michael Lehr; Journal of Investigative Dermatology (2020) 140, 243e246

DOI link to the formal publication on ScienceDirect: <https://doi.org/10.1016/j.jid.2019.05.02>

Reprinted from Journal of Investigative Dermatology, Nanoparticle Targeting to Scalp Hair Follicles: New Perspectives for a Topical Therapy for Alopecia Areata; Rebekka Christmann, Carla Thomas, Nadine Jager, Anne S. Raber, Brigitta Loretz, Ulrich F. Schaefer, Thomas Tschernig, Thomas Vogt, and Claus-Michael Lehr, 2020, 140, 243e246.

“Copyright © (2019) The Authors, published by Elsevier, Inc. on behalf of the Society for Investigative Dermatology”¹²².

Nanoparticle Targeting to Scalp Hair Follicles: New Perspectives for a Topical Therapy for Alopecia Areata



Journal of Investigative Dermatology (2020) **140**, 243–246; doi:10.1016/j.jid.2019.05.028

TO THE EDITOR

Alopecia areata (AA) is a hair follicle (HF) disorder, in which the immune system attacks the HF and causes reversible hair loss. Even though AA is not a life-threatening disease, an association with psychosocial diseases and a severe drop in quality of life is common (Pratt et al., 2017). There is, as yet, no approved medicine in the therapy for AA. New potent drugs, such as Jak inhibitors, show promising results but incur severe adverse effects (Wang et al., 2018). For such drugs, targeted delivery to the site of action is essential.

The concept for follicular delivery of drug-loaded nanoparticles (NPs) for

treatment of hair disorders shows potential. The key benefits of targeted biodegradable polymeric NP delivery into HFs include (i) protection of the encapsulated drug, (ii) minimization of drug exposure to the skin surface, as well as interfollicular permeation, (iii) maximization of the penetration into the HF compared with the free drug (Mathes et al., 2016), (iv) the possibility of building a drug depot in the upper part of the HF, creating possible protection of the NPs from external influences such as, textile contact, washing (Lademann et al., 2007), and (v) the concurrent ability of a sustained drug release from the depot to reduce

the application frequency and enhance patient compliance (Hofmeier and Surber, 2017). Taking this into account, Jak inhibitor-loaded NPs could deposit in the upper part of the HF, release the drug in a controlled manner, which diffuses to the site of action (hair bulb), and be taken up by the follicular epithelial cells and immune cells (Divito and Kupper, 2014); thus reducing adverse effects with less systemic drug and skin exposure.

However, a hypothesized penetration mechanism for NP uptake into human HF postulates that, by the movement of the hair shaft, overlapping cuticle cells serve as a gear pump and push the NPs into the HF (Lademann et al., 2007; Radtke et al., 2017). Additionally, appropriate massage seems to be important in this context (Li et al., 2019). Thus,

Abbreviations: AA, alopecia areata; HF, hair follicle; NP, nanoparticle; PLGA, poly (lactic-co-glycolic acid)
Accepted manuscript published online 2 July 2019; corrected proof published online 6 September 2019
© 2019 The Authors. Published by Elsevier, Inc. on behalf of the Society for Investigative Dermatology.

R Christmann et al.
Follicle Targeting in Alopecia Areata

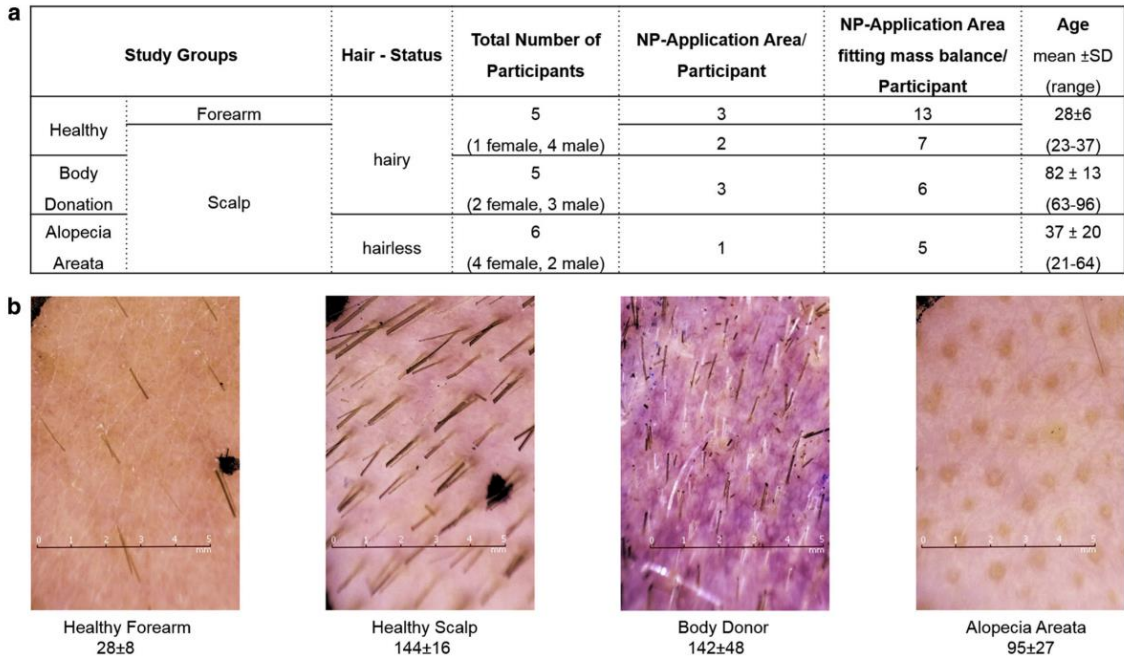


Figure 1. Study groups. (a) Overview of study groups included in the NP uptake study in vivo and in body donors: on one application area (1,767 cm²), 15 μ l of 50 mg/ml fluorescently covalently labeled poly (lactic-co-glycolic acid)-NP suspension was applied by a 3-minute massage with a gloved fingertip and incubated for 1 hour. Additionally, 15 μ l of water was applied on one vehicle blank area per participant. Experimental sets were excluded if they did not meet the mass balance limits of 85–115% as recommended by Scientific Committee on Consumer Safety guidelines (2018). (b) Dermatoscopic documentation of application areas: each application area was documented using a dermatoscope for manual count of hair follicle orifices by ImageJ (results shown as mean \pm SD). (brightness, saturation, focus, black and white balance of pictures enhanced by Corel PaintShop Pro X8 [18.2.0.61 x64]). NP, nanoparticle. Scale bar = 5 mm

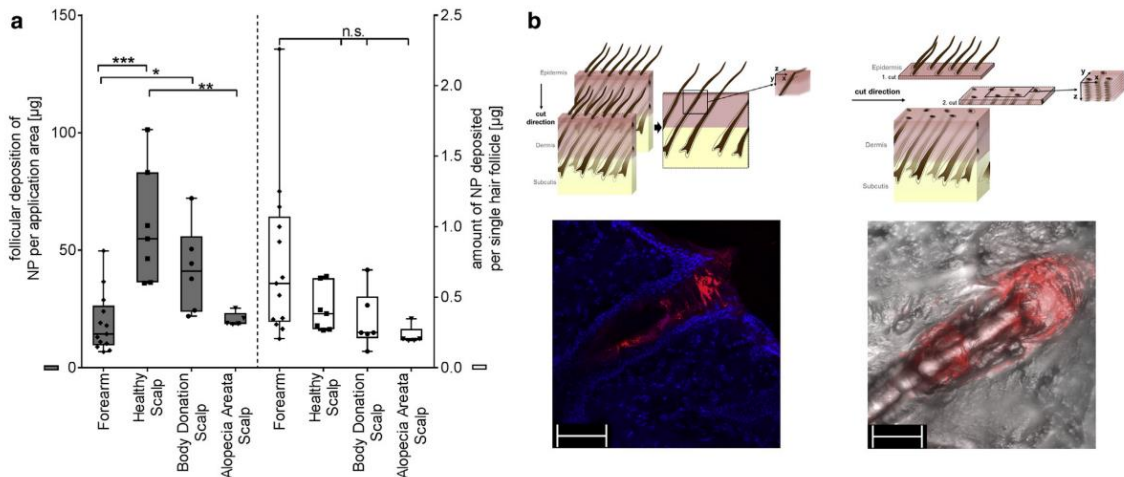


Figure 2. Follicular deposition of nanoparticles. (a) Amount of NPs in HF: gray bars, amount of applied NPs (μ g) per application area deposited in HF; white bars, amount of applied NPs (μ g) deposited in one single HF. Statistics: one-way analysis of variance with corrections (Tukey) of multiple comparisons (mean of each group with the mean of every other group; GraphPad Prism 7; $P = 0.05$). n.s. $P > 0.05$, * $P \leq 0.05$, ** $P \leq 0.01$, *** $P \leq 0.001$. (b) Confocal laser scanning microscopy images of DiD-loaded PLGA-NPs applied on Body Donor scalp: punch biopsy was performed after application of DiD-loaded PLGA-NPs (red; HeNe 633 laser, emission: 665–680 nm) on the skin surface (no skin surface cleaning). Left: longitudinal section 20 μ m, counterstained with DAPI (blue; detection: diode 405 laser, emission: 430–450 nm). Right: transversal section 100 μ m, transmission light (see Supplementary Materials and Methods and Supplementary Figure S3). NP, nanoparticle. Scale bar = 100 μ m

we questioned if NPs are able to penetrate into AA-affected HFs, where there is no hair present. To fill these critical knowledge gaps, we studied NP deposition in AA-affected HFs with a previously developed quantification method for NP uptake into human forearm HFs, demonstrating an excellent *in vivo*–*in vitro* correlation with pig ear skin (Raber et al., 2014). However, there are no quantitative data for human scalp skin. Because hair density and hair type (vellus vs. terminal) differ between the healthy forearm and scalp, such data are critical to assess treatment options.

Therefore, we transferred the quantification method of NP uptake into human forearm HF to human scalp skin of healthy volunteers, subsequently transferred it to AA patients. However, the recruitment of participants for such studies is limited. Accordingly, we assessed the quantification method also in the hairy scalp of body donors as a possible alternative to future *in vivo* studies (experiments were conducted with the skin attached to the corpus; body donors were not fixated before the experiment and kept at 4 °C; maximal post mortem interval was 3 days) (for study group details see Figure 1a). The studies were approved by the Ärztekammer des Saarlandes ethical committee, including informed written consent of participants.

For the model NPs, we continued to use the NPs used in the previously developed quantification method for NP uptake into the HF (Raber et al., 2014). The NPs, size of 150 nm, narrow size distribution and negative zeta potential, consisted of fluorescently covalently labeled poly (lactic-co-glycolic acid) (PLGA), a biodegradable, biocompatible polymer (Weiss et al., 2006; Mittal et al., 2013). For a detailed description of the procedure, see *Supplementary Materials and Methods*. In brief, differential stripping was proceeded 1 hour after applying 15 µl of aqueous fluorescently covalently labeled PLGA-NP suspension (concentration = 50 mg/ml) per application area by a 3-minute massage (Teichmann et al., 2005), which comprises skin surface cleaning by tape stripping and subsequent removal of HF casts by cyanoacrylate

biopsies. For mass balance, all samples in contact with the formulation were extracted in organic solvent and analyzed using fluorescence intensity. Stratum corneum recovery after differential stripping was monitored by transepidermal water loss measurements (Supplementary Figure S1). Experimental sets were excluded if they did not meet the 85–115% mass balance limits as recommended by the Scientific Committee on Consumer Safety guidelines (2018; Figure 1a).

Comparing percentage of dose (mean ± SD) of applied NPs recovered on the skin surface ($61.0 \pm 4.1\%$ vs. $56.4 \pm 3.7\%$), the percentage of dose remaining on the glove ($28.1 \pm 5.5\%$ vs. $24.1 \pm 3.7\%$), and the percentage left on the skin ($0.1 \pm 0.2\%$ vs. $1.3 \pm 1.1\%$) after cyanoacrylate biopsies, results for forearm and healthy scalp, respectively, showed no significant differences (Supplementary Table S1; Supplementary Figure S2, red and purple bars), demonstrating successful transfer of the method from forearm to scalp skin.

Owing to higher HF density on a healthy scalp, we hypothesized a higher amount of NP deposition in scalp HFs than in forearm HFs. Indeed, the amount of NPs deposited in the HFs per application area of healthy scalp ($8.5 \pm 3.6\%$ equals $59.79 \pm 24.46 \mu\text{g}/\text{HF}$ per area) was significantly higher than for forearm ($2.5 \pm 0.9\%$ equals $19.05 \pm 12.78 \mu\text{g}/\text{HF}$ per area) ($P \leq 0.001$; Figure 2a, gray bars). To assess the influence of HF density, we documented each application area using a dermatoscope (handyscope, Foto-Finder, Bad Birnbach, Germany) (Figure 1b) and determined the number of HF orifices visible on the skin surface of each individual application area manually using ImageJ (ImageJ 1.51j8, NIH). After normalizing the NPs deposited per application area for the different HF orifice densities on the human forearm ($0.75 \pm 0.57 \mu\text{g}/\text{one HF}$) and healthy scalp ($0.42 \pm 0.16 \mu\text{g}/\text{one HF}$), the differences were no longer statistically significant (Figure 2b), that is, the amount of NPs deposited per HF was about the same, regardless of the body site. Given that this study is limited by its number of participants, the results need to be considered carefully. Nevertheless, this is an interesting result, because vellus and terminal HF

show fundamental morphometric differences (Vogt et al., 2007). Also, the HF densities and infundibular surfaces significantly differ between different vellus HF covered body sites (Otberg et al., 2004). This study takes only human forearm HF into account.

There was no significant difference when comparing the data of a healthy scalp with a body donation scalp regarding the amount of follicular deposition per application area ($59.79 \pm 24.46 \mu\text{g}$ vs. $41.83 \pm 18.53 \mu\text{g}$) (Figure 2b) or the deposition per single HF ($0.42 \pm 0.16 \mu\text{g}$ vs. $0.33 \pm 0.21 \mu\text{g}$, healthy scalp and body donor scalp, respectively). This implies that body donors may be used as models to develop future follicle-targeted drug carriers for dermatological applications.

Finally, we investigated the NP uptake *in vivo* into AA-affected hairless scalp HFs. Despite the postulated NP uptake mechanism in HF (Lademann et al., 2007), we demonstrated NP deposition in human HF in healthy ($8.5 \pm 3.6\%$ equals $59.79 \pm 24.46 \mu\text{g}$) and AA-affected HFs ($2.7 \pm 0.4\%$ equals $20.49 \pm 2.90 \mu\text{g}$); the difference of NP deposition per application area (Figure 2b, gray bars) between the two groups was significant ($P \leq 0.01$). Interestingly, after correction for the number of HF orifices per application area, the NP deposition per single HF (Figure 2b, white bars) was no longer significantly different ($P > 0.05$; $0.42 \pm 0.16 \mu\text{g}$ vs. $0.23 \pm 0.07 \mu\text{g}$, healthy vs. AA scalp, respectively).

In conclusion, we were able to demonstrate that topically applied NPs do penetrate into human scalp HFs. This phenomenon appeared to be of the same scale as the previously reported follicular penetration in human forearm HFs (Raber et al., 2014) and thus to be independent of the HF type. Moreover, and, most importantly, NPs were found to penetrate into HFs also in the absence of a hair shaft. This opens possibilities for the treatment of inflammatory hair loss, most importantly AA, by designing appropriate nanomedicines capable of penetrating and delivering their cargo directly to the affected HFs.

Data availability statement

Datasets related to this article can be found at <https://doi.org/10.17632/fn6gg3f4py.1>, hosted at Mendeley Data.

AM Carvalho et al.

NLRP3 Inhibitor in Leishmaniasis

ORCID

Rebekka Christmann: <http://orcid.org/0000-0003-1775-2113>
 Carla Thomas: <http://orcid.org/0000-0002-9809-9533>
 Nadine Jager: <http://orcid.org/0000-0002-5216-8441>
 Anne S. Raber: <http://orcid.org/0000-0003-0018-2652>
 Brigitta Loretz: <http://orcid.org/0000-0003-0057-5181>
 Ulrich F. Schaefer: <http://orcid.org/0000-0002-2470-2168>
 Thomas Tschernig: <http://orcid.org/0000-0002-7788-1796>
 Thomas Vogt: <http://orcid.org/0000-0002-2824-5005>
 Claus-Michael Lehr: <http://orcid.org/0000-0002-5864-8462>

CONFLICT OF INTEREST

The authors declare no conflict of interest.

ACKNOWLEDGMENTS

This work was supported by Dr. Rolf M. Schwiete Stiftung, Mannheim, Germany (Project-Nr. 14/2016). We thank Olga Hartwig for help with confocal laser scanning microscope, UHU, Bühl/Baden, Germany, and tesa SE, Norderstedt, Germany for the kind donation of materials.

AUTHOR CONTRIBUTIONS

Conceptualization: TV, UFS, CML; Funding Acquisition: TV, CML; Investigation: RC, CT, NJ; Methodology: ASR, UFS, RC, CT; Project Administration: BL, TV; Resources: TT, CT, TV, RC; Supervision: BL, UFS, CML, TV; Writing - Original Draft Preparation: RC, UFS, BL; Writing - Review and Editing: RC, CT, NJ, ASR, BL, UFS, TT, TV, CML.

**Rebekka Christmann^{1,2,4,5},
 Carla Thomas^{4,5}, Nadine Jager^{4,5},
 Anne S. Raber², Brigitta Loretz¹,
 Ulrich F. Schaefer²,
 Thomas Tschernig³, Thomas Vogt^{4,5}
 and Claus-Michael Lehr^{1,2,*}**

¹Helmholtz-Institute for Pharmaceutical Research Saarland (HIPS)—Helmholtz Centre for Infection Research (HZI), Saarbrücken, Germany; ²Department of Pharmacy, Saarland University, Saarbrücken, Germany; ³Medical Faculty, Institute of Anatomy and Cell Biology, Saarland University, Homburg/Saar, Germany; ⁴Department of Dermatology, Saarland University Hospital, Homburg/Saar, Germany; and ⁵Hair Research Institute Dr. Rolf M. Schwiete, Saarland University Hospital, Homburg/Saar, Germany
 *Corresponding author e-mail: Claus-Michael.Lehr@helmholtz-hips.de

SUPPLEMENTARY MATERIAL

Supplementary material is linked to the online version of the paper at www.jidonline.org, and at <https://doi.org/10.1016/j.jid.2019.05.028>.

REFERENCES

- Divito SJ, Kupper TS. Inhibiting Janus kinases to treat alopecia areata. *Nat Med* 2014;20:989–90.
- Hofmeier KS, Surber C. Nanomedicine in dermatology: nanotechnology in prevention, diagnosis, and therapy. In: Müller B, van de Voorde MH, editors. *Nanoscience and nanotechnology for human health. Nanotechnology innovation & applications*. Weinheim, Germany: Wiley-VCH Press; 2017. p. 329–56.
- Lademann J, Richter H, Teichmann A, Otberg N, Blume-Peytavi U, Luengo J, et al. Nanoparticles— an efficient carrier for drug delivery into the hair follicles. *Eur J Pharm Biopharm* 2007;66:159–64.
- Li BS, Cary JH, Maibach HI. Should we instruct patients to rub topical agents into skin?: the evidence. *J Dermatolog Treat* 2019;30:328–32.
- Mathes C, Melero A, Conrad P, Vogt T, Rigo L, Selzer D, et al. Nanocarriers for optimizing the balance between interfollicular permeation and follicular uptake of topically applied clobetasol to minimize adverse effects. *J Control Release* 2016;223:207–14.
- Mittal A, Raber AS, Schaefer UF, Weissmann S, Ebensen T, Schulze K, et al. Non-invasive delivery of nanoparticles to hair follicles: a perspective for transcutaneous immunization. *Vaccine* 2013;31:3442–51.
- Otberg N, Richter H, Schaefer H, Blume-Peytavi U, Sterry W, Lademann J. Variations of hair follicle size and distribution in different body sites. *J Invest Dermatol* 2004;122:14–9.
- Pratt CH, King LE, Messenger AG, Christiano AM, Sundberg JP. Alopecia areata. *Nat Rev Dis Primers* 2017;3:17011.
- Raber AS, Mittal A, Schäfer J, Bakowsky U, Reichrath J, Vogt T, et al. Quantification of nanoparticle uptake into hair follicles in pig ear and human forearm. *J Control Release* 2014;179:25–32.
- Radtke M, Patzelt A, Knorr F, Lademann J, Netz RR. Ratchet effect for nanoparticle transport in hair follicles. *Eur J Pharm Biopharm* 2017;116:125–30.
- Scientific Committee on Consumer Safety. The SCCS Notes of Guidance for the Testing of Cosmetic Ingredients and their Safety Evaluation 10th Revision, https://ec.europa.eu/health/sites/health/files/scientific_committees/consumer_safety/docs/sccs_o_224.pdf; 2018 (accessed 28 January 2019).
- Teichmann A, Jacobi U, Ossadnik M, Richter H, Koch S, Sterry W, et al. Differential stripping: determination of the amount of topically applied substances penetrated into the hair follicles. *J Invest Dermatol* 2005;125:264–9.
- Vogt A, Hadam S, Heiderhoff M, Audring H, Lademann J, Sterry W, et al. Morphometry of human terminal and vellus hair follicles. *Exp Dermatol* 2007;16:946–50.
- Wang EHC, Sallee BN, Tejada CI, Christiano AM. JAK inhibitors for treatment of alopecia areata. *J Invest Dermatol* 2018;138:1911–6.
- Weiss B, Schaefer UF, Zapp J, Lamprecht A, Stallmach A, Lehr CM. Nanoparticles made of fluorescence-labelled Poly(L-lactide-co-glycolide): preparation, stability, and biocompatibility. *J Nanosci Nanotechnol* 2006;6:3048–56.

SUPPLEMENTARY MATERIALS AND METHODS**Quantification method for nanoparticle uptake in human hair follicles adjusted after Raber et al. (2014)**

Initially, hair was cut to 1 mm with an electrical shaver (Braun Bartschneider, BT3040, Procter & Gamble Service, Schwalbach am Taunus, Germany) and the skin surface was cleansed of free hair. Application areas, each 1,767 cm², were marked with a permanent black marker (Faber-Castell MULTI-MARK permanent 152399, A.W. Faber-Castell Vertrieb, Stein, Germany) using a Teflon mask. Each application area was documented using a dermatoscope (handscope, FotoFinder, Bad Birnbach, Germany) for counting hair follicle (HF) orifices. Then, 15 µl of an aqueous nanoparticle (NP) suspension (concentration = 50 mg/ml) composed of fluoresceinamine covalently labeled poly (lactic-co-glycolic acid) (PLGA) NPs (Mittal et al., 2013; Weiss et al., 2006) was applied per application area. Particle size, 149.04 ± 3.46 nm; polydispersity index, 0.06 ± 0.02; zeta potential -24.64 ± 6.85 mV. On blank areas (one per participant), 15 µl of purified water was applied for individual vehicle control. For NP penetration enhancement into the HF, a 3-minute circular massage with slight pressure (60 r.p.m., ~2 Newton) was applied by a trained person with a gloved fingertip (Mathes et al., 2016; Lademann et al., 2007). Differential stripping was proceeded after a 1-hour incubation time (Teichmann et al., 2005). First, the skin surface was cleaned by tape stripping, followed by removal of HF casts by cyanoacrylate biopsies. For the tape stripping, the application area was covered by one tape strip (tesafilm kristall-klar, Norderstedt, Germany), pressed onto the skin surface by a paint roller (to reach furrows and crinkles) (Lademann et al., 2005), and removed in one swoop with forceps. A total of 12 successive tape strips were used to clean the skin surface by removal of stratum corneum layers. The removal of the HF casts was carried out using the following two cyanoacrylate biopsies. One drop of superglue (UHU blitzschnell Pipette, Bühl/Baden, Germany)

was applied to the cleaned surface area and covered by a tape strip. After polymerization of the cyanoacrylate (5 minutes), the tape strip was removed with a forceps in one swoop. This was done twice. It has been shown by Raber et al. (2014), that with two biopsies a complete removal of the HFs on the application area can be achieved. For mass balance, the treated skin surface and its surroundings were cleaned with a cotton ball. All samples were analyzed separately: glove fingertip, tape strips (one and two separately, then two together), cyanoacrylate biopsies, and cotton ball (skin rest). Extraction and analysis by fluorescence spectroscopy were done according to Raber et al. (2014). Relative fluorescence unit values were corrected by the individual blank matrix value. Lower limit of quantification of fluorescently covalently labeled PLGA-NP suspension calibration curve was calculated according to the FDA *Bio-analytical Method Validation guideline* (FDA/CDER, 2018). Values lower than the lower limit of quantification were excluded. Experimental sets were excluded if they did not meet 85–115% as the recommended range of mass balance by the Scientific Committee on Consumer Safety guidelines (2018). Count of HF orifices on dermatoscopic pictures was done manually by ImageJ (ImageJ 1.51j8, NIH) for each application area individually. By correction of the follicular deposition of NPs per application area to the number of HF orifices counted, the amount of NPs (in µg) deposited into one single HF was determined. Recovery of skin barrier function was monitored by transepidermal water-loss measurements according to the ethical committee (Supplementary Figure S1).

Visualization of nanoparticle penetration inside human scalp hair follicles

DiD-loaded PLGA-NPs were chosen for the visualization of NPs inside the HF, because fluorescently covalently labeled -PLGA-NPs in conjugation with skin and HFs are difficult to differentiate, because of the high auto fluorescence of the organs (Na et al., 2000) and the terminated fluorescence

intensity of Fluorescein. DiD-loaded PLGA-NPs were prepared as described previously (Mittal et al., 2013) with addition of Vybrant DiD cell-labeling solution (Vybrant Multicolor Cell-Labeling Kit, Invitrogen, Waltham, MA) to the organic polymer solution. The free dye was separated from NPs by dialysis in purified water (Spectra/Por Float-a-Lyzer, 100 kDa, Spectrum Europe B.V., Breda, The Netherlands) for 29 hours. NPs were 124.0 ± 0.9 nm, and had a polydispersity index of 0.07 ± 0.02 and a zeta potential of -21.8 ± 0.2 mV. To visualize the DiD-loaded PLGA-NP deposition inside HFs (before the scalp hair was shortened to 1 mm) per application area (1,767 cm²), 20 µl of the NP formulation (250 mg PLGA/ml) was applied by massage. After the incubation time, no further procedure for skin cleaning (no tape stripping) or hair removal was applied; the applied NP formulation remained on the skin surface and in the HFs. An 8-mm punch biopsy was taken. Blank application areas (Control without NP) were treated the same without application of NP formulation. Subsequently, the skin tissue was imbedded in Tissue-Tek O.C.T. Compound (Sakura Finetek Europe B.V., Alphen aan den Rijn, The Netherlands) and cut by cryostat (SLEE, Mainz, Germany) (Supplementary Figure S3). Images were taken with a confocal laser scanning microscope (CLSM) (Leica TCS SP8, Leica, Mannheim, Germany) and processed with Leica Application Suite X (LAS X) software (Leica, Mannheim, Germany). Transversal sections to 100 µm were cut (Supplementary Figure S3c, S3d). On the first section, the amount of NPs on the skin surface was too high for a sufficient differentiation between NPs remaining on the skin surface and deposited in the HF. Therefore, the second 100-µm section is shown in Supplementary Figure S3c, demonstrating the DiD-loaded PLGA-NP (red fluorescence) inside the HF (hair shaft is present) (overlay with transmission light image). On the third 100-µm section, no NPs were detectable (not shown). The second transversal 100-µm section of the blank biopsy is shown in Supplementary Figure S3d (control without NP [HF with hair shaft] [overlay transmission

R Christmann et al.

Follicle Targeting in Alopecia Areata

light image and red fluorescence channel). Results of longitudinal tissue sections of 20 μm are shown in [Supplementary Figure S3a](#) and [b](#). DiI-loaded PLGA-NPs (red fluorescence) can be detected only on the skin surface and inside the HF (hair shaft is present), counterstaining with DAPI (Sigma, Darmstadt, Germany) (blue fluorescence) ([Supplementary Figure S3a](#), NP in HF). In the blank tissue sections, no strong red fluorescence was detectable ([Supplementary Figure S3b](#), control without NP [HF with hair shaft]) (blue fluorescence: DAPI). Visualization of NPs inside the scalp HFs can only be shown by Body Donors, because ethical reasons do not allow invasive procedures in living participants. In addition, because of ethical reasons, only fluorescently covalently labeled -PLGA-NP for the human in vivo studies could be used.

SUPPLEMENTARY REFERENCES

FDA/CDER. Bioanalytical method validation guidance for industry, <https://www.fda.gov/files/drugs/published/Bioanalytical-Method-Validation-Guidance-for-Industry.pdf>; 2018 (accessed 08 October 2019).

Lademann J, Richter H, Teichmann A, Otberg N, Blume-Peytavi U, Luengo J, et al. Nanoparticles—an efficient carrier for drug delivery into the hair follicles. *Eur J Pharm Biopharm* 2007;66:159–64.

Lademann J, Weigmann HJ, Schanzer S, Richter H, Audring H, Antoniou C, et al. Optical investigations to avoid the disturbing influences of furrows and wrinkles quantifying penetration of drugs and cosmetics into the skin by tape stripping. *J Biomed Opt* 2005;10:054015.

Mathes C, Melero A, Conrad P, Vogt T, Rigo L, Selzer D, et al. Nanocarriers for optimizing the balance between interfollicular permeation and follicular uptake of topically applied clobetasol to minimize adverse effects. *J Control Release* 2016;223:207–14.

Mittal A, Raber AS, Schaefer UF, Weissmann S, Ebensen T, Schulze K, et al. Non-invasive delivery of nanoparticles to hair follicles: a

perspective for transcutaneous immunization. *Vaccine* 2013;31:3442–51.

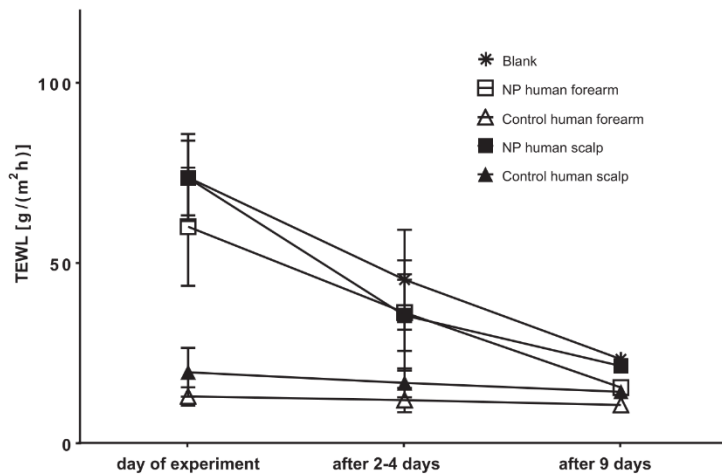
Na R, Stender IM, Ma L, Wulf HC. Auto-fluorescence spectrum of skin: component bands and body site variations. *Skin Res Technol* 2000;6:112–7.

Raber AS, Mittal A, Schäfer J, Bakowsky U, Reichrath J, Vogt T, et al. Quantification of nanoparticle uptake into hair follicles in pig ear and human forearm. *J Control Release* 2014;179:25–32.

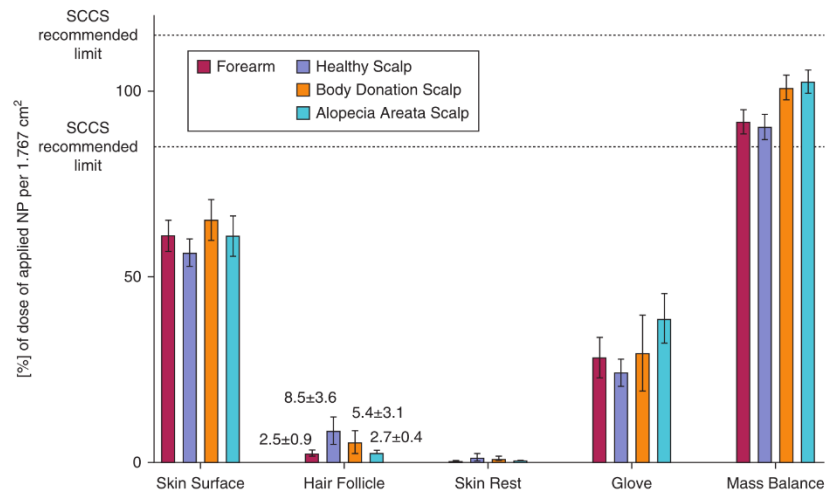
Scientific Committee on Consumer Safety. The SCCS Notes of Guidance for the Testing of Cosmetic Ingredients and their Safety Evaluation 10th Revision, https://ec.europa.eu/health/sites/health/files/scientific_committees/consumer_safety/docs/sccs_o_224.pdf; 2018 (accessed 28 January 2019).

Teichmann A, Jacobi U, Ossadnik M, Richter H, Koch S, Sterry W, et al. Differential stripping: determination of the amount of topically applied substances penetrated into the hair follicles. *J Invest Dermatol* 2005;125:264–9.

Weiss B, Schaefer UF, Zapp J, Lamprecht A, Stallmach A, Lehr CM. Nanoparticles made of fluorescence-labelled Poly(L-lactide-co-glycolide): preparation, stability, and biocompatibility. *J Nanosci Nanotechnol* 2006;6(9-10):3048–56.

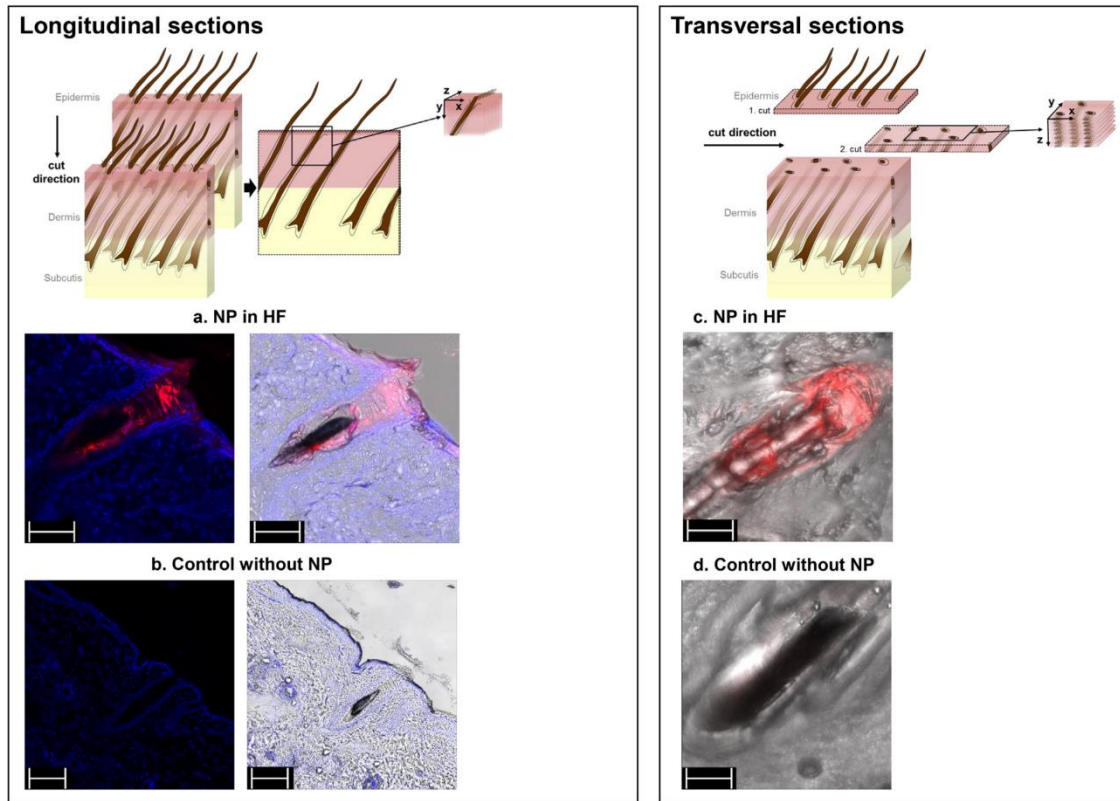


Supplementary Figure S1. Transepidermal water loss (TEWL) measurements for skin damage control through differential stripping. Exemplary measurements on healthy forearm and healthy scalp on four participants (after 9 days from one participant). Control measurements were taken on untreated skin (control forearm, white triangle; control scalp, black triangle), Blank measurements on Blank application areas (star) and treated measurements on NP application areas (treated forearm, white square; treated scalp, black square). Results are presented as mean ± SD. Results show slight stratum corneum damage after differential stripping and fast recovery, without permanent skin surface damage by the method. Similar results have been reported by [Raber et al. \(2014\)](#).



Supplementary Figure S2. Overview of differential stripping results of study groups. Percentage of dose of applied NPs per 1,767 cm² recovered on skin surface, hair follicles, skin rest, glove, and calculated mass balance are shown as mean ± SD. The limits of 85–115% for desired mass balance range recommended by the Scientific Committee on Consumer Safety guidelines (2018) are marked, experimental sets were excluded if they did not meet this criteria.

R Christmann et al.
Follicle Targeting in Alopecia Areata



Supplementary Figure S3. Confocal laser scanning microscope (CLSM) images of DiD-loaded PLGA-NPs applied on the scalp of a Body Donor. (a, b) 20- μm longitudinal sections, counterstained with DAPI; left-hand images, no transmission light overlay; right-hand images, with transmission light overlay. (a) CLSM image of DiD-loaded PLGA-NPs (red) in HF (with hair shaft); DiD detection: HeNe 633 laser, emission: 665–680 nm, gain 40; DAPI detection: diode 405 laser, emission: 430–450 nm, gain 60; magnification $\times 25$; pixel size/voxel size: $x = 0.455 \mu\text{m}$, $y = 0.455 \mu\text{m}$, $z = 2.664 \mu\text{m}$; 15 frames. Scale bars = 100 μm . (b) CLSM image of Control without NP in HF (with hair shaft); DiD detection: HeNe 633 laser, emission: 665–680 nm, gain 100; DAPI detection: diode 405 laser, emission: 430–450 nm, gain 60; magnification $\times 10$; pixel size: $x = 0.001 \text{ mm}$, $y = 0.001 \text{ mm}$; 1 frame. Scale bars = 200 μm . (c, d) 100- μm transversal sections, overlay with transmission light channel. (c) CLSM image of DiD-loaded PLGA-NPs (red) in HF (with hair shaft); DiD detection: HeNe 633 laser, emission: 665–680 nm, gain 40; magnification $\times 25$; pixel size/voxel size: $x = 0.104 \mu\text{m}$, $y = 0.104 \mu\text{m}$, $z = -0.568 \mu\text{m}$; 137 frames. Scale bar = 100 μm . (d) CLSM image of Control without NP in HF (with hair shaft); DiD detection: HeNe 633 laser, emission: 665–680 nm, gain 40; magnification $\times 25$; pixel size/voxel size: $x = 0.455 \mu\text{m}$, $y = 0.455 \mu\text{m}$, $z = 3.582 \mu\text{m}$; 25 frames. Scale bar = 100 μm .

Supplementary Table S1. Differential stripping data (Mean \pm SD) of healthy forearm and healthy scalp, Body Donor scalp and alopecia areata-affected scalp

	No. of experimental sets	Forearm	Scalp		
		Healthy 13	Healthy 7	Body Donor 6	Alopecia Areata 5
% of dose of applied NP per 1,767 cm ² application area	Skin surface	61.0 \pm 4.1	56.4 \pm 3.7	65.2 \pm 5.5	60.9 \pm 5.4
	Skin rest	0.1 \pm 0.2	1.3 \pm 1.1	0.9 \pm 0.7	0.2 \pm 0.20
	Glove	28.1 \pm 5.5	24.1 \pm 3.7	29.3 \pm 10.2	38.7 \pm 6.7
	HF	2.5 \pm 0.9	8.5 \pm 3.6	5.4 \pm 3.1	2.7 \pm 0.4
	Mass balance	91.7 \pm 3.2	90.3 \pm 3.4	100.9 \pm 3.4	102.6 \pm 3.1
NP deposited in HFs per application area (μ g)	HF	19.05 \pm 12.78	59.79 \pm 24.46	41.83 \pm 18.53	20.49 \pm 2.90
NP deposited per HF (μ g)	HF	0.75 \pm 0.57	0.42 \pm 0.16	0.33 \pm 0.21	0.23 \pm 0.07

Boldface indicates deposition in HFs.

For statistical analysis, refer to [Figure 2b](#).

Abbreviations: HF, hair follicle; NP, nanoparticle.

This proof of concept blazes the trail for the targeted drug delivery in the treatment of AA via NDDS and leads to the next chapter:

2.2. CHAPTER 2 – CHOICE OF AN APPROPRIATE NANOPARTICULATE DRUG DELIVERY SYSTEM FOR TARGETED FOLLICULAR DRUG DELIVERY OF TOFACITINIB – CHARACTERIZATION AND DEVELOPMENT OF VERSATILE AMPHIPHILIC SQUALENYL DERIVATIVE NANOPARTICULATE DRUG DELIVERY SYSTEM PLATFORMS

Chapter 2 deals with the following investigations:

Development of potent drug loaded NDDS with the aim of high drug loading to enable sufficient targeted follicular drug delivery. As the potent drug the JAK inhibitor TFB was chosen. Of course, **biocompatible NDDS** had to be used. First attempts involved loading TFB into long established NDDS consisting of biocompatible polymers, e.g., PLGA and polycaprolactone (PCL). Unfortunately, no satisfactory TFB-loaded NDDS could be established, particularly in regard to drug loading and reproducibility of the manufacturing process. Difficulties were due to the pH-dependent water solubility¹²³ and instability in aqueous basic solutions^{124,125} of TFB. The idea to use the squalenylation technique arose⁶⁸. This technique is known to achieve high drug loading capacities of over 30 % (w/w)^{68,69}. An additional benefit of this technique would be the involved excipient – squalene. Squalene is one of the main components of human sebum, which represents the human natural environment in HFs⁷⁸. The squalenylation technique, consists of the bioconjugation of a squalenyl moiety to the drug molecule forming an amphiphilic prodrug, able to build NPs upon nanoprecipitation into aqueous solutions^{68,69}. However, this technique is not available for drugs with missing functional groups or multiple functional groups, complicating the bioconjugation. Unfortunately, TFB presents only a weak chemical reactivity for covalently coupling reactions, which was also reported by other groups⁷⁴. Fortunately, the squalenylation technique was developed further to overcome this drawback^{75,76}. The synthesis of an amphiphilic SqD – squalenyl hydrogen sulfate – consisting of a hydrophobic squalenyl tail and a hydrophilic hydrogen sulfate group enables a stable NPs formation upon nanoprecipitation into aqueous solutions without the addition of further surfactants and excipients⁷⁶. A core-shell structure formation of the NPs is postulated, with a hydrophobic core of squalenyl moieties and a hydrophilic shell of hydrogen sulfate groups, enabling drug loading for both, hydrophobic, as well as hydrophilic drugs (positively charged) either by intercalation, hydrophobic interactions, and/or charge interactions⁷⁶. However, the development of squalenyl based NPs calls for an experienced person in handling and manufacturing these NPs to minimize the failure of the manufacturing process due to the experimenter and to be able to adapt

and develop a sufficient manufacturing process for the to be-loaded drug. **Therefore, before TFB-loaded SqD NPs could be developed, the SqD NDDS platform was further developed and explored** ¹²⁶. Besides the squalenyl hydrogen sulphate (negatively charged SqD), a positively charged as well as PEGylated SqDs were synthesized and different loading processes were investigated to open the NDDS platforms for a broader field of application ¹²⁶; this part is further elucidated in the following publication. The loading of different model drugs and substances demonstrates the broad usability of the SqD based NDDS platforms by achieving high drug loading capacities of up to 45 % (w/w) ¹²⁶. For example, as representative of glucocorticoids, the drug loading of dexamethasone in each different SqD was explored ¹²⁶. Impressive drug loading capacities for all SqDs of ~ 32 to 35 % (w/w) were demonstrated ¹²⁶. Furthermore, the colloidal stability of the SqD NDDS in physiological relevant pH solutions as well as the biocompatibility were elucidated ¹²⁶.

These approaches are further addressed by the publication: "***Synthesis and Biopharmaceutical Characterization of Amphiphilic Squalenyl Derivative Based Versatile Drug Delivery Platform***".

Duy-Khiet Ho*, Rebekka Christmann*, Xabier Murgia, Chiara de Rossi, Sarah Frisch, Marcus Koch, Ulrich F. Schaefer, Brigitta Loretz, Didier Desmaele, Patrick Couvreur, Claus-Michael Lehr; *Frontiers in Chemistry* (2020) 8:584242.

DOI: 10.3389/fchem.2020.584242

* These authors have contributed equally to this work and share first authorship

Reprinted from *Frontiers in Chemistry, Synthesis and Biopharmaceutical Characterization of Amphiphilic Squalenyl Derivative Based Versatile Drug Delivery Platform*; Duy-Khiet Ho*, Rebekka Christmann*, Xabier Murgia, Chiara de Rossi, Sarah Frisch, Marcus Koch, Ulrich F. Schaefer, Brigitta Loretz, Didier Desmaele, Patrick Couvreur, and Claus-Michael Lehr; (2020) 8:584242

"Copyright © (2020) Ho, Christmann, Murgia, De Rossi, Frisch, Koch, Schaefer, Loretz, Desmaele, Couvreur and Lehr. This is an open-access article distributed under the terms of the Creative Commons Attribution License (CC BY). The use, distribution or reproduction in other forums is permitted, provided the original author(s) and the copyright owner(s) are credited and that the original publication in this journal is cited, in accordance with accepted academic practice. No use, distribution or reproduction is permitted which does not comply with these terms" ¹²⁶.



OPEN ACCESS

Edited by:

Jianliang Shen,
Wenzhou Medical University, China

Reviewed by:

Haihua Xiao,
Chinese Academy of Sciences, China
Qian Cao,
SYSU, China

***Correspondence:**

Brigitta Loretz
brigitta.loretz@helmholtz-hips.de
Didier Desmaele
didier.desmaele@u-psud.fr
Claus-Michael Lehr
claus-michael.lehr@helmholtz-hips.de

[†] These authors have contributed
equally to this work and share first
authorship

***Present address:**

Duy-Khiet Ho,
Department of Bioengineering, School
of Medicine, University of Washington,
Seattle, WA, United States
Xabier Murgia,
Kusudama Therapeutics, Parque
Científico y Tecnológico de Gipuzkoa,
Donostia-San Sebastián, Spain

Specialty section:

This article was submitted to
Supramolecular Chemistry,
a section of the journal
Frontiers in Chemistry

Received: 16 July 2020

Accepted: 08 September 2020

Published: 19 October 2020

Citation:

Ho D-K, Christmann R, Murgia X, De
Rossi C, Frisch S, Koch M,
Schaefer UF, Loretz B, Desmaele D,
Couvreur P and Lehr C-M (2020)
Synthesis and Biopharmaceutical
Characterization of Amphiphilic
Squalenyl Derivative Based Versatile
Drug Delivery Platform.
Front. Chem. 8:584242.
doi: 10.3389/fchem.2020.584242

Synthesis and Biopharmaceutical Characterization of Amphiphilic Squalenyl Derivative Based Versatile Drug Delivery Platform

Duy-Khiet Ho^{1,2†}, Rebekka Christmann^{1,2†}, Xabier Murgia^{1,2†}, Chiara De Rossi¹,
Sarah Frisch^{1,2}, Marcus Koch³, Ulrich F. Schaefer², Brigitta Loretz^{1*}, Didier Desmaele^{4*},
Patrick Couvreur⁴ and Claus-Michael Lehr^{1,2*}

¹ Helmholtz Institute for Pharmaceutical Research Saarland, Helmholtz Centre for Infection Research, Saarbrücken, Germany, ² Department of Pharmacy, Saarland University, Saarbrücken, Germany, ³ INM-Leibniz Institute for New Materials, Saarbrücken, Germany, ⁴ Faculté de Pharmacie, Institut Galien Paris Sud, Université Paris-Saclay, Chatenay-Malabry, France

Limited drug loading capacity (LC), mostly below 5% w/w, is a significant drawback of nanoparticulate drug delivery systems (DDS). Squalenylation technology, which employs bioconjugation of squalenyl moiety and drug, allows self-assembly of nanoparticles (NPs) in aqueous media with significantly high LC (>30% w/w). The synthesis and particle preparation of squalenoylated prodrugs are, however, not facile for molecules with multiple reactive groups. Taking a different approach, we describe the synthesis of amphiphilic squalenyl derivatives (SqDs) as well as the physicochemical and biopharmaceutical characterizations of their self-assembled NPs as DDSs. The SqDs included in this study are (i) cationic squalenyl diethanolamine (ii) PEGylated SqD (PEG 750 Da), (iii) PEGylated SqD (PEG 3,000 Da), and (iv) anionic squalenyl hydrogen sulfate. All four SqDs self-assemble into NPs in a size range from 100 to 200 nm in an aqueous solution. Furthermore, all NP derivatives demonstrate appropriate biocompatibility and adequate colloidal stability in physiological relevant pH environments. The mucoprotein binding of PEGylated NPs is reduced compared to the charged NPs. Most importantly, this technology allows excellent LC (at maximum of 45% w/w) of a wide range of multifunctional compounds, varying in physicochemical properties and molecular weight. Interestingly, the drug release profile can be tuned by different loading methods. In summary, the SqD-based NPs appear as versatile drug delivery platforms.

Keywords: drug delivery, self-assembly, pegylated, squalenyl derivatives, squalene, nanoparticles, protein-interaction

INTRODUCTION

Nano-sized drug delivery systems (DDS) having the size range from 10 to 1,000 nm have been investigated intensively to improve the treatment efficacy of severe diseases (Bobo et al., 2016; Ho et al., 2019). DDS protect drugs from biodegradation, improve drug solubility, enhance the delivery of drugs specifically to their target sites and reduce adverse effects (Danhier et al., 2012; Sanna et al., 2012; Kalepu and Nekkanti, 2015; Kim et al., 2017). The major challenge in DDS formulation is to improve the drug loading capacity (LC), which have been mostly

reported as lower than 5% w/w while using pharmaceutically accepted excipients (Couvreur, 2013; Ho et al., 2019). With the aim to formulate nanomedicines having a maximized LC, Couvreur et al. (2006) invented the squalenoylation approach. This unique technique creates a prodrug by bioconjugation of a drug molecule and a hydrophobic squalenyl moiety. The squalenoylated prodrug could self-assemble into uniform and stable nanoparticles (NPs) in aqueous solution without using additional surfactants (Desmaële et al., 2012), which cannot be achieved by other lipid prodrugs, e.g., employing stearyl moiety (Couvreur et al., 2006). Importantly, the squalenyl drug bioconjugates, e.g., squalenyl gemcitabine, squalenyl penicillin G, as well as squalenyl dideoxycytidine or didanosine, have not only shown a high LC (>30% w/w) but also improved pharmacological profile and efficacy compared to the parent drugs (Couvreur et al., 2006; Desmaële et al., 2012; Sémiramoth et al., 2012; Hillaireau et al., 2013; Maksimenko et al., 2013; Buchy et al., 2015). Moreover, squalene is a natural lipid, which is also found in humans as a precursor of the cholesterol biosynthesis (Schroepfer, 1981). Hence, using squalenyl derivatives in developing DDS is favorable (Reddy and Couvreur, 2009).

However, it is challenging to bio-conjugate squalene and drug molecules with multiple functional groups or without functional groups (Ralay-Ranaivo et al., 2014). Furthermore, if possible, the chemical synthesis would not be facile and easily scaled-up, and poor solubility of the resulting prodrugs in common solvents could be an additional issue. Taking advantage of squalenoylation approach and extending its use in versatile DDS preparation, Lepeltier et al. (2015) proposed the core-shell structured squalenoylated chitosan NPs allowing the loading of both hydrophilic and hydrophobic compounds. However, the LC in such a system was not as high as expected, and the particles size could not be tuned easily due to the poor solubility of squalenoylated chitosan in common solvents (Lepeltier et al., 2015). Taking a different approach, without employing bioconjugation Ho et al. (2020) reported self-assembled NPs based on an anionic squalenyl derivative (aSq)—squalenyl hydrogen sulfate—which showed excellent simultaneous LC of both hydrophobic alkyl quinolone (~10% w/w) and hydrophilic tobramycin (~30% w/w). Importantly, this DDS also demonstrated an improved penetration through biological barriers, such as biofilms, and enhanced synergistic therapeutic effects of both actives (Ho et al., 2020). Hence, we aimed to expand such a promising DDS platform to further applications, like drug loading of anionic hydrophilic drugs and the minimization of interactions between the NPs and proteins. For these purposes, we here propose, in addition to the synthesis of aSq, the preparation of other squalenyl derivatives (SqDs), namely, (i) cationic squalenyl diethanolamine (cSq), (ii) PEGylated squalenyl derivative (PEG 750 Da, PEG750Sq),

and (iii) PEGylated squalenyl derivative (PEG 3,000 Da, PEG3000Sq). Especially, the low molecular weight of SqDs in comparison to excipients used in conventional carrier systems [e.g., from biodegradable polymers like poly (lactic-co-glycolic acid)] promises to lead to a higher LC in these DDS. We studied their ability to self-assemble into NPs in aqueous solution, their morphology, as well as their colloidal stability in biophysically relevant pH milieus and cytotoxicity as surrogate for their biocompatibility. At their first contact with the human body, NPs are mostly confronted with proteins. By adsorption on the NP surface (formation of a “protein-corona”), the proteins can change the characteristics of NPs dramatically (Raesch et al., 2015; Kokkinopoulou et al., 2017). These protein–NP interactions not only play a role for systemic applications but also for non-invasive drug delivery, where the first main challenge is to overcome a protective mucus barrier (e.g., vaginal, pulmonary, gastrointestinal delivery) (Ruge et al., 2013; Murgia et al., 2018). Mucus is a hydrogel consisting mainly of water and mucins, which are high molecular weight glycoproteins with a negative net charge at physiological pH (Bansil and Turner, 2006; Lock et al., 2018; Murgia et al., 2018). One of the main defense mechanisms of mucus against xenobiotics is the physicochemical interaction with mucin glycoproteins (Lai et al., 2007; Lieleg and Ribbeck, 2011; Murgia et al., 2016). In this study, these possible interactions were investigated using nanoparticle tracking analysis (NTA), to evaluate the mucoadhesive and mucoinert characteristics of the charged and PEGylated SqDs, respectively. To assess the LC of SqDs for a broad range of molecules, a representative set of compounds, varying in physicochemical properties and molecular weight (Mw), was chosen. Depending on the drug properties, the loading procedure has been optimized using different methods, namely, (i) coprecipitation, (ii) solvent evaporation, or (iii) dropping. Subsequently, the tuning possibility of drug release by different preparation methods was studied by *in vitro* release profiles of the drug from SqD–NPs, at pH 7.4 (PBS), and 37°C.

MATERIALS AND METHODS

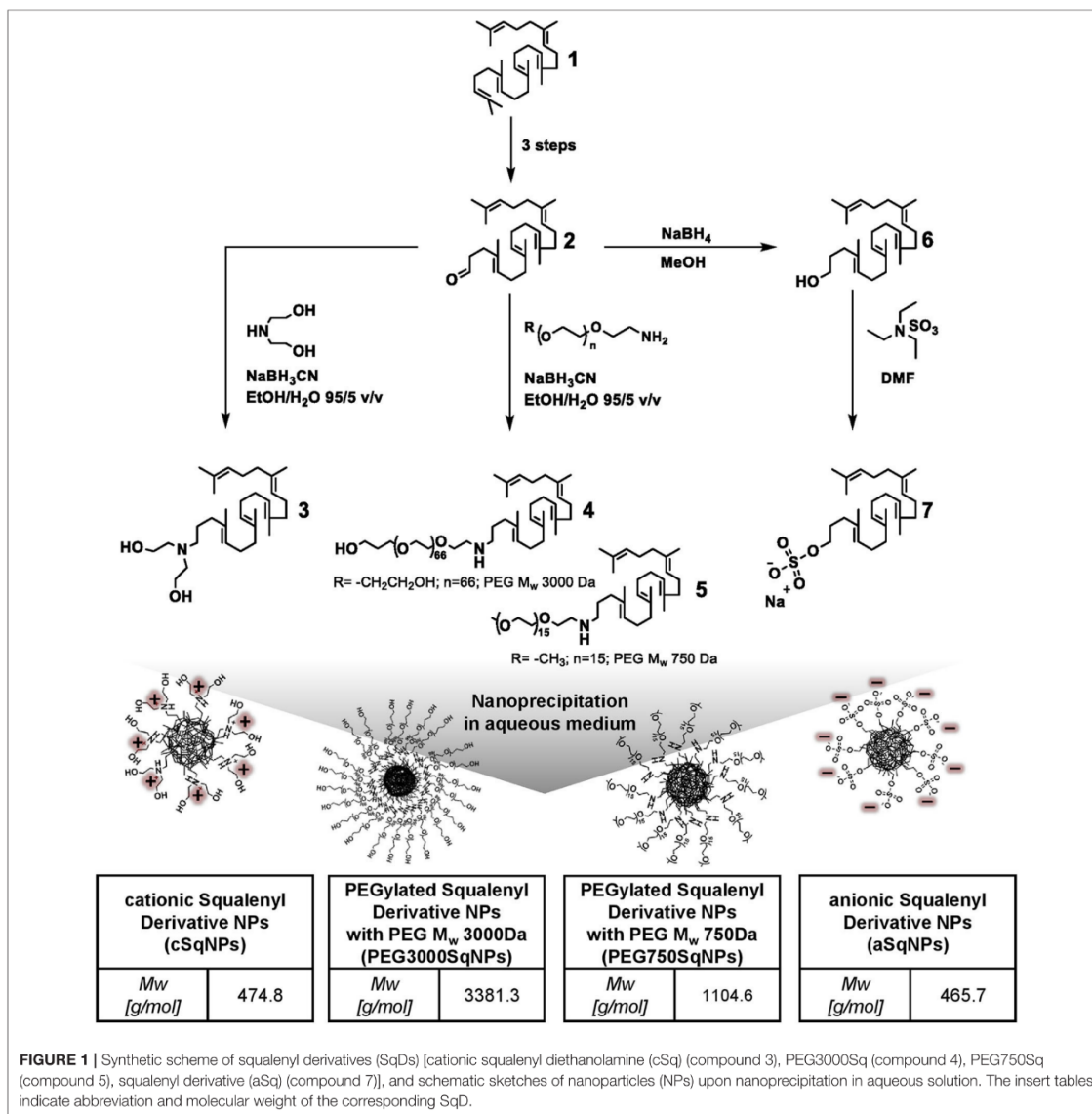
Materials

All chemicals were purchased from Sigma-Aldrich unless otherwise specified. Tetrahydrofuran (HPLC grade) (THF), ethanol, absolute (HPLC grade) (EtOH), ethyl acetate (analytical grade reagent), and Formic Acid Optima LCMS were purchased from Fisher Scientific. Acetonitrile and methanol (MeOH) were obtained from VWR Chemicals. Yeast extract was obtained from Fluka. Bacto™ Tryptone was obtained from BD Biosciences. Luria Bertani (LB) agar was obtained from Carl Roth. Gibco® HBSS (1x) Hanks' Balanced Salt Solution and Gibco® PBS was obtained from Life Technologies. Purified water was prepared by a Milli-Q water purification system (Merck Millipore, Billerica, MA, USA) (called water in the manuscript).

Synthesis and Characterization of SqDs

The preparation of 1,1',2-trisnorsqualenic aldehyde (compound 2) and 1,1',2-trisnorsqualenol (compound 6) (Figure 1) from squalene (compound 1) was performed as reported in previous

Abbreviations: LC, drug loading capacity; SqD, squalenyl derivative; aSq, anionic squalenyl derivative; cSq, cationic squalenyl derivative; PEG750Sq, PEG750 squalenyl derivative; PEG3000Sq, PEG3000 squalenyl derivative; NP, nanoparticle; NTA, nanoparticle tracking analysis; DLS, dynamic light scattering; ELS, electrophoretic light scattering; cryo-TEM, cryogenic transmission electron microscopy; MS, mass spectrometry; PDI, polydispersity index; HPLC, high performance liquid chromatography; SD, standard deviation; SE, standard error.



studies (van Tamelen and Curphey, 1962; Ceruti et al., 1987; Skarbek et al., 2015).

Synthesis and Characterization of PEGylated SqDs and cSq

cSq (compound 3), PEG3000Sq (compound 4), and PEG750Sq (compound 5) were synthesized using the same procedure from 1,1',2-trisnorsqualenic aldehyde (compound 2) (Figure 1). The conjugation was achieved *via* reductive amination reaction between amine and aldehyde groups, using sodium

cyanoborohydride (NaBH_3CN) as reducing agent. Briefly, 1 molar equivalent of 1,1',2-trisnorsqualenic aldehyde (compound 2) was solubilized in a mixed solvent of EtOH:water (95:5 v/v) at a concentration of 10% w/w. Following the addition of 1.2 molar equivalent of amine—methoxyl-PEG750- NH_2 (methoxypolyethylene glycol amine, M_w 750 Da), PEG3000- NH_2 [O-(2-aminoethyl) polyethylene glycol, M_w 3,000 Da], or diethanolamine—the reaction was carried out at room temperature for 3 h. NaBH_3CN , 1.2 molar equivalent, was subsequently added, and the reaction was kept for an additional

20 h allowing imine reduction. EtOH was then removed under reduced pressure, and water was added, allowing precipitation of the resulted SqD. The product was then collected by centrifugation and washed three times with water. The isolated yield was >90% in all reactions. The cSq product (compound 3) was characterized by $^1\text{H-NMR}$ (Supplementary Figure 3), $^{13}\text{C-NMR}$ (Supplementary Figure 4), and MS (mass spectroscopy), while the PEG750Sq product (compound 5) and PEG3000Sq product (compound 4) were characterized by $^1\text{H-NMR}$ (Supplementary Figures 5, 7, respectively) and $^{13}\text{C-NMR}$ (Supplementary Figures 6, 8, respectively) before further use.

Synthesis and Characterization of aSq (Compound 7)

aSq was synthesized from 1,1',2-trisnorsqualenol as described by Ho et al. (2020) (Figure 1). Briefly, 1 molar equivalent of 1,1',2-trisnorsqualenol (compound 6) was prepared in DMF (dimethylformamide) at a concentration of 10% w/w. The solution was degassed using N_2 , and 1.1 molar equivalent of TEA. SO_3 (sulfur trioxide triethylamine complex) was slowly dropped into the solution at room temperature. The temperature was then increased to 60°C . Following 16 h of reaction, the resulting system was quenched with an appropriate amount of water. The solvent mixture, DMF and water, was partly removed under reduced pressure. After being diluted in an excess amount of MeOH, NaOH 1 N was added under stirring. MeOH was subsequently removed under reduced pressure, and water was added allowing precipitation of aSq. The aSq product was extracted using ethyl acetate and dried over MgSO_4 . The solvents were completely removed under reduced pressure at 40°C . The isolated yield was 95%. The aSq product was characterized by $^1\text{H-NMR}$ (Supplementary Figure 1), $^{13}\text{C-NMR}$ (Supplementary Figure 2), and MS (mass spectroscopy) before further use.

Preparation of Drug-Free SqD-NPs

All drug-free self-assembled SqD-NPs in this study were prepared by nanoprecipitation in aqueous solution as described previously (Fessi et al., 1989; Ho et al., 2020). In brief, a SqD was solubilized in THF and dropped into the water at a speed of 12 drops/min under constant stirring (1,000 rpm). Afterward, THF was evaporated at 40°C , 40 mbar, and 280 rpm using a rotary evaporator (Rotavapor, Büchi, Essen, Germany) resulting in a drug-free SqD-NPs suspension in water, which was further stored at 4°C .

Figure 1 presents the schemes of the optimal representatives of SqD-NPs, including:

- (i) cSq-NPs, which was prepared as follows: 0.15 ml of cSq solution in THF at a concentration of ~ 7 mg/ml was dropped into 1 ml of water under stirring. THF was then removed under reduced pressure resulting in a cSq-NPs suspension in water at a concentration of 1 mg/ml.
- (ii) PEG750Sq-NPs and PEG3000Sq-NPs, which were prepared using the same protocol as follows: 0.5 ml PEGylated SqD in THF:water (1:1 v/v) mixture at a concentration of 1 mg/ml was dropped into 0.75 ml of water. THF was then removed under reduced pressure

resulting in the PEGylated SqD-NPs in water at a concentration of 0.5 mg/ml.

- (iii) aSq-NPs, which were prepared as follows: 0.1 ml of aSq solution in THF at a concentration of 10 mg/ml was dropped into 1 ml of water under stirring. THF was then removed under reduced pressure resulting in an aSq-NPs suspension in water at a concentration of 1 mg/ml.

The NP characteristics, especially size and polydispersity index (PDI), of the drug-free cSq-NPs and aSq-NPs were studied by varying the initial SqD concentration in THF and the final NP concentration in water. The detailed information is reported in the supplementary information (Supplementary Table 1).

Physicochemical Characterization of Drug-Free SqD-NPs Size, PDI, Zeta-Potential

The intensity-based hydrodynamic size (reported as z-average), PDI, and zeta-potential of the SqD-NPs were determined at 25°C by dynamic and electrophoretic light scattering (DLS, ELS) using a Zetasizer (Zetasizer Nano ZSP, ZEN5600, Malvern, Software 7.02) equipped with a He-Ne Laser at a 633 nm wavelength, backscattering angle of 173° for DLS. For the measurements, 20 μl of SqD-NPs suspension was diluted into 800 μl of water.

Morphology

The morphology of each drug-free SqD-NPs was investigated by cryogenic transmission electron microscopy (cryo-TEM). In brief, after plotting 3 μl of SqD-NPs suspension on a holey carbon grid (S147-4, Plano Wetzlar, Germany) for 2 s, the sample was frozen by plunging into -165°C liquid ethane, then transferred to the sample holder under liquid nitrogen conditions. All samples were examined using a JEOL (Akishima, Tokio, Japan) JEM-2100 LaB6 TEM equipped with a Gatan model 914 cryo-TEM sample holder (Pleasanton, CA, USA) and a Gatan Orius SC1000 CCD camera to gain bright-field images. Sample analysis was done at -170°C , under low-dose conditions, meaning conservative settings of $\sim 10 \mu\text{a}/\text{cm}^2$ radiation level to avoid sample destruction.

Colloidal Stability

The colloidal stability of the drug-free SqD-NPs was studied in physiological relevant pH milieus, including pH 2, pH 5 (acetate buffer solution), and pH 7.4 (HBSS buffer solution). The tested samples were prepared by adding 25 μl of SqD-NPs suspension into 975 μl of buffer solution. NP characteristics, including size, PDI, and zeta-potential, were determined by DLS and ELS using a Zetasizer after 1, 3, and 24 h at 25°C .

Interaction of SqD-NPs With Biological Systems

Biocompatibility

As surrogate for biocompatibility, the determination of cytotoxicity by MTT assay on A549 cells was chosen. Briefly, prior to the assays, 10^4 cells were seeded in each well of the 96-well plates and grown until reaching 80% cell confluence. The SqD-NPs were suspended in HBSS at concentrations ranging

from 0.0652 to 1 mg/ml and incubated with cells for 4 h at 37°C and 5% CO₂. After the incubation time, cells were washed twice with PBS, and MTT reagent (0.5 mg/ml in HBSS) was added. The cells were then incubated for an additional 4 h, at 37°C, and 5% CO₂ allowing the formation of formazan crystals intracellularly (Mosmann, 1983). Following the removal of the supernatant, cells and formed formazan crystals were dissolved in DMSO for 30 min, and the absorbance was measured at 550 nm using a Tecan microplate reader Infinite M200Pro (Tecan, Crailsheim, Germany). Cells incubated with 1% Triton TM X-100 in HBSS served as positive controls (0% cell viability), while cells incubated with plain HBSS served as negative controls (100% cell viability), respectively. The percentage of cell viability was calculated relating to the negative controls (Ho et al., 2020).

Protein–SqD–NPs Interactions

The interaction between fluorescent SqD–NPs and mucin glycoproteins was studied *via* NTA by NanoSight (LM-10, Laser 532 nm) (Malvern, UK). NTA is able to determine the hydrodynamic diameter of NPs. Under random Brownian motions, NPs scatter light from a laser beam. The scattered light can be visualized by the NTA and captured by a video camera, to enable the software to track the movement of the NPs individually. Using the Stoke–Einstein equation, the hydrodynamic diameter of the particles can be determined.

To study the protein–SqD–NP interaction, the Brownian motion of fluorescent NPs in water was compared to their movement in water containing non-fluorescent 0.1% mucin solution (mucin from porcine stomach, type II, Sigma). For the measurements, used dilutions of the NPs, either in 0.1% mucin solution or water, were 1:100 (aS–NPs), 1:200 (cS–NPs), and 1:50 (PEG750S–NPs). To detect only the movement of the SqD–NPs, the particles were fluorescently labeled, and the fluorescence mode of the NTA was used. Therefore, SqD–NPs were loaded with 0.5% Nile red by coprecipitation; a detailed description of the method is in the Preparation of Drug-Loaded SqD–NPs section. As a vehicle control sample, the 0.1% aqueous mucin solution was studied with and without the fluorescence filter, to show the ability of the filter to exclude optical interferences of the proteins (**Supplementary Figure 9**, green line: with filter, gray line: without filter). Videos with a duration of 20–30 s were taken and analyzed by NanoSight Software NTA 3.3. The results of the particle concentration as a function of particle size are reported as mean ± standard error (SE).

Carrier Properties of SqD–NPs

Preparation of Drug-Loaded SqD–NPs

The LC of the synthesized SqDs was investigated using compounds representing different physicochemical properties, namely:

- (i) hydrophobic compounds: cholesteryl BODIPY, Nile red, and dexamethasone,
- (ii) hydrophilic and charged compounds: isoniazid, colistin, tigecycline, and FITC-albumin.

With the aim to maximize the LC while maintaining the NP stability, appropriate preparation methods for generating drug-loaded NPs were chosen depending on the drug properties. In brief, we explored three NP preparation methods as follows:

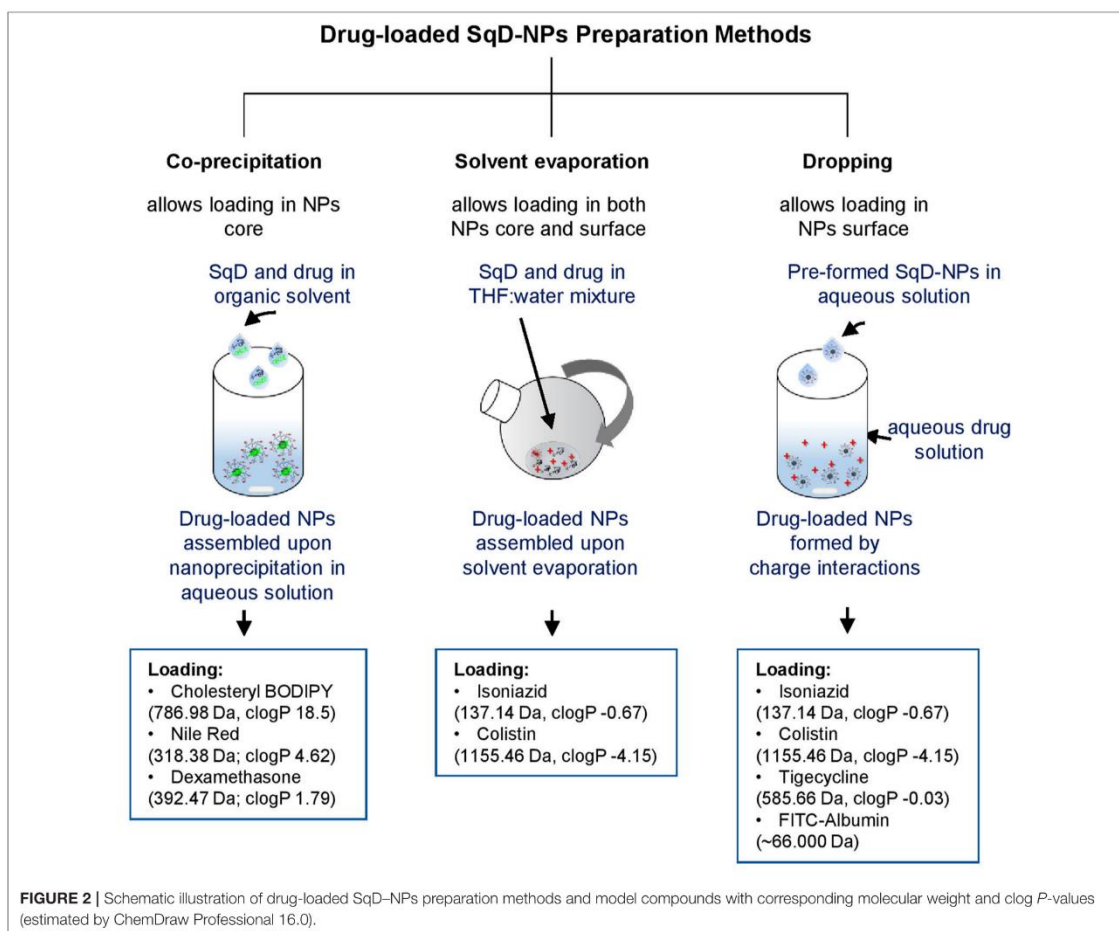
- (i) *Co-precipitation method*: In this study, we found that this method worked best for loading hydrophobic compounds (cholesteryl BODIPY, Nile red, and dexamethasone). Briefly, hydrophobic compound and SqD were dissolved in THF. Upon NP self-assembling in water by nanoprecipitation, the hydrophobic compound localized in the core of the SqD–NPs by hydrophobic interaction.
- (ii) *Solvent evaporation method*: In this study, we found that this method worked best for loading hydrophilic compounds having multiple functional groups, especially for small Mw hydrophilic compounds (e.g., isoniazid) and amphiphilic compounds (e.g., colistin). Briefly, the SqD and drug were dissolved completely in the mixture of THF:water (1:1 v/v) at desired concentrations (0.25–0.125 mg NPs/ml of NP suspension). The solution was then stirred for 24 h at room temperature allowing charge interaction of SqD and drug molecules, while the hydrophobic interaction between SqD and drug could be induced upon removal of THF using a rotary evaporator (Rotavapor, Büchi, Essen, Germany) at 40 mbar, 40°C and 65 rpm.
- (iii) *Dropping method*: In this study, we found that this method worked best for loading both small (e.g., tigecycline) and high Mw hydrophilic compounds (FITC-albumin) having multiple functional groups. Briefly, the charged drug-free SqD–NPs were prepared in water as described in the Preparation of Drug-Free SqD–NPs section and diluted to a concentration of 0.25 mg/ml. SqD–NPs suspension (1 ml) was then dropped into 1 ml of the prepared drug solution in water under stirring at 200 rpm. The resulting drug-loaded SqD–NPs were further stirred for 1 day at room temperature.

The “solvent evaporation method” and “dropping method,” which allowed the loading of drugs in both compartments, core and shell, of the NPs could be used in multiple drug-loading purposes. As an example, Nile red and FITC-albumin co-loaded cS–NPs are presented in **Supplementary Material Part 4**. Briefly, the Nile red-loaded cS–NPs were prepared by “coprecipitation method” and then dropped into an aqueous solution of FITC-albumin (“dropping method”) allowing the dual-loading of both compounds.

Figure 2 summarizes an overview of the preparation methods for drug-loaded SqD–NPs, listing all the model cargos with corresponding Mw and clog *P*-values (estimated by ChemDraw Professional 16.0).

Quantification of loading capacity and encapsulation efficiency

The loading capacity (LC) and encapsulation efficiency (EE) of the drugs loaded to SqD–NPs were determined indirectly using the amount of non-loaded drug in the supernatant of the SqD–NPs suspension. The hydrophobic compound (dexamethasone, cholesteryl BODIPY, or Nile red) was extracted



from the supernatant using ethyl acetate (Ho et al., 2018). The hydrophilic compound was analyzed in the supernatant after centrifugation of the SqD-NPs suspension. Isoniazid was collected by loading the NPs in a Centriscart filter (MWCO 10,000 Da) (Sartorius, Göttingen, Germany) and centrifuging at 2,000 *g* for 30 min. Colistin, tigecycline, or FITC-albumin was collected by centrifuging the drug-loaded NPs at 24,400 *g* for 30 min. The amount of cholesteryl BODIPY, Nile red, tigecycline, or FITC-albumin in the supernatant, respectively, was analyzed by a plate reader (details described in **Supplementary Material Part 6**), while dexamethasone, isoniazid, or colistin were quantified by high-performance liquid chromatography (HPLC) (details described in **Supplementary Material Part 6**).

$$EE [\%] = \frac{\text{drug amount loaded in NPs [mg]}}{\text{initial drug amount [mg]}} * 100 \quad (1)$$

$$LC [\%] = \frac{\text{drug amount loaded in NPs [mg]}}{\text{total amount of NPs [mg]}} * 100 \quad (2)$$

The drug amount loaded in NPs is calculated by subtraction of the non-loaded drug amount from the initial one. The total amount of NPs equals the sum of the amount of SqD and the amount of drug, which is loaded to the NPs.

Release Studies

The release studies of selected drug-loaded SqD-NPs were performed using the same procedure in PBS (pH 7.4) at 37°C and constant shaking at 250 rpm. Briefly, the optimal LC sample of the drug-loaded SqD-NPs was concentrated and then diluted in PBS to have a final concentration of the corresponding drug at 10% w/w. The cumulative drug release in percent was evaluated over a 24 h period. Samples were collected after 1, 2, 4, 6, 8, 16, and 24 h, while the release acceptor volume was always kept constant. The drug amount in the acceptor fluid was analyzed. The hydrophobic drugs were extracted using ethyl acetate before further analysis. The drug quantification was done by plate reader or HPLC (**Supplementary Material Part 6**).

Statistics

If not stated otherwise, all procedures were conducted at least in three independent experiments and measured in technical triplicate. Results are presented as mean \pm standard deviation (SD). Calculations were done using either Excel, Microsoft 2016 and 2019, or GraphPad Prism 8.0. Physicochemical information of molecules was predicted by ChemDraw Professional 16.0.

RESULTS AND DISCUSSION

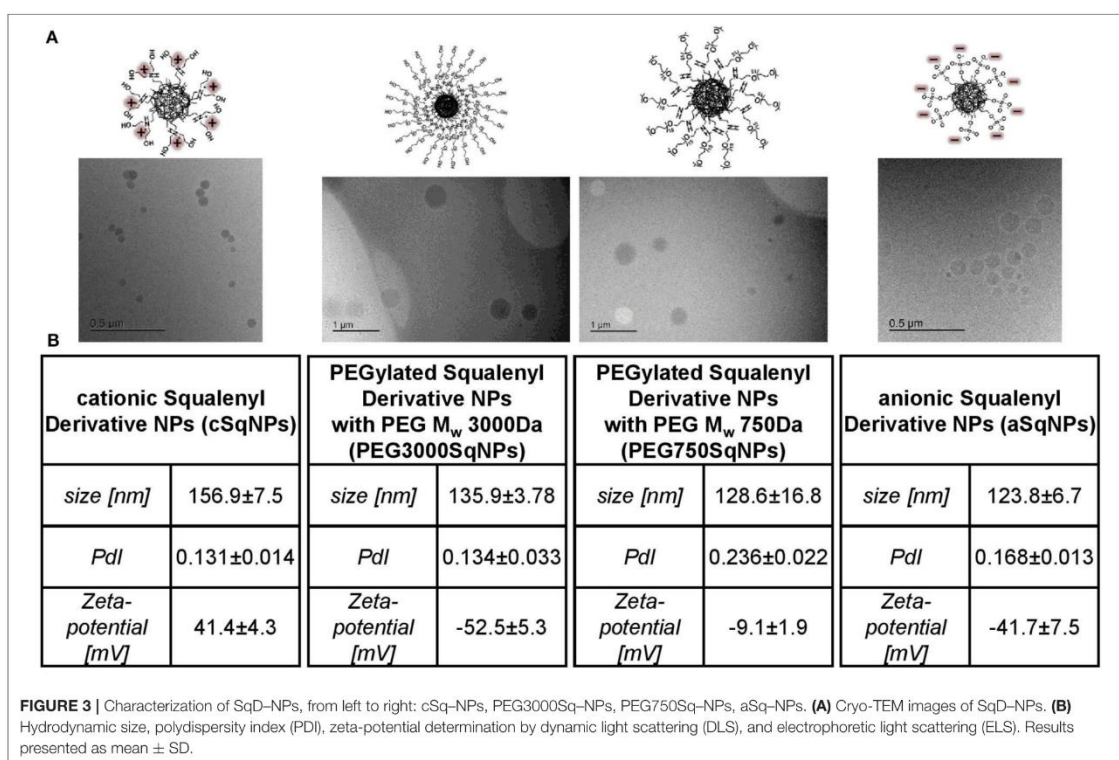
Synthesis and Characterization of SqDs

The cSq and PEGylated SqDs were straightforwardly obtained by simple reductive amination reaction from 1,1',2-trisnorsqualenic aldehyde. The successful synthesis and purification of all SqDs were confirmed by $^1\text{H-NMR}$ and $^{13}\text{C-NMR}$ (Supplementary Figures 1–8). These results were confirmed by MS for aSq [(ESI-) $m/z(\%)$ 465.3 (100) (M-H) $^-$] and cSq [(ESI-) $m/z(\%)$ 474.4 (100) (M-H) $^+$], respectively. The synthetic schemes are facile and allowed isolating the final products in high yields (>90%), which, moreover, could be scaled-up easily. Notably, the synthesis of cSq with a diethanolamino polar head was further optimized with one step less compared to that of the previously reported squalene-amine derivative (van Tamelen and Curphey, 1962; Ralay-Ranaivo et al., 2014).

Preparation and Physicochemical Characterization of Drug-Free SqD-NPs Size, PDI, Zeta-Potential, and Morphology

Overall, the introduction of anionic, cationic, or PEG moiety into squalene enhanced the amphiphilic properties of the synthesized SqDs and enabled the facile self-assembly into uniform and stable NPs in aqueous solution. Regardless of the SqD, the drug-free NPs had mean sizes ranging from 100 to 200 nm and a narrow size distribution (PDI < 0.25) (Figure 3B, Supplementary Table 1). The zeta-potential of aSq-NPs and cSq-NPs were around -40 and $+40$ mV, respectively, indicating the presence of their corresponding charged groups on the NP surface (Figure 3B, Supplementary Table 1). Such strong charges facilitate the further drug loading on the surface *via* electrostatic interaction and enable NP stability (Bhattacharjee, 2016).

We prepared two PEGylated SqDs having PEG with different chain length and terminal groups. The PEG750Sq terminates with a methyl group, while the PEG3000Sq terminates with a hydroxyl group. The self-assembling of these PEGylated SqDs allowed the formation of NPs with a dense surface layer of PEG. Regardless of the recorded zeta-potential, this PEG layer is expected to stabilize the NPs and minimize surface interactions between NPs and other molecules (Suk et al., 2016).



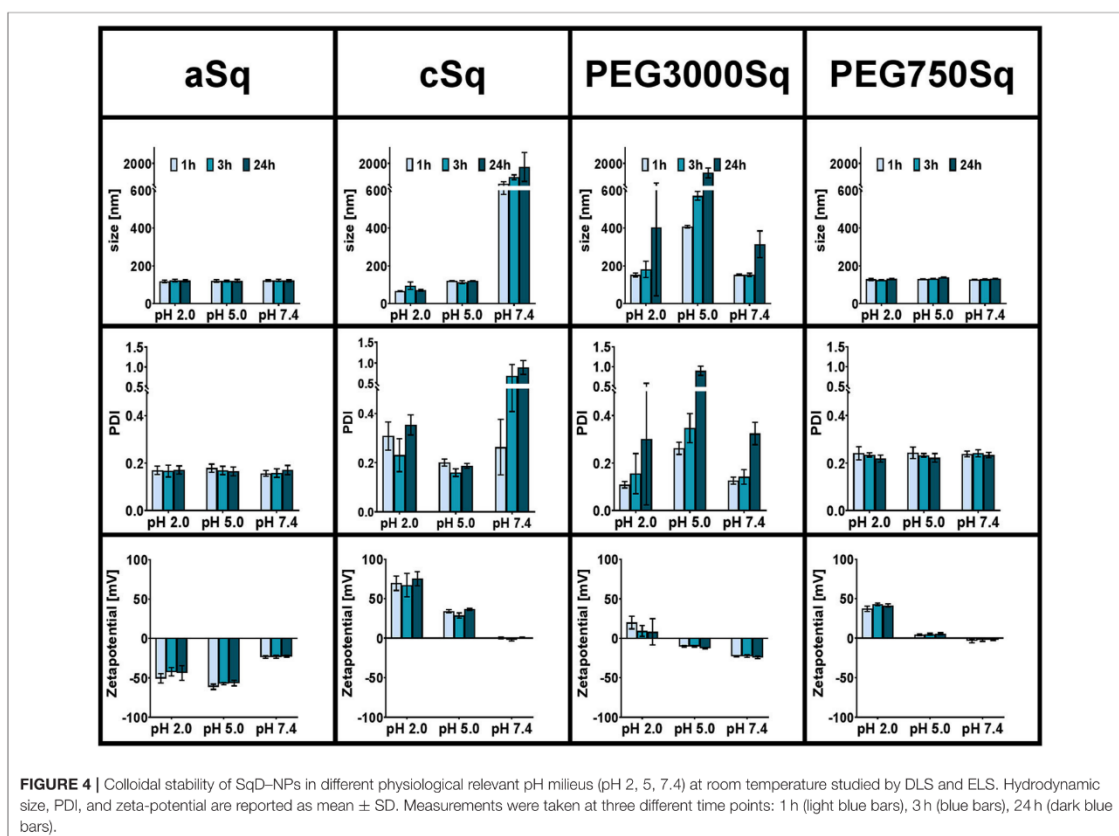
Different initial concentrations of aSq in THF could slightly tune the size of aSq-NPs that were prepared by nanoprecipitation in water at a final concentration of 1 mg/ml (Supplementary Table 1). By increasing the aSq concentration in THF from 2.5 to 25 mg/ml, the aSq-NPs had the size raised from 90 to 160 nm. This phenomenon could be explained by the assembly of more squalenyl moieties in the core compartment at higher concentrations (Ho et al., 2018). In contrast, varying the final aSq-NPs concentration in water and using the same initial aSq concentration in THF did not influence the NP size (Supplementary Table 1). A similar observation was reported previously for squalenoylated chitosan NPs, which showed an increase rather in NP count than in NP size (Lepeltier et al., 2015). The drug-free cSq-NPs, in turn, could be only formed in the size range of 200 nm regardless of the variation of either initial cSq concentration in organic solvent or final NP concentration in water. The cryo-TEM images of the drug-free SqD-NPs are presented in Figure 3A illustrating the amorphous and spherical-shaped NPs. No differences in morphology between the SqD-NPs were observed.

Colloidal Stability

The colloidal stability of drug-free SqD-NPs was investigated in different pH values representing gastric acid (pH 1–3), skin (pH ~5), and common physiological pH environments at 7.4 (Schmid-Wendtner and Korting, 2006; Koziolok et al., 2015). The colloidal stability in the corresponding pH was evaluated based on the changes of NP size, PDI, and zeta-potential at 1, 3, and 24 h post-incubation. Overall, the aSq-NPs and PEG750Sq-NPs were stable after 24 h of incubation in all studied pH milieus, while the stability of cSq-NPs could only be maintained at pH 5 or lower. In contrast, the incubation of PEG3000Sq-NPs in all tested buffers resulted in colloidal aggregation over time (Figure 4).

The hydrogen sulfate groups on aSq-NPs surface were strongly acidic and deprotonated at all tested pH values resulting in a low zeta-potential (around -50 and -25 mV in pH 2/5 and 7.4, respectively), which helped stabilizing the NP suspension (Bhattacharjee, 2016). At 24 h post-incubation in all conditions, the aSq-NPs hydrodynamic diameter was always around 120 nm, while the PDI was lower than 0.2.

The cSq-NPs, in turn, exposing the diethanolamine moiety on its surface, in which pK_a -value is estimated at 8.44 (ChemDraw



Professional 16.0), showed positive zeta-potential of 71 ± 11 and 33 ± 4 mV at pH 2 and 5, respectively, reflecting the protonation of the amine groups. The size and PDI of stable cSq-NPs after 24 h of incubation at pH 5 were 120.5 ± 1.5 nm and 0.19 ± 0.01 nm, respectively. Interestingly, a slightly smaller particle size (76.9 ± 17.1 nm) and a larger PDI (0.30 ± 0.07) were recorded when dispersing cSq-NPs at pH 2. The cSq-NPs could be fully charged at pH 2, which enhanced the amphiphilicity of cSq molecules. Consequently, this induced intermolecular forces and hydrophobic interactions between the squalenyl moieties leading to a denser particle packing (Ho et al., 2018). The same phenomenon was also observed before in farnesylated glycol chitosan NPs (Ho et al., 2018). At neutral pH 7.4, amine functional groups might become partly uncharged causing a decrease in zeta-potential from ~ 70 mV at pH 2 to around zero, and the aggregation of cSq-NPs was observed. The colloidal instability of cSq-NPs at pH 7.4 makes these DDS rather unfavorable for systemic drug delivery. However, cSq-NPs demonstrate a good colloidal stability at pH 5, which represents the pH milieu of the skin barrier (Schmid-Wendtner and Korting, 2006). Topical application of NPs to the skin surface are known to enhance the follicular drug delivery. cSq-NPs could be especially further explored to be used for follicular vaccination (Mittal et al., 2015). In addition to the possible complexation of DNA, squalene was already used in adjuvants, boosting an immune response against vaccine antigens. Even the *in vitro* and *in vivo* transfection efficiency of a DNA complex emulsion was improved in the presence of squalene compared to the control complexes (Kwon et al., 2008; Reddy and Couvreur, 2009).

PEGylation offers plenty of advantages to nano-sized drug carriers especially to improve the *in vivo* stability and therapeutic efficacy (Suk et al., 2016; Thomas and Weber, 2019). Previously, PEGylated SqD with a Mw of 1,955 Da was incorporated into squalenoylated gemcitabine prodrug NPs in order to enhance their stability at pH 7.4 and gemcitabine performance (Bekkara-Aounallah et al., 2008). In this study, we aim to investigate the potential of PEGylated SqDs as a platform for drug delivery. Hence, the stability of NPs assembled from PEG3000Sq or PEG750Sq was studied individually. As shown in Figure 4, PEG3000Sq-NPs were unstable in all tested buffer media making it unfavorable for use as DDS. Although the small molecule squalene ($Mw = 410$ Da) holds excellent assembling properties, the monoconjugation with PEG having a Mw of 3,000 Da might result in a better water solubility. Thus, the hydrophobic interaction of squalenyl moieties would not be strong enough to stabilize the PEG3000Sq-NPs. On the complete opposite, SqPEG750-NPs demonstrated excellent colloidal stability in all pH milieus at all time points. The hydrodynamic diameter and PDI were always around 129.7 ± 4.5 nm and lower than 0.23 ± 0.02 , respectively. The zeta-potential of SqPEG750-NPs was nearly neutral at pH 5 and 7.4; however, it increased to 40 ± 3 mV at pH 2 due to the protonation of the amino conjugation.

The particles holding appropriate colloidal stability in physiological relevant pH milieus were used in further investigations, including aSq-NPs, cSq-NPs, and PEG750Sq-NPs.

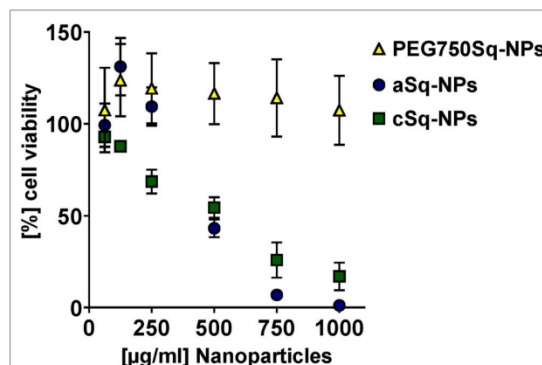


FIGURE 5 | Biocompatibility study via MTT assay at different concentrations of PEG750Sq-NPs (yellow triangle), aSq-NPs (dark blue circles), and cSq-NPs (green squares) diluted in HBSS on A549 cells over 4 h at 37°C and 5% CO₂. Results are presented as (% cell viability relating to negative control in plain HBSS at different NP concentrations and reported as mean \pm SD.

Interaction of SqD-NPs With Biological Systems

Biocompatibility

The biocompatibility of the SqD-NPs was tested on A549 cells via MTT assay (Figure 5). In good agreement with Ho et al. (2020) aSq-NPs demonstrated 100% viability for up to 250 μ g/ml (blue circles in Figure 5). The cSq-NPs (green squares in Figure 5) showed slightly lower tolerability than aSq-NPs, which might have an explanation in the instability of cSq-NPs in HBSS buffer causing large aggregates on cells. Moreover, the nature of a cationic lipid can enhance the toxicity due to its potential interaction with anionic biological molecules like proteins and nucleic acids (Knudsen et al., 2015). Thus, only 70% cell viability was found when incubating cSq-NPs at a concentration of 250 μ g/ml. Similar findings were previously described: the incubation of 250 μ g/ml of positively charged squalenoylated chitosan NPs and farnesylated glycol chitosan NPs resulting in ~ 80 and $>70\%$ A549 cell viability, respectively (Lepeltier et al., 2015; Ho et al., 2018). The PEG750Sq-NPs (yellow squares in Figure 5) were highly biocompatible demonstrating 100% cell viability at the highest tested concentration of 1 mg/ml.

Protein-SqD-NPs Interactions

Exemplary for a protein interaction study, the physicochemical interactions between fluorescent SqD-NPs and mucin glycoproteins were studied using NTA. The hydrodynamic size of the SqD-NP suspension was compared either in (i) water (blue line in Figure 6) or in (ii) 0.1% mucin glycoprotein aqueous solution (green line in Figure 6). It was hypothesized that non-interacting, fluorescent SqD-NPs would display the same particle size distribution irrespective of dispersion in water or in the low-viscosity mucin glycoprotein-containing solution. Conversely, the fluorescence signal of SqD-NPs interacting

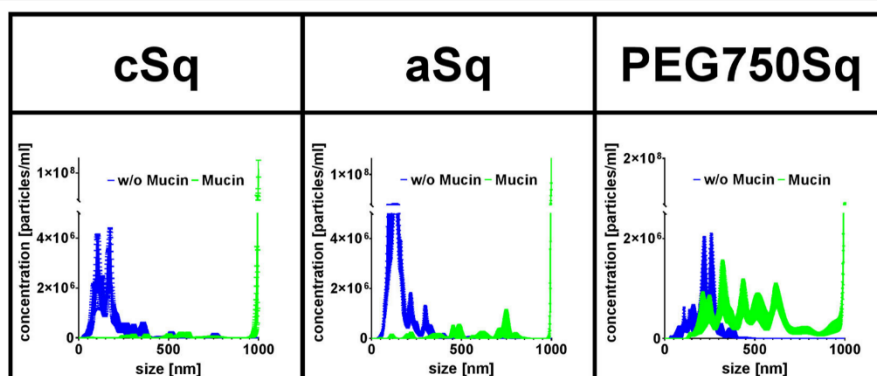


FIGURE 6 | Fluorescent SqD-NPs interaction study with mucin glycoproteins. Interactions detected by size shift determined by nanoparticle tracking analysis (NTA) measurements. Blue lines: measurement of fluorescent SqD-NPs in water. Green lines: measurement of fluorescent SqD-NPs in non-fluorescent 0.1% mucin glycoprotein aqueous solution. Results are presented as mean \pm SE.

with non-fluorescent mucin glycoproteins would display a different Brownian motion, indicative of a movement hindrance, and resulting in a particle size distribution shifted toward larger particle diameters. By comparing the results of the measurements of SqD-NPs in both aqueous solution (**Figure 6**) on this basis, the interaction between the mucin glycoproteins and NPs can be ranked from high to low as follows: cSq-NPs > aSq-NPs >> PEG750Sq-NPs.

In detail, cSq-NPs were found to present a highly positive surface net charge enabling interaction with the negatively charged mucin glycoproteins. These strong interactions are demonstrated by a size shift to a larger size from ~ 180 to ~ 960 nm (mean of number-weighted distribution) (blue and green lines in **Figure 6**, respectively). Further, the negatively charged aSq-NPs showed interactions with the mucin glycoproteins, shifting the mean particle size from ~ 160 to ~ 930 nm (blue and green lines in **Figure 6**, respectively), which is less pronounced than for cSq-NPs. We assumed that those interactions are mainly caused by the hydrophobic squalenyl moiety (Murgia et al., 2018). As expected, PEG750Sq-NPs demonstrated only minor interactions with mucin glycoproteins (mean size shift from ~ 230 to ~ 575 nm, blue and green lines in **Figure 6**, respectively). Still PEG750Sq-NPs resulted in partial mucin adsorption, which can be explained by hydrophobic interactions between mucin glycoproteins and the NP core.

Our results, showing that interactions between mucin glycoproteins and charged NPs, cSq-NPs, and aSq-NPs are more pronounced than interactions with neutral PEG750Sq-NPs, are in good concordance with previous findings (Crater and Carrier, 2010). PEGylated NPs, with a sufficiently high PEG density on the NP surface, are widely known to be mucus penetrating because they are inert to hydrophobic interactions and hydrogen bonding (Wang et al., 2008; Xu et al., 2015; Maisel et al., 2016).

Carrier Properties of SqD-NPs Optimal Loading Capacities of SqD-NPs

We investigated the LC of the SqD-NPs using a variety of compounds owning multiple functional groups as well as representing different physicochemical characteristics and Mw. The suitable SqD and drug-loading method to obtain optimal LC for each model compound are reported in **Table 1**, while detailed guidance for choosing appropriate SqD and preparation method is shown in **Figure 2**. Generally, the SqD-NPs are composed of two compartments—a hydrophilic shell and a hydrophobic core. The hydrophobic drugs were loaded in the core by hydrophobic interactions *via* the coprecipitation method or the solvent evaporation method. For the hydrophobic compounds, e.g., Nile red, cholesteryl BODIPY, or dexamethasone, the coprecipitation method offers more facile loading procedure and better LC. The hydrophilic drugs, in turn, could be loaded onto the NP shell by charge interactions and hydrogen bonding *via* the dropping method or the solvent evaporation method. Interestingly, by allowing the drug to distribute in both the lipophilic and hydrophilic domains of the squalenyl nanoassemblies, the solvent evaporation method is a good loading technique for amphiphilic compounds, e.g., colistin.

In this study, the model compounds dexamethasone, cholesteryl BODIPY, and Nile red—representing different Mw and hydrophobicity—could be loaded in the core of any SqD-NPs. The drug-loaded NPs had a size range of 130–250 nm and a narrow size distribution (PDI < 0.3). Notably, the optimal LC of dexamethasone was ~ 33 , ~ 32 , and $\sim 24\%$ in aSq-NPs, cSq-NPs, and PEG750Sq-NPs, respectively, while the EE values in all cases were $\sim 90\%$ (**Table 1**). The optimal LC and EE of cholesteryl BODIPY in aSq-NPs were $10.35 \pm 0.66\%$ and $87.6 \pm 8.2\%$, respectively. The optimal LC and EE of Nile red in cSq-NPs were $9.03 \pm 0.91\%$ and $60.2 \pm 6.7\%$, respectively. The lower EE recorded in loading Nile red could be explained by its low Mw

TABLE 1 | Summary of preparation methods used to load model compounds to squalenyl derivative–nanoparticles (SqD-NPs).

Squalenyl-derivative	Drug	Preparation method	Size (nm)	PDI	Zeta-potential (mV)	EE (%)	LC (%)
aSq	Cholesteryl BODIPY	Coprecipitation	254.3 ± 2.4	0.094 ± 0.011	−18.6 ± 0.1	87.6 ± 8.2	10.35 ± 0.66
		Dexamethasone	Coprecipitation	140.2 ± 25.7	0.203 ± 0.061	−40.0 ± 7.1	90.6 ± 1.2
	Isoniazid	Solvent evaporation	198.9 ± 8.6	0.249 ± 0.029	−29.5 ± 1.0	42.6 ± 1.7	27.43 ± 0.79
		Dropping	112.9 ± 2.0	0.125 ± 0.017	−35.6 ± 2.3	07.4 ± 1.2	06.17 ± 0.97
	Colistin	Solvent evaporation	325.0 ± 7.1	0.152 ± 0.041	22.9 ± 1.1	90.1 ± 2.3	45.31 ± 0.73
		Dropping	195.6 ± 2.6	0.184 ± 0.002	25.1 ± 1.0	83.6 ± 4.1	35.83 ± 0.51
cSq	Tigecycline	Dropping	198.6 ± 4.8	0.014 ± 0.010	28.6 ± 1.3	85.3 ± 6.7	44.26 ± 2.03
	Nile Red	Coprecipitation	208.0 ± 3.2	0.185 ± 0.069	38.6 ± 3.7	60.2 ± 6.7	09.03 ± 0.91
		Dexamethasone	Coprecipitation	146.9 ± 8.9	0.183 ± 0.027	44.1 ± 5.7	87.9 ± 6.6
	Fluorescent Albumin	Dropping	205.6 ± 2.8	0.174 ± 0.010	17.4 ± 1.7	92.1 ± 3.8	03.52 ± 0.33
PEG750Sq	Dexamethasone	Coprecipitation	162.95 ± 59.45	0.255 ± 0.075	00.1 ± 9.2	92.4 ± 2.5	23.49 ± 0.48

The characteristics of optimal drug-loaded SqD-NPs, including hydrodynamic size, polydispersity index (PDI), zeta-potential, encapsulation efficiency (EE), and loading capacity (LC) are reported. Results are presented as mean ± SD.

and less interaction with the squalenyl core. Squalene is known as a precursor in the endogenous cholesterol biosynthesis, which implies its strong interaction with dexamethasone—a derivative of cholesterol—thereof enhancing the LC and EE (Reddy and Couvreur, 2009; Ghimire et al., 2016). The same holds true for cholesteryl BODIPY, which has a high clog *P*-value and contains a cholesteryl moiety.

Isoniazid, colistin, tigecycline, and FITC-albumin, representing different Mw and hydrophobicity, were loaded in either aSq-NPs or cSq-NPs. Accordingly, the loading of these compounds was investigated using solvent evaporation method and/or dropping method (Figure 2), while the optimal LC and EE for each compound and the corresponding loading method are reported in Table 1.

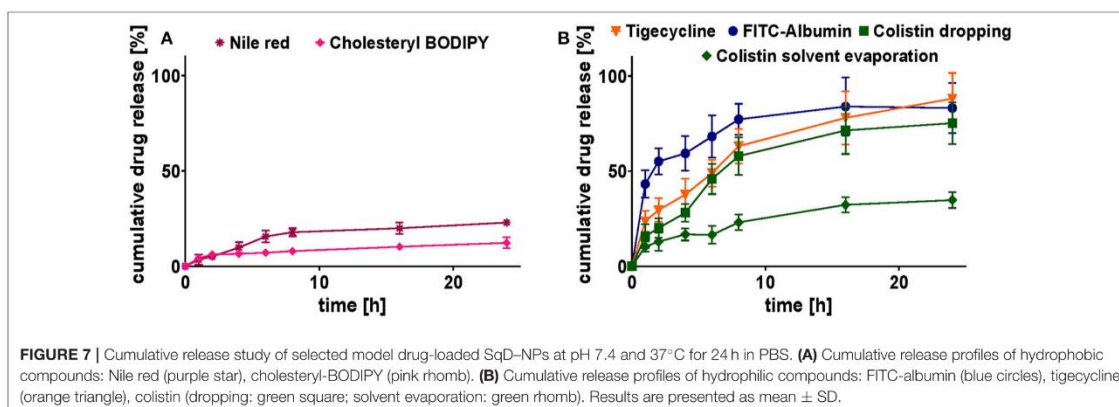
Isoniazid—a positively charged and small molecule (Mw 137.14 Da)—was loaded in aSq-NPs. The solvent evaporation method resulted in a significantly higher LC of isoniazid at 27.43 ± 0.79% compared to that of the dropping method at 6.17 ± 0.97%. Using the solvent evaporation method, the preparation of isoniazid and aSq in the solvent mixture (THF:water 1:1 v/v) allowed the maximum charged interaction between the two reagents, thus, increased the EE and LC. In contrast, the preformed aSq-NPs and dropping method limited the interaction with isoniazid molecules. The optimal isoniazid-loaded aSq-NPs had the size of 198.9 ± 8.6 nm and PDI below 0.25.

The molecules with multiple functional groups—tigecycline (Mw 585.66 Da), colistin (Mw 1,155.46 Da), and FITC-albumin (Mw ~60,000 Da)—could be loaded in NPs using the dropping method. The optimal LC and EE of stable tigecycline-loaded aSq-NPs (198.6 ± 4.8 nm, PDI 0.014 ± 0.010) were 44.26 ± 2.03 and 85.3 ± 6.7%, respectively. The LC and EE of colistin in aSq-NPs were significantly high at 35.83 ± 0.51 and 83.6

± 4.1%, respectively, which also produced a stable DDS having the size of 195.6 ± 2.6 nm and PDI lower than 0.2. The reasonable LC and EE of FITC-albumin—a representative of negatively charged protein molecules—in cSq-NPs were 3.52 ± 0.33 and 92.1 ± 3.8%, respectively. The stable protein-loaded cSq-NPs had the size of 205.6 ± 2.8 nm and PDI below 0.2. As shown in Table 1, the zeta-potential values of these drug-loaded NPs changed significantly compared to the corresponding drug-free NPs reflecting the loading *via* charged interactions.

The positively charged colistin contains a lipophilic moiety and could interact with aSq molecules *via* both charged and hydrophobic interactions (Yasar et al., 2018; Menina et al., 2019). We, thus, hypothesized that the solvent evaporation method could enhance the LC and EE of colistin in aSq-NPs. In fact, colistin LC and EE obtained by using such an approach were 45.31 ± 0.73 and 90.1 ± 2.3%, respectively, which were higher than the ones obtained by the dropping method. The integration of the lipophilic moiety of colistin into aSq-NPs increased the NP size from 195.6 ± 2.6 to 325.0 ± 7.1 nm, while the positive zeta-potential (22.9 ± 1.1 mV) of the drug-loaded aSq-NPs indicated also the presence of colistin on the NP surface.

The dual loading capacity of the SqD-NPs was illustrated by loading both hydrophobic Nile red and hydrophilic FITC-albumin in cSq-NPs. The Nile red-loaded cSq-NPs (LC ~0.5%) were prepared by the coprecipitation, and then further loaded with hydrophilic FITC-albumin (LC ~0.5%) by the dropping method. The colocalization of both fluorescent compounds in NPs was confirmed by confocal laser scanning microscopy images (Supplementary Figure 10). Such simultaneous drug loadings could benefit the delivery of actives with synergistic effects (Ho et al., 2020).



In short, the SqD-NPs are capable of loading a broad range of drug molecules differing in physicochemical characteristics, thus, are versatile drug delivery platforms.

Release Studies

In vitro release profiles were conducted under the same conditions at physiological pH 7.4 (PBS), 37°C, and over 24 h (Figures 7A,B).

The release profiles of hydrophobic compounds were determined for the ones with the highest and lowest Mw, cholesteryl BODIPY, and Nile red, respectively. The release profiles for both compounds are shown in Figure 7A. They clearly demonstrate their affection by the strength of hydrophobic interactions. Compared to cholesteryl BODIPY, Nile red released twice the cumulative percentage after 24 h. Nevertheless, the release of both compounds was sustained for the period over at least 24 h.

The release profiles of hydrophilic compounds were conducted for tigecycline (highest achieved LC), FITC-albumin (protein representative) and colistin (comparison of two preparation methods), respectively. The association of hydrophilic drugs loaded onto the NP surface by the dropping method is not as strong as a covalent conjugation, leading to the assumption of a complete drug release. Cumulative release of tigecycline, colistin, and FITC-albumin reached 88 ± 13 , 75 ± 11 , and $83 \pm 13\%$, respectively, after 24 h in PBS at 37°C (Figure 7B). The burst release at the early time points were avoided suggesting the strong charged interactions between the SqD and drug molecules. In comparison to that, the tight interaction of colistin to aSq-NPs by using the solvent evaporation method resulted in a sustained release for colistin. Only $35 \pm 4\%$ of colistin was released from aSq-NPs after 24 h in PBS at 37°C (Figure 7B).

Furthermore, IC90 values of tigecycline and colistin-loaded aSq-NPs were determined by the minimum inhibitory concentration (MIC) assay performed on *Pseudomonas aeruginosa* strain PA14 wild type and *Staphylococcus aureus* strain Newman. As shown in

Supplementary Table 3, the antimicrobial effect of both antibiotic-loaded NPs was similar to that of the drug alone, even though drug release after 24 h from the NPs is not completed.

CONCLUSION

In this study, we explored the use of self-assembling amphiphilic SqDs as DDS, which had started with the aSq. We have further described the straightforward synthesis of cSq and PEGylated SqDs. In addition to the ability of self-assembling to supramolecular colloids, the latter demonstrated that SqD-NPs showed excellent stability in physiological relevant media and biocompatibility. The application of different methods for the preparation of drug-loaded SqD-NPs allowed to modulate not only the LC but also the release rate, as desired. In further studies of carrier properties, the SqD-NPs showed significantly high LC of various cargos. Our findings postulate the self-assembled SqD-NPs as versatile drug delivery platforms.

DATA AVAILABILITY STATEMENT

The raw data supporting the conclusions of this article will be made available by the authors, without undue reservation.

AUTHOR CONTRIBUTIONS

D-KH, BL, DD, PC, and C-ML conceptualized and initiated the study. PC and C-ML acquired funding and provided resources. XM, US, BL, DD, PC, and C-ML were supervisors. D-KH did chemical synthesis and characterization. D-KH and RC investigated NP self-assembly and drug-loading capacities. CDR, RC, and D-KH validated the drug quantification methods. D-KH conducted *in vitro* assays and drug release. CDR and MK visualized the NPs. XM conceptualized and validated the mucin-NPs interaction studies. RC and SF performed NP

stability and mucin–NPs interaction studies. RC and D-KH analyzed the data, prepared the figures, and wrote the original draft. RC reviewed and edited the final draft. All authors read and revised the manuscript.

FUNDING

This project received funding from the European Union's Framework Programme for Research and Innovation Horizon 2020 (2014–2020) under the Marie Skłodowska-Curie Grant Agreement No. 642028. We acknowledged the support by the Deutsche Forschungsgemeinschaft (DFG; German Research Foundation) and Saarland University within the funding program Open Access Publishing.

REFERENCES

- Bansil, R., and Turner, B. S. (2006). Mucin structure, aggregation, physiological functions and biomedical applications. *Curr. Opin. Colloid Interface Sci.* 11, 164–170. doi: 10.1016/j.cocis.2005.11.001
- Bekkara-Aounallah, F., Gref, R., Othman, M., Reddy, L. H., Pili, B., Allain, V., et al. (2008). Novel PEGylated nanoassemblies made of self-assembled squalenyl nucleoside analogues. *Adv. Funct. Mater.* 18, 3718–3725. doi: 10.1002/adfm.200800705
- Bhattacharjee, S. (2016). DLS and zeta potential - What they are and what they are not? *J. Control. Release* 235, 337–351. doi: 10.1016/j.jconrel.2016.06.017
- Bobo, D., Robinson, K. J., Islam, J., Thurecht, K. J., and Corrie, S. R. (2016). Nanoparticle-based medicines: a review of FDA-approved materials and clinical trials to date. *Pharm. Res.* 33, 2373–2387. doi: 10.1007/s11095-016-1958-5
- Buchy, E., Valetti, S., Mura, S., Mouglin, J., Troufflard, C., Couvreur, P., et al. (2015). Synthesis and cytotoxic activity of self-assembling squalene conjugates of 3-[(Pyrrol-2-yl)methylidene]-2,3-dihydro-1H-indol-2-one anticancer agents. *Eur. J. Org. Chem.* 2015, 202–212. doi: 10.1002/ejoc.201403088
- Ceruti, M., Balliano, G., Viola, F., Cattel, L., Gerst, N., and Schuber, F. (1987). Synthesis and biological activity of azasqualenes, bis-azasqualenes and derivatives. *Eur. J. Med. Chem.* 22, 199–208. doi: 10.1016/0223-5234(87)90050-X
- Couvreur, P. (2013). Nanoparticles in drug delivery: past, present and future. *Adv. Drug Deliv. Rev.* 65, 21–23. doi: 10.1016/j.addr.2012.04.010
- Couvreur, P., Stella, B., Reddy, L. H., Hillaireau, H., Dubernet, C., Desmaële, D., et al. (2006). Squalenyl nanomedicines as potential therapeutics. *Nano Lett.* 6, 2544–2548. doi: 10.1021/nl061942q
- Crater, J. S., and Carrier, R. L. (2010). Barrier properties of gastrointestinal mucus to nanoparticle transport. *Macromol. Biosci.* 10, 1473–1483. doi: 10.1002/mabi.201000137
- Danhier, F., Ansorena, E., Silva, J. M., Coco, R., Le Breton, A., and Préat, V. (2012). PLGA-based nanoparticles: an overview of biomedical applications. *J. Control. Release* 161, 505–522. doi: 10.1016/j.jconrel.2012.01.043
- Desmaële, D., Gref, R., and Couvreur, P. (2012). Squalenoylation: a generic platform for nanoparticulate drug delivery. *J. Control. Release* 161, 609–618. doi: 10.1016/j.jconrel.2011.07.038
- Fessi, H., Puisieux, F., Devissaguet, J. Ph, Ammoury, N., and Benita, S. (1989). Nanocapsule formation by interfacial polymer disposition following solvent displacement. *Int. J. Pharm.* 55, 1–4. doi: 10.1016/0378-5173(89)90281-0
- Ghimire, G. P., Thuan, N. H., Koirala, N., and Sohng, J. K. (2016). Advances in biochemistry and microbial production of squalene and its derivatives. *J. Microbiol. Biotechnol.* 26, 441–451. doi: 10.4014/jmb.1510.10039
- Hillaireau, H., Dereuddre-Bosquet, N., Skanji, R., Bekkara-Aounallah, F., Caron, J., Lepêtre, S., et al. (2013). Anti-HIV efficacy and biodistribution of nucleoside reverse transcriptase inhibitors delivered as squalenoylated prodrug nanoassemblies. *Biomaterials* 34, 4831–4838. doi: 10.1016/j.biomaterials.2013.03.022
- RC was supported by Dr. Rolf M. Schwiete Stiftung, Mannheim, Germany.

ACKNOWLEDGMENTS

The authors would like to thank the kind support from Dr. Sangeun Lee, Petra König, Jana Westhues, Dr. Arnaud Peramo, and Sandrine Gouazou.

SUPPLEMENTARY MATERIAL

The Supplementary Material for this article can be found online at: <https://www.frontiersin.org/articles/10.3389/fchem.2020.584242/full#supplementary-material>

- Ho, D.-K., Frisch, S., Biehl, A., Terriac, E., Rossi, C. de, Schwarzkopf, K., et al. (2018). Farnesylated glycol chitosan as a platform for drug delivery: synthesis, characterization, and investigation of mucus-particle interactions. *Biomacromolecules* 19, 3489–3501. doi: 10.1021/acs.biomac.8b00795
- Ho, D.-K., Murgia, X., Rossi, C. de, Christmann, R., Hüfner de Mello Martins, A. G., Koch, M., et al. (2020). Squalenyl hydrogen sulfate nanoparticles for simultaneous delivery of tobramycin and an alkylquinolone quorum sensing inhibitor enable the eradication of *P. aeruginosa* biofilm infections. *Angew. Chem. Int. Ed. Engl.* 59:10296. doi: 10.1002/anie.202001407
- Ho, D.-K., Nichols, B. L. B., Edgar, K. J., Murgia, X., Loretz, B., and Lehr, C.-M. (2019). Challenges and strategies in drug delivery systems for treatment of pulmonary infections. *Eur. J. Pharm. Biopharm.* 144, 110–124. doi: 10.1016/j.ejpb.2019.09.002
- Kalepu, S., and Nekkanti, V. (2015). Insoluble drug delivery strategies: review of recent advances and business prospects. *Acta Pharm. Sin. B* 5, 442–453. doi: 10.1016/j.apsb.2015.07.003
- Kim, S. M., Faix, P. H., and Schnitzer, J. E. (2017). Overcoming key biological barriers to cancer drug delivery and efficacy. *J. Control. Release* 267, 15–30. doi: 10.1016/j.jconrel.2017.09.016
- Knudsen, K. B., Northeved, H., Kumar, P. E. K., Permin, A., Gjetting, T., Andresen, T. L., et al. (2015). *In vivo* toxicity of cationic micelles and liposomes. *Nanomedicine* 11, 467–477. doi: 10.1016/j.nano.2014.08.004
- Kokkinopoulou, M., Simon, J., Landfester, K., Mailänder, V., and Lieberwirth, I. (2017). Visualization of the protein corona: towards a biomolecular understanding of nanoparticle-cell-interactions. *Nanoscale* 9, 8858–8870. doi: 10.1039/C7NR02977B
- Koziolek, M., Grimm, M., Becker, D., Iordanov, V., Zou, H., Shimizu, J., et al. (2015). Investigation of pH and temperature profiles in the GI tract of fasted human subjects using the Intellipac® system. *J. Pharm. Sci.* 104, 2855–2863. doi: 10.1002/jps.24274
- Kwon, S. M., Nam, H. Y., Nam, T., Park, K., Lee, S., Kim, K., et al. (2008). *In vivo* time-dependent gene expression of cationic lipid-based emulsion as a stable and biocompatible non-viral gene carrier. *J. Control. Release* 128, 89–97. doi: 10.1016/j.jconrel.2008.02.004
- Lai, S. K., O'Hanlon, D. E., Harrold, S., Man, S. T., Wang, Y.-Y., Cone, R., et al. (2007). Rapid transport of large polymeric nanoparticles in fresh undiluted human mucus. *PNAS* 104, 1482–1487. doi: 10.1073/pnas.0608611104
- Lepeltier, E., Loretz, B., Desmaële, D., Zapp, J., Herrmann, J., Couvreur, P., et al. (2015). Squalenoylation of chitosan: a platform for drug delivery? *Biomacromolecules* 16, 2930–2939. doi: 10.1021/acs.biomac.5b00840
- Liele, O., and Ribbeck, K. (2011). Biological hydrogels as selective diffusion barriers. *Trends Cell Biol.* 21, 543–551. doi: 10.1016/j.tcb.2011.06.002
- Lock, J. Y., Carlson, T. L., and Carrier, R. L. (2018). Mucus models to evaluate the diffusion of drugs and particles. *Adv. Drug Deliv. Rev.* 124, 34–49. doi: 10.1016/j.addr.2017.11.001
- Maisel, K., Reddy, M., Xu, Q., Chattopadhyay, S., Cone, R., Ensign, L. M., et al. (2016). Nanoparticles coated with high molecular weight PEG penetrate mucus

- and provide uniform vaginal and colorectal distribution *in vivo*. *Nanomedicine* 11, 1337–1343. doi: 10.2217/nnm-2016-0047
- Maksimenko, A., Mougín, J., Mura, S., Sliwinski, E., Lepeltier, E., Bourgaux, C., et al. (2013). Polyisoprenoyl gemcitabine conjugates self assemble as nanoparticles, useful for cancer therapy. *Cancer Lett.* 334, 346–353. doi: 10.1016/j.canlet.2012.08.023
- Menina, S., Eisenbeis, J., Kamal, M. A. M., Koch, M., Bischoff, M., Gordon, S., et al. (2019). Bioinspired liposomes for oral delivery of colistin to combat intracellular infections by *Salmonella enterica*. *Adv. Healthc. Mater.* 8:e1900564. doi: 10.1002/adhm.201900564
- Mittal, A., Schulze, K., Ebsen, T., Weißmann, S., Hansen, S., Lehr, C. M., et al. (2015). Efficient nanoparticle-mediated needle-free transcutaneous vaccination *via* hair follicles requires adjuvantation. *Nanomedicine* 11, 147–154. doi: 10.1016/j.nano.2014.08.009
- Mosmann, T. (1983). Rapid colorimetric assay for cellular growth and survival: application to proliferation and cytotoxicity assays. *J. Immunol. Methods* 65, 55–63. doi: 10.1016/0022-1759(83)90303-4
- Murgia, X., Loretz, B., Hartwig, O., Hittinger, M., and Lehr, C.-M. (2018). The role of mucus on drug transport and its potential to affect therapeutic outcomes. *Adv. Drug Deliv. Rev.* 124, 82–97. doi: 10.1016/j.addr.2017.10.009
- Murgia, X., Pawelczyk, P., Schaefer, U. F., Wagner, C., Willenbacher, N., and Lehr, C.-M. (2016). Size-limited penetration of nanoparticles into porcine respiratory mucus after aerosol deposition. *Biomacromolecules* 17, 1536–1542. doi: 10.1021/acs.biomac.6b00164
- Raesch, S. S., Tenzer, S., Storck, W., Rurainski, A., Selzer, D., Ruge, C. A., et al. (2015). Proteomic and lipidomic analysis of nanoparticle corona upon contact with lung surfactant reveals differences in protein, but not lipid composition. *ACS Nano* 9, 11872–11885. doi: 10.1021/acs.nano.5b04215
- Ralay-Ranaivo, B., Desmaële, D., Bianchini, E. P., Lepeltier, E., Bourgaux, C., Borgel, D., et al. (2014). Novel self assembling nanoparticles for the oral administration of fondaparinux: synthesis, characterization and *in vivo* evaluation. *J. Control. Release* 194, 323–331. doi: 10.1016/j.jconrel.2014.07.060
- Reddy, L. H., and Couvreur, P. (2009). Squalene: a natural triterpene for use in disease management and therapy. *Adv. Drug Deliv. Rev.* 61, 1412–1426. doi: 10.1016/j.addr.2009.09.005
- Ruge, C. A., Kirch, J., and Lehr, C.-M. (2013). Pulmonary drug delivery: from generating aerosols to overcoming biological barriers—therapeutic possibilities and technological challenges. *Lancet Respir. Med.* 1, 402–413. doi: 10.1016/S2213-2600(13)70072-9
- Sanna, V., Roggio, A. M., Siliani, S., Piccinini, M., Marceddu, S., Mariani, A., et al. (2012). Development of novel cationic chitosan-and anionic alginate-coated poly(D,L-lactide-co-glycolide) nanoparticles for controlled release and light protection of resveratrol. *Int. J. Nanomed.* 7, 5501–5516. doi: 10.2147/IJN.S36684
- Schmid-Wendtner, M.-H., and Korting, H. C. (2006). The pH of the skin surface and its impact on the barrier function. *Skin Pharmacol. Physiol.* 19, 296–302. doi: 10.1159/000094670
- Schroepfer, G. J. (1981). Sterol biosynthesis. *Annu. Rev. Biochem.* 50, 585–621. doi: 10.1146/annurev.bi.50.070181.003101
- Sémiramoth, N., Di Meo, C., Zouhiri, F., Saïd-Hassane, F., Valetti, S., Gorges, R., et al. (2012). Self-assembled squalenoylated penicillin bioconjugates: an original approach for the treatment of intracellular infections. *ACS Nano* 6, 3820–3831. doi: 10.1021/nn204928v
- Skarbak, C., Lesueur, L. L., Chapuis, H., Deroussent, A., Pioche-Durieu, C., Daville, A., et al. (2015). Preactivated oxazaphosphorines designed for isophosphoramidate mustard delivery as bulk form or nanoassemblies: synthesis and proof of concept. *J. Med. Chem.* 58, 705–717. doi: 10.1021/jm501224x
- Suk, J. S., Xu, Q., Kim, N., Hanes, J., and Ensign, L. M. (2016). PEGylation as a strategy for improving nanoparticle-based drug and gene delivery. *Adv. Drug Deliv. Rev.* 99, 28–51. doi: 10.1016/j.addr.2015.09.012
- Thomas, O. S., and Weber, W. (2019). Overcoming physiological barriers to nanoparticle delivery—are we there yet? *Front. Bioeng. Biotechnol.* 7:415. doi: 10.3389/fbioe.2019.00415
- van Tamelen, E. E., and Curphey, T. J. (1962). The selective *in vitro* oxidation of the terminal double bonds in squalene. *Tetrahedron Lett.* 3, 121–124. doi: 10.1016/S0040-4039(00)71112-9
- Wang, Y.-Y., Lai, S. K., Suk, J. S., Pace, A., Cone, R., and Hanes, J. (2008). Addressing the PEG mucoadhesivity paradox to engineer nanoparticles that “slip” through the human mucus barrier. *Angew. Chem. Int. Ed. Engl.* 47, 9726–9729. doi: 10.1002/anie.200803526
- Xu, Q., Ensign, L. M., Boylan, N. J., Schön, A., Gong, X., Yang, J.-C., et al. (2015). Impact of surface polyethylene glycol (PEG) density on biodegradable nanoparticle transport in mucus *ex vivo* and distribution *in vivo*. *ACS Nano* 9, 9217–9227. doi: 10.1021/acs.nano.5b03876
- Yasar, H., Ho, D.-K., Rossi, C. de, Herrmann, J., Gordon, S., Loretz, B., et al. (2018). Starch-chitosan polyplexes: a versatile carrier system for anti-infectives and gene delivery. *Polymers*. 10:252. doi: 10.3390/polym10030252

Conflict of Interest: The authors declare that the research was conducted in the absence of any commercial or financial relationships that could be construed as a potential conflict of interest.

Copyright © 2020 Ho, Christmann, Murgia, De Rossi, Frisch, Koch, Schaefer, Loretz, Desmaële, Couvreur and Lehr. This is an open-access article distributed under the terms of the Creative Commons Attribution License (CC BY). The use, distribution or reproduction in other forums is permitted, provided the original author(s) and the copyright owner(s) are credited and that the original publication in this journal is cited, in accordance with accepted academic practice. No use, distribution or reproduction is permitted which does not comply with these terms.

With the experience gained after the successful characterization and evaluation of the versatile amphiphilic SqD NDDS platforms, further research focused on the development, characterization and evaluation of TFB-loaded SqD NPs, discussed in the third and last chapter:

2.3. CHAPTER 3 – DEVELOPMENT OF TOFACITINIB LOADED SQUALENYL DERIVATIVE NANOPARTICULATE DRUG DELIVERY SYSTEM AND CHARACTERIZATION OF ITS ABILITY FOR TARGETED FOLLICULAR DRUG DELIVERY AND BIOLOGICAL RESPONSE – EX VIVO AND IN VIVO

Chapter 3 deals with the following investigations:

For TFB, a weak base, the negatively charged SqD with a hydrogen sulfate head group, was chosen ¹²⁷. Since the charge interaction between the hydrogen sulfate head group and the TFB did not show satisfactory results, the intercalation of TFB with the hydrophobic squalenyl moiety was desirable. Therefore, the pH of the aqueous solution was controlled to repress the water solubility of TFB ¹²⁷. However, a topical skin application was desired. Therefore, the pH of the skin had to be taken into account. As a compromise for both desired aspects, the final formulation had a pH of ~ 6.3 ¹²⁷. The TFB-loaded NDDS demonstrated an impressive drug loading capacity of ~ 20 % (w/w) and an enhanced solubility of TFB of up to 40 times compared to the plain drug formulation ¹²⁷. **After the successful development of TFB SqD NPs was achieved, the targeted delivery of TFB into HFs had to be investigated. The HF penetration of the NDDS and the delivery of TFB into the HFs was studied in the *ex vivo* pig ear model ¹²⁷.** Unfortunately, the differential stripping method could not be used to determine the TFB amount delivered into HFs by NDDS in the *ex vivo* pig ear skin model ¹²⁷. The polymerized cyanoacrylate interfered with TFB in the analytical method, so **another method to determine the amount deposited into HFs** had to be found. Accordingly, the skin surface cleaning step of the differential stripping method ¹¹⁹ was combined with the “single HF harvesting method” ⁶³ (for further information on the methods see section 1.5.4.) to reap the benefits of each method: open HFs by retaining pig ear skin on the cartilage ¹¹⁹, differentiation between formulation amount remaining on skin surface and amount penetrated into HFs ^{113,119}, no disturbance of the analytical method caused by additional substances ⁶³, and determination of mass balance ¹¹⁹. Therefore, after skin surface cleaning by tape stripping ^{113,119}, the application area was divided into two halves. On one half all HFs were punched by a 1 mm diameter punch biopsy, on the other half the same amount of interfollicular skin biopsies were taken ¹²⁷. For mass balance purposes all devices and the skin rest coming into contact with the formulation were extracted and

analyzed¹²⁷. Apart from the TFB SqD NPs formulation, aqueous drug formulations as well as an acetone:DMSO drug solution were studied¹²⁷. The TFB acetone:DMSO solution was chosen for comparison reasons to a previous study¹²⁸. In this previous study, topically applied TFB acetone:DMSO solution demonstrated a reduction of ear swelling 24 hours after the challenging with allergen in an *in vivo* dermatitis mouse model¹²⁹ as compared to the control group, using a drug-free acetone:DMSO solution¹²⁸. **To investigate the biological effect of TFB, the *in vivo* dermatitis mouse model was chosen**, where the TFB acetone:DMSO solution could serve as a positive control.

The *ex vivo* pig ear model clearly demonstrated higher impact of follicular delivery compared to interfollicular skin penetration and permeation¹²⁷. Moreover, the TFB-loaded NDDS delivered a significantly larger amount of TFB into HFs compared to aqueous drug solutions¹²⁷. The TFB acetone:DMSO solution transported similar amounts of TFB as the NDDS to follicular skin, but slightly higher ones to interfollicular skin¹²⁷. Interestingly, as the only tested formulation, TFB acetone:DMSO solution did not meet the mass balance criteria¹²⁷. By the *in vivo* dermatitis mouse model TFB acetone:DMSO solution showed a significant difference in ear swelling reduction in comparison to the drug-free control group¹²⁷. Moreover, the TFB SqD NPs demonstrated a biological effect by reducing ear swelling after a 24-hour allergen challenge¹²⁷.

These approaches and findings are further addressed by the publication: “***Tofacitinib Loaded Squalenyl Nanoparticles for Targeted Follicular Delivery in Inflammatory Skin Diseases***”.

Rebekka Christmann, Duy-Khiet Ho, Jenny Wilzopolski, Sangeun Lee, Marcus Koch, Brigitta Loretz, Thomas Vogt, Wolfgang Bäumer, Ulrich F. Schaefer, Claus-Michael Lehr; *Pharmaceutics* (2020) 12, 1131.

DOI: 10.3390/pharmaceutics12121131



Reprinted from *Pharmaceutics*, Tofacitinib Loaded Squalenyl Nanoparticles for Targeted Follicular Delivery in Inflammatory Skin Diseases; Rebekka Christmann, Duy-Khiet Ho, Jenny Wilzopolski, Sangeun Lee, Marcus Koch, Brigitta Loretz, Thomas Vogt, Wolfgang Bäumer, Ulrich F. Schaefer, and Claus-Michael Lehr; *Pharmaceutics* (2020) 12, 1131.

“Copyright © (2020) by the authors. Licensee MDPI, Basel, Switzerland. This article is an open access article distributed under the terms and conditions of the Creative Commons Attribution (CC BY) license (<http://creativecommons.org/licenses/by/4.0/>)”¹²⁷.



Article

Tofacitinib Loaded Squalenyl Nanoparticles for Targeted Follicular Delivery in Inflammatory Skin Diseases

Rebekka Christmann ^{1,2}, Duy-Khiet Ho ^{1,2,†} , Jenny Wilzopolski ³, Sangeun Lee ¹, Marcus Koch ⁴, Brigitta Loretz ¹ , Thomas Vogt ⁵, Wolfgang Bäumer ³, Ulrich F. Schaefer ² and Claus-Michael Lehr ^{1,2,*}

¹ Helmholtz-Institute for Pharmaceutical Research Saarland (HIPS)—Helmholtz Centre for Infection Research (HZI), 66123 Saarbrücken, Germany; Rebekka.Christmann@helmholtz-hips.de (R.C.); DuyKhiet.Ho@helmholtz-hips.de (D.-K.H.); Sangeun.Lee@helmholtz-hips.de (S.L.); Brigitta.Loretz@helmholtz-hips.de (B.L.)

² Department of Pharmacy, Saarland University, 66123 Saarbrücken, Germany; ufs@mx.uni-saarland.de

³ Institute of Pharmacology and Toxicology, Department of Veterinary Medicine, Freie Universität Berlin, 14195 Berlin, Germany; Jenny.Wilzopolski@fu-berlin.de (J.W.); Wolfgang.Baeumer@fu-berlin.de (W.B.)

⁴ INM-Leibniz Institute for New Materials, 66123 Saarbrücken, Germany; Marcus.Koch@leibniz-inm.de

⁵ Department of Dermatology, Saarland University Hospital, 66421 Homburg/Saar, Germany; Thomas.Vogt@uks.eu

* Correspondence: Claus-Michael.Lehr@helmholtz-hips.de; Tel.: +49-681-98806-1000

† Current address: Department of Bioengineering, School of Medicine, University of Washington, Seattle, WA 98195, USA.

Received: 30 October 2020; Accepted: 20 November 2020; Published: 24 November 2020



Abstract: Tofacitinib (TFB), a Janus kinase inhibitor, has shown excellent success off-label in treating various dermatological diseases, especially alopecia areata (AA). However, TFB's safe and targeted delivery into hair follicles (HFs) is highly desirable due to its systemic adverse effects. Nanoparticles (NPs) can enhance targeted follicular drug delivery and minimize interfollicular permeation and thereby reduce systemic drug exposure. In this study, we report a facile method to assemble the stable and uniform 240 nm TFB loaded squalenyl derivative (SqD) nanoparticles (TFB SqD NPs) in aqueous solution, which allowed an excellent loading capacity (LC) of 20%. The SqD NPs showed an enhanced TFB delivery into HFs compared to the aqueous formulations of plain drug in an *ex vivo* pig ear model. Furthermore, the therapeutic efficacy of the TFB SqD NPs was studied in a mouse model of allergic dermatitis by ear swelling reduction and compared to TFB dissolved in a non-aqueous mixture of acetone and DMSO (7:1 *v/v*). Whereas such formulation would not be acceptable for use in the clinic, the TFB SqD NPs dispersed in water illustrated a better reduction in inflammatory effects than plain TFB's aqueous formulation, implying both encouraging good *in vivo* efficacy and safety. These findings support the potential of TFB SqD NPs for developing a long-term topical therapy of AA.

Keywords: targeted drug delivery; hair follicle; *in vivo* allergic dermatitis mouse model; follicular delivery; interfollicular delivery; nanoparticles; squalene

1. Introduction

Alopecia areata (AA) is one of the major non-scarring hair loss disorders with a lifetime incidence of 2% [1–3]. AA is a complex disorder that involves breakdown of the immune privilege of anagen hair follicles (HFs), leads to an attack of the immune system, and causes reversible hair loss with a

preserved HF [1,4]. Although AA is a non-life-threatening disease, it still has a significant effect on the patients' quality of life [1,5]. The most common off-labeled treatment regimens for AA include corticosteroids—applied intralesionally, topically or systemically, topical minoxidil, oral methotrexate, or topical immunotherapy [6], while an approved medicine is not available due to the missing therapeutic outcome prediction and the often-seen relapses [6].

A recently developed Janus kinase inhibitor (JAK-inhibitor) has demonstrated an impressive hair regrowth in long-term alopecia universalis [7,8]. Namely, tofacitinib (TFB)—an FDA-approved immunosuppressant against rheumatoid arthritis, psoriasis arthritis, and ulcerative colitis [9], which inhibits JAK 1 and 3, has shown promising treatment progress on human and mice [10–13]. However, continuous treatment is necessary to gain a possible persistent success in hair regrowth [12,13]. Unfortunately, long-term systemic treatment with TFB can cause a broad and severe spectrum of adverse effects due to the wide bioactive range of such JAKs [14]. JAKs are part of the intracellular signaling pathway transducing cytokine signaling of both the types I and II cytokine receptor family. Thus, JAK/STAT (signal transducers and activators of transcription) dependent cytokines have a broad spectrum of action in humans, especially in hematopoiesis, inflammation induction, and immune response control [14,15]. In 2019, TFB received an FDA-boxed warning due to an “increased risk of blood clots and death with higher dose” [16]. Those facts emphasize the necessity of generating a safer treatment profile for TFB, especially in non-life-threatening diseases like AA [5,17].

The TFB targeted HF delivery is considered as a good strategy to reduce the high systemic drug levels and adverse effects. The topical application of the nanoparticulate drug delivery system (NDDS) to the skin is able to (i) enhance drug solubility [18], (ii) deliver drugs targeted into HFs [19,20], (iii) build up a drug depot [20,21], and (iv) release the drug in a controlled manner [22,23]. Consequently, nanoparticles (NPs) can deliver a higher amount of drug to HFs compared to plain drug solution—meaning to maximize the follicular penetration while minimizing the interfollicular permeation of drug molecules [22–24]. The primary mechanism of NPs deposition in HFs is the postulated ratchet effect of cuticle cells in the hair shaft [20,25]. However, we have previously demonstrated the deposition of NPs also in AA affected hairless human scalp HFs [26].

NDDS excipients composition can be chosen depending on their purpose, beside the conventional approach of biodegradable polymers, for example, metal-based NDDS are used as antimicrobial agents [27]. In addition, NDDS can release their cargo upon a triggering stimulus, e.g., by ultrasound or infrared A radiation [28–30].

Taking advantage of an NP approach, we aimed to develop a NDDS for TFB targeted delivery to AA affected HFs. Importantly, since a high dose of TFB—up to 5 or 10 mg orally twice daily—is clinically required [9], a NDDS for TFB must have a high drug loading capacity (LC). Moreover, such a NDDS should also be safe and easily prepared to meet future translational requirements [31]. The conventional NDDS's based on biodegradable polymers (e.g., poly (lactic-co-glycolic acid) (PLGA)) or nanostructured lipid carriers (NLCs) offer good biocompatibility and are facile to produce. LC had, however, been reported to be lower than 5% (*w/w*) [32,33], which was in good agreement with our attempts, although previously a study claimed around 30% LC for TFB citrate salt loaded PLGA particles [34].

Squalene alone accounts for around 12% of the human sebum's major components [35] and is a precursor of the cholesterol biosynthesis throughout the human body [35,36]. Interestingly, squalene is not further transformed in the sebaceous cells, which makes the skin the richest squalene containing tissue in the human body [35,36]. Thus, squalene-based NPs for targeted follicular delivery would be an excellent choice. Squalenoylation technology, which consists of linking a hydrophobic squalenyl moiety to a more hydrophilic drug molecule, can significantly improve drug LC in self-assembled squalenoylated NPs. This, moreover, could enhance the therapeutic efficacy of the drugs [37,38]. Unfortunately, the secondary amine in the pyrrole ring, which is the only available reactive group in TFB, is a relatively weak nucleophile for covalently coupling reactions. Possible attempts to synthesize TFB prodrug are not facile [39]. Only the successful formation of a carbamate linkage was reported,

leading to undesired long cleavage times for over three weeks [39]. Moreover, TFB is degraded in harsh conditions making it less favorable in the chemically squalenyl modification [39–41].

Recently, we have reported an alternative to the squalenoylation approach, in which we used amphiphilic squalenyl derivatives to formulate the surfactant-free self-assembled NPs allowing significantly high drug LC in both hydrophilic and hydrophobic compartments [42–44].

Based on these studies we employed an anionic squalenyl derivative (SqD)—squalenyl hydrogen sulfate—to produce the TFB loaded SqD NPs (TFB SqD NPs). This SqD is composed of a hydrophilic hydrogen sulfate head-group covalently bonded to a hydrophobic moiety. We speculated that SqD NPs could potentially allow the loading of TFB via charged interaction in the NPs shell and hydrophobic interaction in the NPs core, hence giving a high LC of TFB. The TFB SqD NPs were moreover expected to provide an enhanced TFB delivery in HFs and therapeutic effects.

We here first describe the preparation and characterization of TFB SqD NPs. In the subsequent studies, we investigated the performance of TFB SqD NPs compared to formulations of the plain drug and vehicle controls in some established *ex vivo* and *in vivo* models. The *ex vivo* pig ear model was adopted from previously reported ones [45,46] and used to determine the TFB penetration and permeation pathways—into either follicular or interfollicular skin areas. A well-established *in vivo* allergic dermatitis mouse model was, in turn, used to evaluate the therapeutic efficacy of the formulations in reducing an inflammatory response, which corresponds to a reduction in the ear swelling upon being challenged with allergen [47]. Our *ex vivo* and *in vivo* findings reveal the TFB SqD NPs as safe and efficient for targeted drug delivery to the hair follicles after topical administration.

2. Materials and Methods

2.1. Materials

TFB free base (TFB) and TFB citrate salt (TFB-C) were purchased from LC Laboratories, Massachusetts, US. TFB-C was manufactured to enhance the water solubility of TFB and was in this study used to prepare an aqueous drug reference solution. SqD was synthesized as described previously [43,44]. Ammonium acetate (LC-MS grade) was purchased from Sigma-Aldrich, Munich, Germany. Disodium hydrogen phosphate heptahydrate and sodium dihydrogen phosphate hydrate were purchased from Carl Roth, Karlsruhe, Germany. Tetrahydrofuran (HPLC grade) (THF), ethanol, absolute (HPLC grade; EtOH), formic acid (LC-MS grade), and dimethyl sulfoxide (DMSO) were purchased from Fisher Scientific, Leicestershire, UK. Acetone (HPLC grade) was purchased from Honeywell Riedel-deHäen, Fisher Scientific GmbH, Schwerte, Germany. Methanol (MeOH) was obtained from VWR Chemicals, Darmstadt, Germany. A disposable biopsy punch with plunger with a 1 mm diameter was obtained from kai europe GmbH, Solingen, Germany. Millex[®]-LG syringe driven filter units (PTFE, 0.20 µm) were purchased from Merck Millipore, Darmstadt, Germany. Faber Castell[®] MULTIMARK permanent 152399, 0.4 mm in black was purchased from A.W. Faber-Castell Vertrieb GmbH, Stein, Germany. Tesafilm kristallklar 33 m × 19 mm was a gift from tesa SE, Hamburg, Germany. Dialysis bag SpetraPor[®]7, MWCO 10 kDa, consisting of regenerative cellulose was purchased from Repligen Corporation, California, US. Milli-Q water purification system from Merck Millipore (Darmstadt, Germany) was used to prepare purified water (water).

2.2. Animal Procedure and Ethics Statement

The animal experiment was approved on 27th of November in 2017 by state agency (LAGeSo Berlin, approval number: G 0234/17). The experiments were conducted in female BALB/c (BALB/cAnNCrl) aged 6–8 weeks. Mice were obtained from Charles River Laboratories (Sulzfeld, Germany). Mice received a standard diet and water ad libitum. After arrival, mice were acclimatized to their environment for 1 week.

2.3. Preparation of TFB SqD NPs

TFB SqD NPs were prepared using free base TFB and anionic squalenyl derivative (SqD)—squalenyl hydrogen sulphate (Figure 1)—whose detailed synthesis and characterization can be found in our previous work [43,44]. The optimal TFB SqD NPs were produced by solvent evaporation technique. In detail, TFB and SqD were separately solubilized in THF at a concentration of 2 mg/mL and 10 mg/mL, respectively. An appropriate volume of each compound solution in THF was mixed to obtain a final TFB:SqD (36.5:63.5 *w/w*) and a total 1 mg/mL concentration. Subsequent, phosphate buffer (10 mM) pH 6.75 (phos-buffer) was added reaching a THF:phos-buffer volume ratio of 1:0.9. The TFB SqD NPs were formed upon slow evaporation of THF, and water was then partially removed (at 40 mbar, 40 °C, in a Rotavapor R-300, Büchi, Essen, Germany) to reach a final TFB SqD NPs concentration of 5.5 mg/mL, which contained an equivalent TFB concentration of 2 mg/mL. Drug-free SqD NPs were prepared using the same procedure and served as controls.

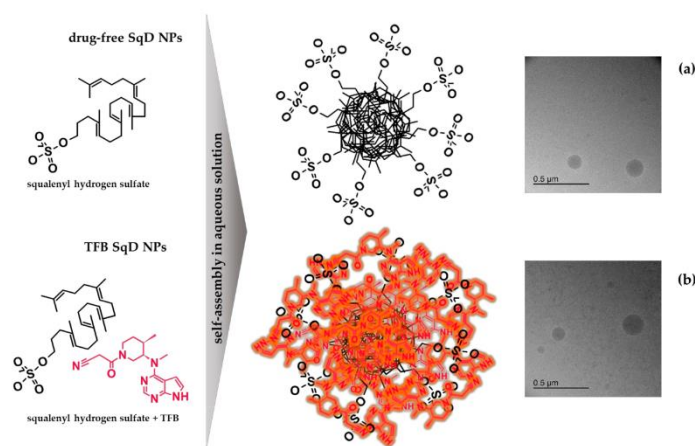


Figure 1. Schematic illustration of SqD and TFB chemical structures, and the self-assembled drug-free SqD NPs and TFB SqD NPs. Morphology of (a) drug-free SqD NPs and (b) TFB SqD NPs visualized by cryo-TEM. Black scale bar equals 0.5 μm.

2.4. Quantification of Drug Loading Capacity and Encapsulation Efficiency

The quantity of drug in the TFB SqD NPs was determined using a direct method. In brief, 500 μL of the TFB SqD NPs 5.5 mg/mL suspension was centrifuged at 24,400 g, 4 °C, for 4 h. Both supernatant and NPs sediment were collected, of which the supernatant was further diluted in MeOH and ready for high performance liquid chromatography (HPLC, Supplemental part 2) analysis, while the NPs sediment was freeze dried (Lyo-Cube 4-8, Alpha 2-4 LSC, Christ, Osterrode am Harz, Germany). Following the total weight measurement of the dried NPs sediment, it was solubilized in a predetermined volume of MeOH, then sonicated for 1 h in an ultrasound bath (Bandelin, Sonorex, Bandelin electronic GmbH and Co. KG, Berlin, Germany). The subsequent solution was diluted in MeOH and analyzed by HPLC (Supplemental part 2). The encapsulation efficiency (EE) and the drug loading capacity (LC) of TFB SqD NPs were calculated as follows:

$$EE (\%) = (\text{TFB amount in NPs sediment} / \text{total TFB amount}) \times 100 \quad (1)$$

$$LC (\%) = (\text{TFB amount in NPs sediment} / \text{total weight of NPs sediment}) \times 100 \quad (2)$$

where in:

$$\text{total TFB amount} = \text{TFB amount in the NPs sediment} + \text{TFB amount in the supernatant} \quad (3)$$

At least three experiments were conducted and results are presented as mean \pm standard deviation (SD).

2.5. Size, Polydispersity Index, Zeta-Potential, and pH Value Determination

The hydrodynamic diameter (reported as intensity-based z-average) and the polydispersity index (PDI) were determined by dynamic light scattering (DLS) using a Zetasizer (Zetasizer Nano ZSP, ZEN5600, Malvern, UK, Software 7.02). The zeta-potential was determined by electrophoretic light scattering (ELS), using the same equipment. The Zetasizer was equipped with a He-Ne Laser at a wavelength of 633 nm, DLS was done at a backscattering angle of 173° and ELS at an angle of 13°. For the measurements, 20 μ L of the final NP-suspension was diluted in 800 μ L water. The pH of the final NP-suspensions and aqueous drug solution of TFB-C in phos-buffer (2 mg TFB/mL) (aqTFB-C) was determined by a pH meter (Mettler Toledo Seven Compact PHS 210 including pH electrode Mettler Toledo InLab® Micro, Switzerland). To determine the colloidal storage stability of TFB SqD NPs and drug-free SqD NPs at 4 °C, the measurements were repeated after 12 and 24 days. Three experiments were conducted and measurements were done in triplicates. Results are reported as mean \pm SD.

2.6. Morphology

The morphology of the TFB SqD NPs and of the drug-free SqD NPs were determined by cryogenic transmission electron microscopy (cryo-TEM). Three microliters of each NP-suspension were plotted for two seconds on a holey carbon grid (S147-4, Plano, Wetzlar, Germany) and subsequently plunged into -165 °C liquid ethane. Under liquid nitrogen conditions they were transferred to a Gatan model 914 cryo-TEM sample holder (Pleasanton, CA, USA). The sample analysis was done at -170 °C under low dose conditions, using a JEOL (Akishima, Tokio, Japan) JEM-2100 LaB6 TEM equipped with a Gatan Orius SC1000 CCD camera to gain bright field images.

2.7. In Vitro Release Study

The *in vitro* release profile of TFB SqD NPs was determined at pH 5.0 (ammonium acetate buffer, 10 mM) and 32 °C to simulate skin conditions [48], over a 24 h period using a dialysis bag method. In brief, following the equilibration of the dialysis membrane in the ammonium acetate buffer, 900 μ L of the final TFB SqD NPs suspension was loaded into a dialysis bag consisting of regenerative cellulose (MWCO 10 kDa). Subsequently, the loaded dialysis bag was sunk in 30.0 mL ammonium acetate buffer, and the whole system was shaken at 100 rpm, 32 °C. At predetermined time points (0.25, 0.5, 0.75, 1, 2, 4, 6, and 24 h), 500 μ L of the release medium was withdrawn, and an equal volume of fresh buffer was added. The samples were then analyzed by HPLC (Supplemental part 2). The maximum solubility of TFB in the ammonium acetate buffer was determined at 115.6 ± 9.3 μ g/mL prior to the experiment. Three experiments were conducted and results are expressed as mean \pm SD.

2.8. Ex Vivo and In Vivo Performance of TFB SqD NPs

We evaluated the HFs targeted transport and therapeutic efficacy of TFB SqD NPs in comparison to plain drug solutions in an *ex vivo* pig ear model and an allergic dermatitis mouse model, respectively.

2.8.1. Targeted Follicular Transport of TFB in a Pig Ear Model

Excised hairy human skin cannot be used for follicular penetration studies of therapeutics, due to the shrinkage of the follicular reservoir of around 90%. This effect can be precluded in the pig ear model, where the skin remains on the cartilage [49–51]. Hence, in this study, we investigated the follicular and interfollicular penetration and permeation of TFB (the terms penetration and permeation are defined in the Supplemental part 4 and used according to Ref. [52]) in a pig ear model, which we optimized from two previously described methods, namely the differential stripping method [45,53] and the single HF harvesting method [46]. The differential stripping consists of two major steps—the surface

cleaning by tape stripping to remove the formulation left on the skin surface, and the harvesting of the follicular casts by cyanoacrylate biopsies, including the formulation deposited in HFs. Unfortunately, the cyanoacrylate biopsies were not compatible and interfered with the TFB LC-MS quantification method. Therefore, the harvesting of the HFs was done as previously described by Kalia and coworkers: intact HFs were collected by 1 mm diameter punch biopsies (follicular skin). Accordingly, interfollicular drug penetration was determined by HF-free 1 mm diameter punch biopsies (interfollicular skin) [46]. The investigated drug formulations and tested vehicle control groups are summarized in Table 1.

Table 1. Abbreviation, composition, formulation type, number of pig ears, and number of application areas used for *ex vivo* pig ear study on topical penetration and permeation pathways.

Group	Abbreviation	Components	Formulation Type	No. Ear	No. Area
Treatment (TFB 2 mg/mL)	TFB SqD NPs	TFB ¹ , SqD ² , phos-buffer ³	suspension	4	7
	aqTFB-C	TFB-C ⁴ , phos-buffer ³	solution	2	4
	TFB-EtOH	TFB ¹ , EtOH ⁵ :H ₂ O (50:50 <i>v/v</i>)	solution	3	6
	TFB-acet:DMSO	TFB ¹ , acetone:DMSO ⁶ (7:1 <i>v/v</i>)	solution	3	6
vehicle control	phos-buffer	phos-buffer ³	solution	4	4
	EtOH:H ₂ O	EtOH ⁵ :H ₂ O (50:50 <i>v/v</i>)	solution	3	3
	acet:DMSO	acetone:DMSO ⁶ (7:1 <i>v/v</i>)	solution	3	3

¹ tofacitinib free base, ² anionic squalenyl derivative, ³ phosphate buffer, ⁴ tofacitinib citrate, ⁵ ethanol, ⁶ dimethyl sulfoxide.

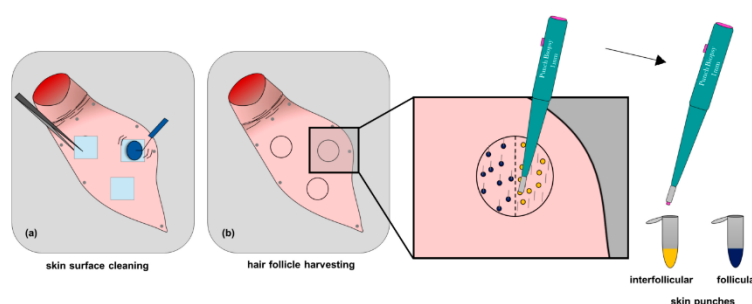
The experiments on the pig ear model were as follows: the ears were collected from freshly slaughtered pigs, cleaned with water, and carefully dried with paper tissues. The ears were stored for a maximum of 7 days at 4 °C. Only ears with intact skin were used and the experiments were conducted on the outer auricle of the ear. In an experiment, a pig ear was firstly fixed on an aluminum foil covered wooden board. Subsequently, the hair shafts were shortened to 1 mm with an electrical clipper, during which the skin barrier was surely maintained (Braun Bartschneider, BT3040, Procter and Gamble Service GmbH, Schwalbach am Taunus, Germany). The areas for investigation with a surface area of 1.767 cm² were marked, and there were at least two areas for the treatment group and one area for the vehicle control on each ear (Table 1). A 15 µL of the formulation—treatment or vehicle control—was applied on each marked area, which was then massaged with a gloved fingertip for 3 min to enhance the penetration into HFs [54]. After 1 h incubation at 32 °C, the skin surface was cleaned by means of tape stripping (Scheme 1a) [45,53].

For sufficient skin surface cleaning, 10 subsequent tape strips were pressed onto the skin surface by using a paint roller to minimize the influence of furrows and wrinkles [45,55]. Afterwards, the 1 mm diameter punch biopsies (equals 0.785 mm²) of follicular and interfollicular skin were collected as described in Scheme 1b. Briefly, the surface-cleaned area of investigation was equally divided into two parts. On one part, all HFs—described in Scheme 1b follicular skin, dark blue punches—were collected by means of a stereomicroscope (Model SZX7, SZX2-ILLTQ, Olympus Corporation, Tokyo, Japan). On the other part, the interfollicular skin—described in Scheme 1b interfollicular skin, orange punches—were collected. Notably, an equal number of punch biopsies were collected in each part and stored in 2 mL tubes. Moreover, a skin area of 4.91 cm² including the rest of the treated area and the surrounding skin was also punched (called “skin rest”) for TFB mass balance calculation purposes [45]. Furthermore, TFB left on the materials that were in contact with the formulation, including glove-fingertip, tape strips, and skin rest, were extracted in 2 mL of a mixed MeOH:ammonium acetate buffer (pH 5.0, 5 mM) ratio of 60:40 *v/v* (called “extraction media”). The 0.785 mm² punch biopsies were extracted in 500 µL extraction media. All samples were sonicated in an ultrasonic bath (Sonorex, Bandelin electronic GmbH and Co. KG, Berlin, Germany) for 1 h, subsequent shaking at 350 rpm for 2 h. Following, the samples were centrifuged at 24,400 *g*, at 20 °C for 5 min, the supernatant was filtered and if necessary diluted prior to LC-MS analysis (Supplemental

part 3). According to the FDA bioanalytical method validation guideline sensitivity criteria [56], the lower limit of quantification (LLOQ) was at least 5 times higher than the response from the blank matrix value. The LLOQ was determined separately for each different matrix type, by multiplying the highest found blank matrix value times 5, and the values below LLOQ were excluded. The TFB mass balance was determined for each treated area as follows:

$$\text{Mass balance (\%)} = \frac{(\text{TFB in glove-fingertip} + \text{TFB in tape strips} + \text{TFB in follicular and interfollicular skin punches} + \text{TFB in skin rest})}{\text{applied TFB amount on treated area}} \times 100 \quad (4)$$

Results are reported as mean \pm SD, illustrated by a scatter dot plot.



Scheme 1. Graphic illustration: targeted follicular transport study of TFB in a pig ear model (a) skin surface cleaning by means of tape stripping and (b) follicular and interfollicular skin harvesting by 0.785 mm² punch biopsies by means of stereomicroscopy.

2.8.2. The Therapeutic Efficacy of TFB in an Allergic Dermatitis Mouse Model

In this study, we employed the allergic dermatitis mouse model to gain the first insights in the therapeutic efficacy of the TFB SqD NPs. The efficacy of the TFB SqD NPs in reducing inflammatory response was compared to the positive control—TFB-acet:DMSO—and aqTFB-C formulation (Table 2). Drug-free SqD NPs and acetone:DMSO solution served as vehicle control groups. The reduction of the ear swelling at 24 h post-challenging by allergen served as readout to evaluate the efficacy of a formulation in reducing inflammatory response in mice.

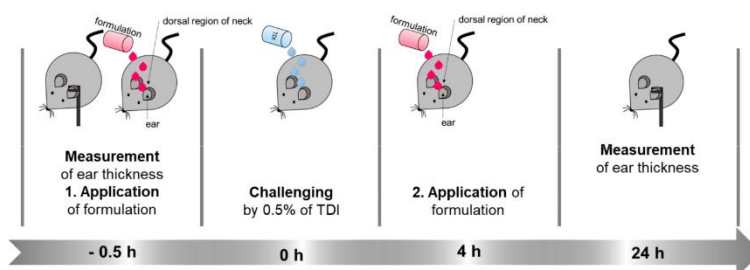
Table 2. Abbreviation, composition, formulation type, and number of treated mice of treatment and respective vehicle control groups for *in vivo* dermatitis mouse model study on biological response upon topical application.

Group	Abbreviation	Components	Formulation Type	No. Mice
Treatment TFB 2 mg/mL	TFB SqD NPs	TFB ¹ , SqD ² , phos-buffer ³	suspension	7
	aqTFB-C	TFB-C ⁴ , phos-buffer ³	solution	7
	TFB-acet:DMSO	TFB ¹ , acetone:DMSO ⁵ (7:1 v/v)	solution	7
vehicle control	Drug-free SqD NPs	SqD ² , phos-buffer ³	suspension	7
	Drug-free acet:DMSO	acetone:DMSO ⁵ (7:1 v/v)	solution	7

¹ tofacitinib free base, ² anionic squalenyl derivative, ³ phosphate buffer, ⁴ tofacitinib citrate, ⁵ dimethyl sulfoxide.

The animal procedure was as follows: prior to the experiments, the allergic dermatitis mouse model was established by sensitizing and challenging the mice for one month with the contact allergen toluene 2,4 diisocyanate (TDI) in acetone as described in previous studies [47,57,58]. On the experiment day, the ear thickness was measured and the formulations were applied (Scheme 2, −0.5 h).

After 30 min, the mice were challenged by applying 20 μ L and 30 μ L of 0.5% TDI in acetone on the mouse ear and the neck's dorsal region, respectively (Scheme 2, 0 h). After 4 h, the formulations were applied for the second time (Scheme 2, 4 h). The ear thickness was measured again at 24 h post-challenge, and the mice were sacrificed afterwards (Scheme 2, 24 h). The reduction of the ear swelling was determined by subtracting the ear thickness after 24 h of challenge from the ear thickness before the challenge. Results are reported as mean \pm standard error (SEM).



Scheme 2. Graphic illustration of the chronology of the formulation application, ear thickness measurements, and challenging time points of the allergic dermatitis mouse model. Each group contained of 7 female BALB/c (BALB/cAnNCrI) mice. The ability of the applied formulations to reduce inflammatory response was monitored by ear swelling reduction 24 h post-allergen challenge (TDI: toluene 2,4 diisocyanate).

2.9. Statistics

Statistical analysis was performed by GraphPad Prism 8.0 or Microsoft Excel 2016/2019. Significant differences between formulations in the *ex vivo* pig ear experiment were tested for follicular and interfollicular skin area separately by one-way ANOVA with multiple comparisons by Tukey's test. Significant difference between the vehicle control group and treatment group in *in vivo* mouse model was detected by an unpaired two-tailed *t*-test. Significance levels are reported as follows: $p \geq 0.05$: n.s., $p = 0.01$ to 0.05 : *, $p = 0.001$ to 0.01 : **, and $p < 0.001$: ***.

3. Results and Discussion

3.1. Characteristics of TFB SqD NPs

The stable and uniform TFB SqD NPs with a size of 239.1 ± 43.5 nm and PdI of 0.21 ± 0.01 (Table 3 and Figure S1) were formed by simultaneous self-assembly of the amphiphilic SqD and TFB using the solvent evaporation method. The anionic SqD (Figure 1) containing a hydrophilic hydrogen sulfate head-group and a hydrophobic squalenyl moiety potentially allows the loading of TFB (Figure 1) in both compartments via charged and hydrophobic interactions, respectively.

Table 3. Physicochemical characteristics, including size, polydispersity index (PdI), zeta-potential, pH, loading capacity (LC) and encapsulation efficiency (EE), of SqD nanoparticles (NPs) determined by dynamic light scattering (DLS), electrophoretic light scattering (ELS), pH measurements, and HPLC. Results are reported as mean \pm SD.

Physicochemical Characteristic	Drug-Free SqD NPs	TFB SqD NPs
size (nm)	225.7 ± 20.3	239.1 ± 43.5
PdI	0.19 ± 0.02	0.21 ± 0.01
zeta-potential (mV)	-54.5 ± 1.7	-59.9 ± 2.3
pH	6.28 ± 0.02	6.31 ± 0.02
LC (%)	N.A.	20.1 ± 2.1
EE (%)	N.A.	19.8 ± 3.6

We have previously reported the significant drug LC of SqD NPs yet also pointed out that the loading of small molecules—containing polar groups and having rather poor water-solubility—is challenging, only allowing e.g., the maximum LC at around 10% of a quorum sensing inhibitor [43] or at around 9% of Nile red [44]. In this study, it is surprising that the LC of TFB could be maximized at $20.1\% \pm 2.2\%$, with a corresponding EE at $19.8\% \pm 3.6\%$. Most importantly, such a high LC of TFB in SqD NPs enhanced the TFB solubility in phos-buffer up to 2 mg TFB/mL, which was around 40 times higher than the maximum solubility of TFB alone in the same buffer ($47.9 \pm 0.2 \mu\text{g/mL}$). The negative zeta-potential of the drug-free SqD NPs ($-54.5 \pm 1.7 \text{ mV}$, Table 3) did not change upon drug loading ($-59.9 \pm 2.3 \text{ mV}$, Table 3), which led to the assumption that TFB might be loaded rather via hydrophobic than charged interactions into SqD NPs [44]. It is worth noting that the pH value plays a crucial role in the optimization of TFB loading. As the pH of human skin is slightly acidic around 5 [59], a comparable pH of the formulation is hence preferred. However, the better solubility of TFB in acidic pH [60] does not benefit the NP encapsulation. In our optimization, an ideal compromise was found by preparing the TFB SqD NPs in a phos-buffer, resulting in a suspension with a pH of 6.3 (Table 3).

The low negative zeta potential of the NPs ($-59.9 \pm 2.3 \text{ mV}$, Table 3) could stabilize the suspension well by strong charge repulsion [61]. The drug-free SqD NPs having similar characteristics to the TFB SqD NPs—a hydrodynamic size of $225.7 \pm 20.3 \text{ nm}$, PdI of 0.19 ± 0.02 , and zeta-potential of $-54.5 \pm 1.7 \text{ mV}$ —served as a control (Table 3 and Figure S2). The morphology of the NP-suspensions was visualized by cryo-TEM, demonstrating homogeneous, dense, and spherical shaped NPs in both drug-free SqD NPs (Figure 1a) and TFB SqD NPs (Figure 1b).

3.2. Stability of TFB SqD NPs

Both drug-free SqD NPs and TFB SqD NPs exhibited good colloidal stability at storage conditions over 24 days (Figure 2a–c). Interestingly, the aqTFB-C solution (2 mg TFB/mL) in phos-buffer, showed a lower pH value at 4.54 ± 0.03 compared to the NP formulations and was further decreasing to 4.17 ± 0.22 after 24 days at 4°C (Figure 2d). This can be explained by the interaction of the citrate salt with the disodium hydrogen phosphate, which forms a new buffer system and lowers pH [62]. Notably, crystals were visible in the TFB-C in phos-buffer solution upon storage at 4°C after 2 weeks. No visual changes were observed over the 24-days in drug-free SqD NPs and TFB SqD NPs.

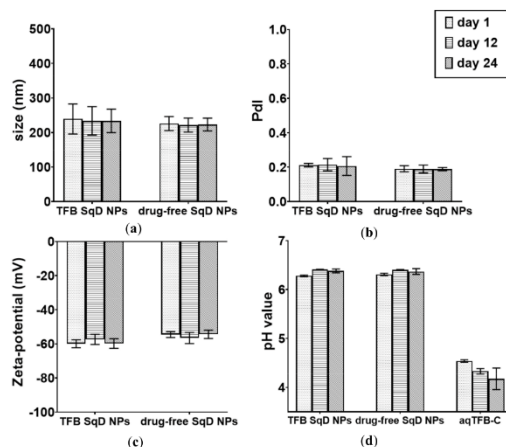


Figure 2. Colloidal stability of TFB SqD NPs, drug-free SqD NPs, and aqTFB-C solution at 4°C , over a 24-day period, investigated by DLS, ELS, and pH measurements. (a) Hydrodynamic diameter (nm), (b) polydispersity index, (c) zeta-potential (mV), and (d) pH-value. Results are presented as mean \pm SD.

3.3. Release Profile of TFB SqD NPs

We evaluated the *in vitro* release profile of TFB SqD NPs and assessed the TFB stability in skin mimicking conditions using HPLC [48,59]. Figure 3 shows a burst TFB release of around 40% in the first 0.25 h followed by a continuous slower release of TFB until complete. This data set proves the releasing capacity of the TFB SqD NPs. Moreover, the HPLC analysis of TFB over 24 h did not show any signs of drug degradation. It is also important to highlight that a simple correlation between *in vitro* and *in vivo* release of TFB SqD NPs cannot be drawn, since the lipid derived SqD NPs would interact differently with the sebum milieu inside the HFs. In addition, the changing pH profile inside HFs was not taken into account [63,64]. Therefore, further *in vivo* experiments would be necessary to evaluate the release profile of TFB SqD NPs in HFs.

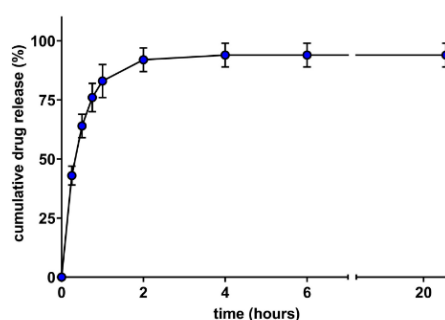


Figure 3. *In vitro* cumulative drug release study of TFB SqD NPs at pH 5.0 and 32 °C over 24 h. Results are presented as mean \pm SD.

3.4. Ex vivo and In vivo Performance of TFB SqD NPs

3.4.1. Targeted Follicular Transport of TFB in a Pig Ear Model

We first investigated the targeted follicular delivery of TFB in a pig ear model. The quantity of TFB in nanograms per 0.785 mm² follicular (Figure 4a) and interfollicular (Figure 4b) skin surface cleaned punch biopsy was analyzed. The results were used to compare the performance of TFB SqD NPs to TFB alone formulations—aqTFB-C, TFB-EtOH, and TFB-acet:DMSO. Moreover, TFB-acet:DMSO has shown a significant effect in an allergic dermatitis mouse model compared to vehicle control [47]. Therefore, it was used as a standard to compare the performance of TFB SqD NPs.

Overall, the results clearly demonstrated that the follicular transport was the major route for drug penetration compared to the interfollicular route. Figure 4a compares the TFB amount in the follicular skin delivered by different formulations. The aqTFB-C and TFB-EtOH delivered 16.03 \pm 5.11 ng/0.785 mm² and 14.68 \pm 5.59 ng/0.785 mm² of TFB, respectively, into the follicular skin, which were significantly less than that of the TFB SqD NPs at 30.06 \pm 8.32 ng/0.785 mm². Interestingly, the ability of SqD NPs to deliver TFB to the follicular skin was found to be as good as the TFB-acet:DMSO, which allowed the TFB delivery of 27.03 \pm 5.60 ng/0.785 mm².

As shown in Figure 4b, the TFB amount in interfollicular skin was, in contrast, relatively low and not significantly different regardless of different tested formulations. The amount of TFB penetrating interfollicular skin was slightly more pronounced when using the TFB-acet:DMSO (5.14 \pm 4.29 ng/0.785 mm², Figure 4b) compared to the other tested formulations (3.28 \pm 1.91 ng/0.785 mm² for TFB SqD NPs, 0.77 \pm 0.20 ng/0.785 mm² for aqTFB-C, and 1.70 \pm 1.26 ng/0.785 mm² for TFB-EtOH, Figure 4b). The overall higher drug penetration by follicular skin compared to interfollicular skin stresses the impact HFs have on general drug penetration into skin, and are in good agreement to previous findings [65].

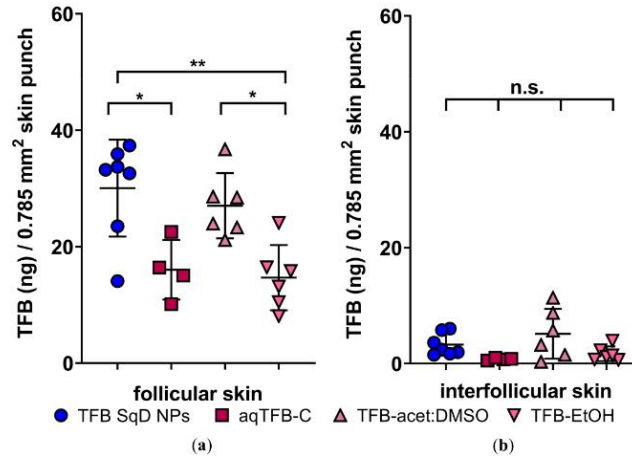


Figure 4. TFB deposition in nanograms per 0.785 mm² skin punch of surface-cleaned application area in (a) follicular skin and (b) interfollicular skin. Treatment groups are presented as TFB SqD NPs in blue circles, aqTFB-C in dark red squares, TFB-acet:DMSO in purple upward triangles, and TFB-EtOH in pink downward triangles respectively. Results presented as mean \pm SD in a scatter dot plot. Significant differences are presented as $p \geq 0.05$: n.s., $p = 0.01$ to 0.05 : *, and $p = 0.001$ to 0.01 : **, tested for follicular and interfollicular skin separately by one-way ANOVA with multiple comparisons by a Tukey's test.

The guideline of the scientific committee on consumer safety recommends a mass balance in the range of $100\% \pm 15\%$ [66], these criteria were met for all formulation types except for the TFB-acet:DMSO (Table 4). In addition to the total organic solvent-based formulation of TFB-acet:DMSO, the lack of mass recovery leads to the assumption of uncontrolled and fast drug penetration and permeation. Taking together, these results imply the advantages of using aqueous SqD NPs for the targeted follicular delivery of TFB.

Table 4. Mass balance of TFB applied on application area in *ex vivo* pig ear skin experiment. Results are presented as mean \pm SD.

Treatment Group	Mass Balance (%)
TFB SqD NPs	90.4 \pm 6.4
aqTFB-C	87.4 \pm 1.9
TFB-acet:DMSO	69.7 \pm 10.7
TFB-EtOH	95.7 \pm 3.3

3.4.2. The Therapeutic Efficacy of TFB in an Allergic Dermatitis Mouse Model

The topical formulation of TFB in an organic mixture of acetone:DMSO (7:1 *v/v*) has previously shown a reduction in inflammatory response in an allergic dermatitis mouse model at all tested TFB concentrations that ranged from 0.1% to 0.5% (*w/v*) compared to vehicle controls [47]. These results implied the therapeutic efficacy of TFB at preclinical levels, and validated the allergic dermatitis mouse model [47]. This Th2 driven mouse model resembles major characteristics of acute atopic dermatitis (AD) lesions in regard to cytokine pattern and prediction of effectiveness of, e.g., phosphodiesterase 4 inhibitors [67], JAK-inhibitors [47], and glucocorticoids [57], all therapeutic options used or in clinical phase for treatment of human AD.

Therefore, we used this model and TFB-acet:DMSO as a positive treatment control to evaluate the therapeutic efficacy of TFB SqD NPs and aqTFB-C. Notably, it should be taken into account that the acetone:DMSO solution cannot be considered as a safe drug delivery system for topical application. DMSO itself might alter the cellular processes and cause some unknown biological effects [68,69].

However, DMSO containing formulations are often used for preclinical research due to good drug solubility in DMSO and penetration enhancing effects [69]. As shown in Figure 5, mice treated with TFB-acet:DMSO demonstrated a significant reduction of around 50% in ear swelling compared to that from the drug-free acet:DMSO ($50.80 \pm 11.09 \mu\text{m}$ and $97.97 \pm 14.05 \mu\text{m}$ ear swelling, respectively), which is in agreement with Fukuyama et al. [47]. The TFB SqD NPs were able to reduce the ear swelling by around 20% compared to drug-free SqD NPs ($76.20 \pm 5.54 \mu\text{m}$ and $94.34 \pm 11.71 \mu\text{m}$ ear swelling, respectively). The aqTFB-C did not show any reducing effect ($112.5 \pm 30.16 \mu\text{m}$ ear swelling).

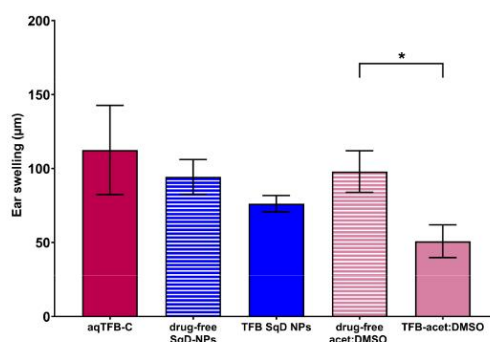


Figure 5. Ear swelling reduction in *in vivo* allergic dermatitis mouse model after 24 h allergen challenge. Application of formulation 30 min prior and 4 h after challenging. Tested treatment groups are: aqTFB-C (filled dark red bar), TFB SqD NPs (filled dark blue bar), including control group drug-free SqD NPs (striped dark blue bar), and TFB-acet:DMSO (filled purple bar), including control group drug-free acet:DMSO (striped purple bar). Results are presented as mean \pm SEM. Significant difference between vehicle control group and treatment group was tested by an unpaired two-tailed *t*-test. Significance levels are reported as $p \geq 0.05$: n.s. and $p = 0.01$ to 0.05 : *.

In general, these results were actually well correlated to the *ex vivo* pig ear outcomes. Particularly, the aqTFB-C provided a very low penetration and permeation in both follicular and interfollicular skin *ex vivo*, also performed poorly in the allergic dermatitis mouse model *in vivo*. Despite resulting a comparable TFB delivery in follicular skin in the pig ear model, TFB SqD NPs did not reduce the inflammatory response as much as TFB-acet:DMSO did in the mouse model. Such results could be explained by the higher TFB interfollicular penetration and permeation of TFB-acet:DMSO, and it has to be taken into account, that not only the follicular skin, but the whole treated skin area (follicular and interfollicular) was affected in the allergic dermatitis mice model. Furthermore, the low mass balance of TFB-acet:DMSO in the pig ear model also suggested that this formulation had uncontrollable penetration and permeation rates and depth into the skin, possibly leading to an overall higher delivered TFB amount into the whole skin tissue. As also discussed in the previous study, the addition of DMSO as a vehicle for NP-suspension is likely to enhance the interfollicular skin permeation, while the aqueous NP-suspension only maximized the follicular deposition [70]. These results demonstrate quite plainly that it is important to take *ex vivo* data of penetration and permeation pathways into account when evaluating *in vivo* data of drug effects of topically applied formulations. Taking the shown follicular targeting of the *ex vivo* pig ear model and the measurable anti-inflammatory effect of the *in vivo* mouse model into consideration, our TFB SqD NP was clearly the best option for safe and efficient delivery of TFB into the HF. The appropriate TFB concentration for a topical delivery and the overall biological effects have to be further determined, to meet the needs for a safe and effective nanomedicine against AA and other skin diseases.

4. Conclusions

In this study, we successfully showed the preparation of TFB SqD NPs with a satisfying drug LC of 20% and an enhanced drug solubility, up to 40 times in phos-buffer compared to the plain drug. Moreover, we maximized the targeted delivery of TFB into the hair follicles, as demonstrated in an *ex vivo* pig ear model. Thereby, NPs were able to provide controlled drug delivery to the target site, which is expected to minimize adverse effects due to high drug amounts in the interfollicular area and high systemic drug levels. While safe and well tolerated by avoiding any organic solvent, TFB SqD NPs showed a pharmacological effect in an *in vivo* mouse dermatitis model. Taking the *ex vivo* and *in vivo* results together, we have clearly demonstrated, that TFB SqD NPs are favorable to achieve controlled and targeted delivery of TFB into HFs.

Supplementary Materials: The following are available online at <http://www.mdpi.com/1999-4923/12/12/1131/s1>, Part 1, Particle size distribution data by dynamic light scattering (DLS) of SqD NPs, Figure S1: Particle size distribution of TFB SqD NPs determined by DLS, Figure S2: Particle size distribution of drug-free SqD NPs determined by DLS; Part 2, High performance liquid chromatography method used for quantitative tofacitinib (TFB) determination; Part 3, LC-MS/MS method used for quantitative tofacitinib (TFB) determination; part 4, Definitions.

Author Contributions: Conceptualization, C.-M.L., B.L., U.F.S., T.V. and W.B.; methodology, R.C., U.F.S., D.-K.H. and W.B.; investigation, R.C., D.-K.H., S.L., J.W. and W.B.; writing—original draft preparation, R.C.; writing—review and editing, all authors; visualization, M.K.; supervision, C.-M.L., B.L., U.F.S., T.V. and W.B.; funding acquisition, T.V. and C.-M.L. All authors have read and agreed to the published version of the manuscript.

Funding: This work was supported by Rolf M. Schwiete Stiftung, Mannheim, Germany (Project-Nr. 14/2016). We acknowledge support by the Deutsche Forschungsgemeinschaft (DFG; German Research Foundation) and Saarland University within the funding program Open Access Publishing.

Acknowledgments: We thank Pascal Paul for help with LC-MS analytic and tesa SE, Norderstedt, GER for the kind donation of material and Schlachthof Färber, Zweibrücken, GER for the kind donation of pig ear skin.

Conflicts of Interest: The authors declare no conflict of interest. The funders had no role in the design of the study; in the collection, analyses, or interpretation of data; in the writing of the manuscript, or in the decision to publish the results.

References

1. Pratt, C.H.; King, L.E.; Messenger, A.G.; Christiano, A.M.; Sundberg, J.P. Alopecia areata. *Nat. Rev. Dis. Primers* **2017**, *3*, 17011. [[CrossRef](#)] [[PubMed](#)]
2. Strazzulla, L.C.; Wang, E.H.C.; Avila, L.; Lo Sicco, K.; Brinster, N.; Christiano, A.M.; Shapiro, J. Alopecia areata: Disease characteristics, clinical evaluation, and new perspectives on pathogenesis. *J. Am. Acad. Dermatol.* **2018**, *78*, 1–12. [[CrossRef](#)] [[PubMed](#)]
3. Mirzoyev, S.A.; Schrum, A.G.; Davis, M.D.P.; Torgerson, R.R. Lifetime incidence risk of alopecia areata estimated at 2.1% by Rochester Epidemiology Project, 1990–2009. *J. Investig. Dermatol.* **2014**, *134*, 1141–1142. [[CrossRef](#)] [[PubMed](#)]
4. Bertolini, M.; McElwee, K.; Gilhar, A.; Bulfone-Paus, S.; Paus, R. Hair follicle immune privilege and its collapse in alopecia areata. *Exp. Dermatol.* **2020**. [[CrossRef](#)] [[PubMed](#)]
5. Gilhar, A.; Keren, A.; Paus, R. JAK inhibitors and alopecia areata. *Lancet* **2019**, *393*, 318–319. [[CrossRef](#)]
6. Strazzulla, L.C.; Wang, E.H.C.; Avila, L.; Lo Sicco, K.; Brinster, N.; Christiano, A.M.; Shapiro, J. Alopecia areata: An appraisal of new treatment approaches and overview of current therapies. *J. Am. Acad. Dermatol.* **2018**, *78*, 15–24. [[CrossRef](#)] [[PubMed](#)]
7. Gupta, A.K.; Carviel, J.L.; Abramovits, W. Efficacy of tofacitinib in treatment of alopecia universalis in two patients. *J. Eur. Acad. Dermatol. Venereol.* **2016**, *30*, 1373–1378. [[CrossRef](#)]
8. Craiglow, B.G.; King, B.A. Killing two birds with one stone: Oral tofacitinib reverses alopecia universalis in a patient with plaque psoriasis. *J. Investig. Dermatol.* **2014**, *134*, 2988–2990. [[CrossRef](#)]
9. FDA. XELJANZ (Tofacitinib). Available online: https://www.accessdata.fda.gov/drugsatfda_docs/label/2018/203214s018lbl.pdf (accessed on 7 August 2020).
10. Divito, S.J.; Kupper, T.S. Inhibiting Janus kinases to treat alopecia areata. *Nat. Med.* **2014**, *20*, 989–990. [[CrossRef](#)]

11. Xing, L.; Dai, Z.; Jabbari, A.; Cerise, J.E.; Higgins, C.A.; Gong, W.; de Jong, A.; Harel, S.; DeStefano, G.M.; Rothman, L.; et al. Alopecia areata is driven by cytotoxic T lymphocytes and is reversed by JAK inhibition. *Nat. Med.* **2014**, *20*, 1043–1049. [[CrossRef](#)]
12. Tegtmeier, K.; Zhao, J.; Maloney, N.J.; Atassi, G.; Beestrup, M.; Lio, P.A. Off-label studies on tofacitinib in dermatology: A review. *J. Dermatol. Treat.* **2019**, 1–11. [[CrossRef](#)] [[PubMed](#)]
13. Shreberk-Hassidim, R.; Ramot, Y.; Zlotogorski, A. Janus kinase inhibitors in dermatology: A systematic review. *J. Am. Acad. Dermatol.* **2017**, *76*, 745–753.e19. [[CrossRef](#)] [[PubMed](#)]
14. Schwartz, D.M.; Kanno, Y.; Villarino, A.; Ward, M.; Gadina, M.; O’Shea, J.J. JAK inhibition as a therapeutic strategy for immune and inflammatory diseases. *Nat. Rev. Drug Discov.* **2017**, *16*, 843–862. [[CrossRef](#)] [[PubMed](#)]
15. Hodge, J.A.; Kawabata, T.T.; Krishnaswami, S.; Clark, J.D.; Telliez, J.-B.; Dowty, M.E.; Menon, S.; Lamba, M.; Zwillich, S. The mechanism of action of tofacitinib—An oral Janus kinase inhibitor for the treatment of rheumatoid arthritis. *Clin. Exp. Rheumatol.* **2016**, *34*, 318–328.
16. FDA Drug Safety Communication. FDA Approves Boxed Warning about Increased Risk of Blood Clots and Death with Higher Dose of Arthritis and Ulcerative Colitis Medicine Tofacitinib (Xeljanz, Xeljanz XR). Available online: <https://www.fda.gov/drugs/drug-safety-and-availability/fda-approves-boxed-warning-about-increased-risk-blood-clots-and-death-higher-dose-arthritis-and> (accessed on 7 August 2020).
17. Blume-Peytavi, U.; Vogt, A. Translational Positioning of Janus Kinase (JAK) Inhibitors in Alopecia Areata. *EBioMedicine* **2015**, *2*, 282–283. [[CrossRef](#)]
18. Kandekar, S.G.; Del Río-Sancho, S.; Lapteva, M.; Kalia, Y.N. Selective delivery of adapalene to the human hair follicle under finite dose conditions using polymeric micelle nanocarriers. *Nanoscale* **2018**, *10*, 1099–1110. [[CrossRef](#)]
19. Mittal, A.; Schulze, K.; Ebensen, T.; Weißmann, S.; Hansen, S.; Lehr, C.M.; Guzmán, C.A. Efficient nanoparticle-mediated needle-free transcutaneous vaccination via hair follicles requires adjuvantation. *Nanomedicine* **2015**, *11*, 147–154. [[CrossRef](#)]
20. Lademann, J.; Richter, H.; Teichmann, A.; Oberg, N.; Blume-Peytavi, U.; Luengo, J.; Weiss, B.; Schaefer, U.F.; Lehr, C.-M.; Wepf, R.; et al. Nanoparticles—An efficient carrier for drug delivery into the hair follicles. *Eur. J. Pharm. Biopharm.* **2007**, *66*, 159–164. [[CrossRef](#)]
21. Lademann, J.; Richter, H.; Schaefer, U.F.; Blume-Peytavi, U.; Teichmann, A.; Oberg, N.; Sterry, W. Hair follicles—A long-term reservoir for drug delivery. *Skin Pharmacol. Physiol.* **2006**, *19*, 232–236. [[CrossRef](#)]
22. Mathes, C.; Melero, A.; Conrad, P.; Vogt, T.; Rigo, L.; Selzer, D.; Prado, W.A.; de Rossi, C.; Garrigues, T.M.; Hansen, S.; et al. Nanocarriers for optimizing the balance between interfollicular permeation and follicular uptake of topically applied clobetasol to minimize adverse effects. *J. Control. Release* **2016**, *223*, 207–214. [[CrossRef](#)]
23. Melero, A.; Ferreira Ourique, A.; Stanisçuaski Guterres, S.; Raffin Pohlmann, A.; Lehr, C.-M.; Ruver Beck, R.C.; Schaefer, U. Nanoencapsulation in lipid-core nanocapsules controls mometasone furoate skin permeability rate and its penetration to the deeper skin layers. *Skin Pharmacol. Physiol.* **2014**, *27*, 217. [[CrossRef](#)] [[PubMed](#)]
24. Patzelt, A.; Mak, W.C.; Jung, S.; Knorr, F.; Meinke, M.C.; Richter, H.; Rühl, E.; Cheung, K.Y.; Tran, N.B.N.N.; Lademann, J. Do nanoparticles have a future in dermal drug delivery? *J. Control. Release* **2017**, *246*, 174–182. [[CrossRef](#)] [[PubMed](#)]
25. Radtke, M.; Patzelt, A.; Knorr, F.; Lademann, J.; Netz, R.R. Ratchet effect for nanoparticle transport in hair follicles. *Eur. J. Pharm. Biopharm.* **2017**, *116*, 125–130. [[CrossRef](#)] [[PubMed](#)]
26. Christmann, R.; Thomas, C.; Jager, N.; Raber, A.S.; Loretz, B.; Schaefer, U.F.; Tschernig, T.; Vogt, T.; Lehr, C.-M. Nanoparticle Targeting to Scalp Hair Follicles: New Perspectives for a Topical Therapy for Alopecia Areata. *J. Investig. Dermatol.* **2020**, *140*, 243–246. [[CrossRef](#)]
27. Sánchez-López, E.; Gomes, D.; Esteruelas, G.; Bonilla, L.; Lopez-Machado, A.L.; Galindo, R.; Cano, A.; Espina, M.; Ettcheto, M.; Camins, A.; et al. Metal-Based Nanoparticles as Antimicrobial Agents: An Overview. *Nanomaterials* **2020**, *10*, 292. [[CrossRef](#)]
28. Roberts, M.S.; Mohammed, Y.; Pastore, M.N.; Namjoshi, S.; Yousef, S.; Alinaghi, A.; Haridass, I.N.; Abd, E.; Leite-Silva, V.R.; Benson, H.; et al. Topical and cutaneous delivery using nanosystems. *J. Control. Release* **2017**, *247*, 86–105. [[CrossRef](#)]

29. Lademann, J.; Richter, H.; Knorr, F.; Patzelt, A.; Darvin, M.E.; Rühl, E.; Cheung, K.Y.; Lai, K.K.; Renneberg, R.; Mak, W.C. Triggered release of model drug from AuNP-doped BSA nanocarriers in hair follicles using IRA radiation. *Acta Biomater.* **2016**, *30*, 388–396. [[CrossRef](#)]
30. Paris, J.L.; Vallet-Regí, M. Ultrasound-Activated Nanomaterials for Therapeutics. *BCSJ* **2020**, *93*, 220–229. [[CrossRef](#)]
31. Ho, D.-K.; Nichols, B.L.B.; Edgar, K.J.; Murgia, X.; Loretz, B.; Lehr, C.-M. Challenges and strategies in drug delivery systems for treatment of pulmonary infections. *Eur. J. Pharm. Biopharm.* **2019**, *144*, 110–124. [[CrossRef](#)]
32. Couvreur, P. Nanoparticles in drug delivery: Past, present and future. *Adv. Drug Deliv. Rev.* **2013**, *65*, 21–23. [[CrossRef](#)]
33. Yichuan, Z. Lipid Nanoparticle-Mediated Delivery of Enhanced Costimulation Blockade to Prevent Type 1 Diabetes. Master of Science, Master's Thesis, Johns Hopkins University, Baltimore, MD, USA, 2019.
34. Bashir, S.; Aamir, M.; Sarfaraz, R.M.; Hussain, Z.; Sarwer, M.U.; Mahmood, A.; Akram, M.R.; Qaisar, M.N. Fabrication, characterization and in vitro release kinetics of tofacitinib-encapsulated polymeric nanoparticles: A promising implication in the treatment of rheumatoid arthritis. *Int. J. Polym. Mater. Polym. Biomater.* **2020**, 1–10. [[CrossRef](#)]
35. Smith, K.R.; Thiboutot, D.M. Thematic review series: Skin lipids. Sebaceous gland lipids: Friend or foe? *J. Lipid Res.* **2008**, *49*, 271–281. [[CrossRef](#)] [[PubMed](#)]
36. Reddy, L.H.; Couvreur, P. Squalene: A natural triterpene for use in disease management and therapy. *Adv. Drug Deliv. Rev.* **2009**, *61*, 1412–1426. [[CrossRef](#)] [[PubMed](#)]
37. Couvreur, P.; Stella, B.; Reddy, L.H.; Hillaireau, H.; Dubernet, C.; Desmaële, D.; Lepêtre-Mouelhi, S.; Rocco, F.; Dereuddre-Bosquet, N.; Clayette, P.; et al. Squalenoyl nanomedicines as potential therapeutics. *Nano Lett.* **2006**, *6*, 2544–2548. [[CrossRef](#)] [[PubMed](#)]
38. Desmaële, D.; Gref, R.; Couvreur, P. Squalenoylation: A generic platform for nanoparticulate drug delivery. *J. Control. Release* **2012**, *161*, 609–618. [[CrossRef](#)] [[PubMed](#)]
39. Wei, X.; Wu, J.; Zhao, G.; Galdamez, J.; Lele, S.M.; Wang, X.; Liu, Y.; Soni, D.M.; Purdue, P.E.; Mikuls, T.R.; et al. Development of a Janus Kinase Inhibitor Prodrug for the Treatment of Rheumatoid Arthritis. *Mol. Pharm.* **2018**, *15*, 3456–3467. [[CrossRef](#)]
40. Wu, X.; Zeng, X.; Wang, L.; Hang, T.; Song, M. Identification of related substances in tofacitinib citrate by LC-MS techniques for synthetic process optimization. *J. Pharm. Biomed. Anal.* **2017**, *143*, 17–25. [[CrossRef](#)]
41. Younis, U.S.; Vallorz, E.; Addison, K.J.; Ledford, J.G.; Myrdal, P.B. Preformulation and Evaluation of Tofacitinib as a Therapeutic Treatment for Asthma. *AAPS PharmSciTech* **2019**, *20*, 167. [[CrossRef](#)]
42. Ralay-Ranaivo, B.; Desmaële, D.; Bianchini, E.P.; Lepeltier, E.; Bourgaux, C.; Borgel, D.; Pouget, T.; Tranchant, J.F.; Couvreur, P.; Gref, R. Novel self assembling nanoparticles for the oral administration of fondaparinux: Synthesis, characterization and in vivo evaluation. *J. Control. Release* **2014**, *194*, 323–331. [[CrossRef](#)]
43. Ho, D.-K.; Murgia, X.; de Rossi, C.; Christmann, R.; Hüfner de Mello Martins, A.G.; Koch, M.; Andreas, A.; Herrmann, J.; Müller, R.; Empting, M.; et al. Squalenyl Hydrogen Sulfate Nanoparticles for Simultaneous Delivery of Tobramycin and an Alkylquinolone Quorum Sensing Inhibitor Enable the Eradication of *P. aeruginosa* Biofilm Infections. *Angew. Chem. Int. Ed. Engl.* **2020**, *59*, 10292–10296. [[CrossRef](#)]
44. Ho, D.-K.; Christmann, R.; Murgia, X.; de Rossi, C.; Frisch, S.; Koch, M.; Schaefer, U.F.; Loretz, B.; Desmaële, D.; Couvreur, P.; et al. Synthesis and biopharmaceutical characterization of amphiphilic squalenyl derivatives based versatile drug delivery platform. *Front. Chem.* **2020**. [[CrossRef](#)] [[PubMed](#)]
45. Raber, A.S.; Mittal, A.; Schäfer, J.; Bakowsky, U.; Reichrath, J.; Vogt, T.; Schaefer, U.F.; Hansen, S.; Lehr, C.-M. Quantification of nanoparticle uptake into hair follicles in pig ear and human forearm. *J. Control. Release* **2014**, *179*, 25–32. [[CrossRef](#)] [[PubMed](#)]
46. Lapteva, M.; Möller, M.; Gurny, R.; Kalia, Y.N. Self-assembled polymeric nanocarriers for the targeted delivery of retinoic acid to the hair follicle. *Nanoscale* **2015**, *7*, 18651–18662. [[CrossRef](#)] [[PubMed](#)]
47. Fukuyama, T.; Ehling, S.; Cook, E.; Bäumer, W. Topically Administered Janus-Kinase Inhibitors Tofacitinib and Oclacitinib Display Impressive Antipruritic and Anti-Inflammatory Responses in a Model of Allergic Dermatitis. *J. Pharmacol. Exp. Ther.* **2015**, *354*, 394–405. [[CrossRef](#)] [[PubMed](#)]
48. Marrakchi, S.; Maibach, H.I. Biophysical parameters of skin: Map of human face, regional, and age-related differences. *Contact Dermat.* **2007**, *57*, 28–34. [[CrossRef](#)] [[PubMed](#)]

49. Lademann, J.; Patzelt, A.; Richter, H.; Schanzer, S.; Sterry, W.; Filbry, A.; Bohnsack, K.; Rippke, F.; Meinke, M. Comparison of two in vitro models for the analysis of follicular penetration and its prevention by barrier emulsions. *Eur. J. Pharm. Biopharm.* **2009**, *72*, 600–604. [CrossRef] [PubMed]
50. Patzelt, A.; Richter, H.; Buettemeyer, R.; Huber, H.J.R.; Blume-Peytavi, U.; Sterry, W.; Lademann, J. Differential stripping demonstrates a significant reduction of the hair follicle reservoir in vitro compared to in vivo. *Eur. J. Pharm. Biopharm.* **2008**, *70*, 234–238. [CrossRef]
51. Lademann, J.; Richter, H.; Meinke, M.; Sterry, W.; Patzelt, A. Which skin model is the most appropriate for the investigation of topically applied substances into the hair follicles? *Skin Pharmacol. Physiol.* **2010**, *23*, 47–52. [CrossRef]
52. Buist, H.; Craig, P.; Dewhurst, I.; Hougaard Bennekou, S.; Kneuer, C.; Machera, K.; Pieper, C.; Court Marques, D.; Guillot, G.; Ruffo, F.; et al. Guidance on dermal absorption. *EFSA J.* **2017**, *15*, e04873.
53. Teichmann, A.; Jacobi, U.; Ossadnik, M.; Richter, H.; Koch, S.; Sterry, W.; Lademann, J. Differential stripping: Determination of the amount of topically applied substances penetrated into the hair follicles. *J. Investig. Dermatol.* **2005**, *125*, 264–269. [CrossRef]
54. Li, B.S.; Cary, J.H.; Maibach, H.I. Should we instruct patients to rub topical agents into skin? The evidence. *J. Dermatol. Treat.* **2019**, *30*, 328–332. [CrossRef] [PubMed]
55. Lademann, J.; Schanzer, S.; Richter, H.; Meinke, M.C.; Weigmann, H.-J.; Patzelt, A. Stripping Procedures for Penetration Measurements of Topically Applied Substances. In *Percutaneous Penetration Enhancers Drug Penetration Into/Through the Skin: Methodology and General Considerations*; Dragicevic, N.I., Maibach, H., Eds.; Springer: Berlin/Heidelberg, Germany, 2017; pp. 205–214. ISBN 978-3-662-53270-6.
56. FDA/CDER. Bioanalytical Method Validation Guidance for Industry. Available online: <https://www.fda.gov/files/drugs/published/Bioanalytical-Method-Validation-Guidance-for-Industry.pdf> (accessed on 7 August 2020).
57. Bäumer, W.; Seegers, U.; Braun, M.; Tschernig, T.; Kietzmann, M. TARC and RANTES, but not CTACK, are induced in two models of allergic contact dermatitis. Effects of cilomilast and diflorasone diacetate on T-cell-attracting chemokines. *Br. J. Dermatol.* **2004**, *151*, 823–830. [CrossRef] [PubMed]
58. Bäumer, W.; Tschernig, T.; Sülzle, B.; Seegers, U.; Lührmann, A.; Kietzmann, M. Effects of cilomilast on dendritic cell function in contact sensitivity and dendritic cell migration through skin. *Eur. J. Pharmacol.* **2003**, *481*, 271–279. [CrossRef]
59. Schmid-Wendtner, M.-H.; Korting, H.C. The pH of the skin surface and its impact on the barrier function. *Skin Pharmacol. Physiol.* **2006**, *19*, 296–302. [CrossRef] [PubMed]
60. Committee for Medicinal Products for Human Use. Assessment Report: Xeljanz; INN-Tofacitinib. Available online: https://www.ema.europa.eu/en/documents/assessment-report/xeljanz-epar-public-assessment-report_en-0.pdf (accessed on 15 September 2020).
61. Bhattacharjee, S. DLS and zeta potential—What they are and what they are not? *J. Control. Release* **2016**, *235*, 337–351. [CrossRef] [PubMed]
62. McIlvaine, T.C. A buffer solution for colorimetric comparison. *J. Biol. Chem.* **1921**, *49*, 183–186.
63. Dimde, M.; Sahle, F.F.; Wycisk, V.; Steinhilber, D.; Camacho, L.C.; Licha, K.; Lademann, J.; Haag, R. Synthesis and Validation of Functional Nanogels as pH-Sensors in the Hair Follicle. *Macromol. Biosci.* **2017**, *17*, 1600505. [CrossRef]
64. Kaden, D.; Dähne, L.; Knorr, F.; Richter, H.; Lademann, J.; Meinke, M.C.; Patzelt, A.; Darvin, M.E.; Jung, S. Determination of the pH Gradient in Hair Follicles of Human Volunteers Using pH-Sensitive Melamine Formaldehyde-Pyranine Nile Blue Microparticles. *Sensors* **2020**, *20*, 5243. [CrossRef]
65. Otberg, N.; Patzelt, A.; Rasulev, U.; Hagemeister, T.; Linscheid, M.; Sinkgraven, R.; Sterry, W.; Lademann, J. The role of hair follicles in the percutaneous absorption of caffeine. *Br. J. Clin. Pharmacol.* **2008**, *65*, 488–492. [CrossRef]
66. Scientific Committee on Consumer Safety SCCS. The ScCs Notes of Guidance for the Testing of Cosmetic Ingredients and Their Safety Evaluation 10th Revision. Available online: https://ec.europa.eu/health/sites/health/files/scientific_committees/consumer_safety/docs/sccs_o_224.pdf (accessed on 8 July 2020).
67. Bäumer, W.; Gorr, G.; Hoppmann, J.; Ehinger, A.M.; Rundfeldt, C.; Kietzmann, M. AWD 12-281, a highly selective phosphodiesterase 4 inhibitor, is effective in the prevention and treatment of inflammatory reactions in a model of allergic dermatitis. *J. Pharm. Pharmacol.* **2003**, *55*, 1107–1114. [CrossRef]

68. Verheijen, M.; Lienhard, M.; Schrooders, Y.; Clayton, O.; Nudischer, R.; Boerno, S.; Timmermann, B.; Selevsek, N.; Schlapbach, R.; Gmuender, H.; et al. DMSO induces drastic changes in human cellular processes and epigenetic landscape in vitro. *Sci. Rep.* **2019**, *9*, 4641. [[CrossRef](#)] [[PubMed](#)]
69. Williams, A.C.; Barry, B.W. Penetration enhancers. *Adv. Drug Deliv. Rev.* **2012**, *64*, 128–137. [[CrossRef](#)]
70. Zou, Y.; Celli, A.; Zhu, H.; Elmahdy, A.; Cao, Y.; Hui, X.; Maibach, H. Confocal laser scanning microscopy to estimate nanoparticles' human skin penetration in vitro. *Int. J. Nanomed.* **2017**, *12*, 8035–8041. [[CrossRef](#)] [[PubMed](#)]

Publisher's Note: MDPI stays neutral with regard to jurisdictional claims in published maps and institutional affiliations.



© 2020 by the authors. Licensee MDPI, Basel, Switzerland. This article is an open access article distributed under the terms and conditions of the Creative Commons Attribution (CC BY) license (<http://creativecommons.org/licenses/by/4.0/>).

3. DISCUSSION

The investigations presented in this thesis offer several new insights into a safer and targeted follicular drug delivery in the treatment of AA:

The *in vivo* study on NP uptake into human scalp HFs is an important first step to gain insights into the possibility of depositing NPs in AA-affected human scalp HFs. These findings are of enormous importance since the postulated gear pump mechanism for NP uptake into HFs involves the hair shaft's outer cuticle cells^{91,102}. However, AA-affected human scalp skin HFs present an intact HF without a hair shaft. Therefore, the key question, of whether targeted delivery via NDDS into AA-affected HFs is feasible had to be addressed. Fortunately, the deposition of NPs inside AA-affected scalp HFs could be demonstrated, in addition to the NP uptake into healthy hairy human scalp HFs and hairy scalp HFs of body donors¹²². No significant differences were found between the NP uptake into healthy hairy scalp HFs and hairy HFs of body donors. However, 9 out of 15 application areas had to be excluded in the study group of the body donors due to failed mass balance¹³⁰ and problems during the differential stripping performance¹²². Therefore, the protocol would have to be further enhanced to use the body donor scalp as a potential model for further investigations. Here, a deeper focus should be on the skin status (aged skin, very dry skin, presence of dandruff, changes over time (post-mortem interval)). Furthermore, no significant differences in the NP uptake into a single HF between different hair types and the presence or absence of a hair shaft were discovered¹²². This leads to the conclusion that the amount of follicular-deposited NPs on an application area depends on HF density, but is independent of HF types and hair shaft presence¹²².

The next aim of the thesis was the development of a NDDS for targeted follicular delivery in the treatment of AA. The JAK inhibitor TFB was selected as a potent drug. Loading processes of TFB to classical NDDS, e.g., based on PLGA or PCL, failed. Difficulties arose from the pH dependent water solubility¹²³, the weak chemical reactivity for chemical conjugation⁷⁴, and the instability in aqueous basic solutions^{124,125} of TFB. SqD NPs were selected as a suitable choice of a NDDS for the targeted follicular delivery of TFB, with the NDDS similar to the natural environment by consisting of squalene, which is one of the major components in human sebum⁷⁸. Moreover, the possibility to achieve high drug loading capacity influenced the choice^{68,126}. Broader investigations into the versatile NDDS platforms of SqDs gave important insights into the biocompatibility, stability in physiological pH environments, and drug loading processes¹²⁶. For dexamethasone, a representative for glucocorticoids, an impressive drug loading capacity was achieved in all SqDs of ~ 32 to 35 % (w/w)¹²⁶. Since glucocorticoids play an important role in topical

treatment of skin diseases, these results are very encouraging and further investigations of SqD NPs loaded with glucocorticoids for targeted follicular topical delivery should be conducted in the future. This leads to the ability to develop a protocol for the manufacturing of TFB SqD NPs with a satisfying drug loading capacity of 20 % and an enhanced drug solubility ¹²⁷.

Follicular drug delivery investigations on the *ex vivo* pig ear model demonstrated a maximized follicular delivery by TFB SqD NPs in comparison to aqueous drug solutions ¹²⁷. Moreover, the higher impact of follicular compared to interfollicular skin on permeation and penetration was stressed, which is in agreement with previous findings ⁸⁸. Further investigation of the biological effect of TFB was done in an *in vivo* dermatitis mouse model ¹²⁹. A previous study demonstrated in this model a significant effect of TFB acetone:DMSO solution by the reduction of inflammatory response in comparison to a drug-free control acetone:DMSO solution ¹²⁸. This model was chosen, instead of an AA mouse model, to study the biological *in vivo* response of TFB delivered by SqD NPs for several reasons: excellent experience with the mouse model existed, a positive control was available with the TFB acetone:DMSO solution, and the application of TFB SqD NPs could be investigated for other skin diseases that might benefit from a targeted TFB delivery ¹²⁷⁻¹²⁹. So, building on these previous results opened the possibility to gain first insights, if the targeted follicular drug delivery can evoke a biological response. Data from the *in vivo* dermatitis mouse model revealed a biological effect of TFB delivered by SqD NDDS ¹²⁷. Even though, in the *ex vivo* pig ear model, the TFB acetone:DMSO solution demonstrated similar follicular penetration effects as the TFB SqD NP formulation, the interfollicular skin permeation and penetration was enhanced. In the *in vivo* dermatitis mouse model TFB acetone:DMSO solution demonstrated a significant reduction in ear swelling compared to drug-free acetone:DMSO solution ¹²⁷. By taking the results of *in vivo* and *ex vivo* investigations together, the enhanced effect *in vivo* by TFB acetone:DMSO solution could result from combined follicular and interfollicular skin penetration ¹²⁷. In addition, the missing mass balance hinted at an uncontrolled and fast penetration into the skin ¹²⁷. However, an acetone:DMSO formulation cannot be considered a suitable drug delivery system. Even though DMSO is often used in preclinical studies, mostly due to its good penetration enhancing and drug solubilizing effects, it can alter and influence biological processes ^{131,132}. This makes TFB-loaded SqD NPs without organic solvents the safer option and moreover, enables controlled, targeted, and maximized drug delivery into the HFs.

4. CONCLUSION & OUTLOOK

In conclusion, this thesis demonstrates that NDDS are able to penetrate inside hairless and hairy scalp HFs. Therefore, proof of concept for follicular delivery by NDDS in the treatment of AA and other skin diseases to facilitate a targeted and thereby safer drug delivery was provided ¹²². The setup of a drug depot inside the HFs seems especially beneficial in long-term treatment. The subsequent development and investigation of the TFB SqD NPs supports the findings by demonstrating excellent follicular drug delivery and a biological effect ¹²⁷. These investigations confirmed that follicular targeting via drug-loaded NDDS is a highly desired drug delivery strategy for safe and effective treatment of skin diseases like AA and others such as acne. For AA, further investigations regarding NP penetration into the AA-affected HFs should focus on the penetration depths. Previous studies highlighted that a long-term continuous treatment seems to be necessary for a successful therapy of AA ^{53,54}. Therefore, the drug-loaded NDDS could serve as a safe low-dose, long-term treatment of a potent drug in AA by residing inside the HF as a drug depot and releasing the drug in a controlled manner. This can reduce the application times and enhance patient compliance. Moreover, due to the adjusted low drug amount, only targeted drug effects would take place and prevent high systemic and intradermal drug levels by the minimization of interfollicular drug permeation ^{64,82,121,133}. However, an important proof of concept is still missing as no demonstration exists of the beneficial effects *in vivo* and the enhanced biological effects for targeted drug delivery into HFs by NDDS. With the biological response evoked in the dermatitis mouse model the first step is done ¹²⁷. Further studies should focus on a sufficient drug dose to result in desired biological responses. The use of humanized mouse models, like the AA humanized mouse model, is desperately needed as the biological effect could be studied in human HFs ^{134,135}. If further investigations can confirm these promising findings, the next steps should focus on the performance of clinical trials to facilitate the translation into medical clinics.

5. REFERENCES

1. Vogt A, McElwee KJ, Blume-Peytavi U. Biology of the hair follicle. In: Blume-Peytavi U, Tosti A, Whiting D, Trüeb R, editors. *Hair growth and disorders*. Berlin, Heidelberg: Springer Berlin Heidelberg; 2008. p. 1–22.
2. Buffoli B, Rinaldi F, Labanca M, Sorbellini E, Trink A, Guanziroli E, Rezzani R, Rodella LF. The human hair: from anatomy to physiology: Education. *Int J Dermatol*. 2014;53(3):331-341. doi:10.1111/ijd.12362.
3. Pratt CH, King LE, Messenger AG, Christiano AM, Sundberg JP. Alopecia areata. *Nat Rev Dis Primers*. 2017;3:17011. doi:10.1038/nrdp.2017.11.
4. Blume U, Ferracin J, Verschoore M, Czernielewski JM, Schaefer H. Physiology of the vellus hair follicle: hair growth and sebum excretion. *Br J Dermatol*. 1991;124(1):21–28. doi:10.1111/j.1365-2133.1991.tb03277.x.
5. Mathes C, Brandner JM, Laue M, Raesch SS, Hansen S, Failla AV, Vidal S, Moll I, Schaefer UF, Lehr C-M. Tight junctions form a barrier in porcine hair follicles. *Eur J Cell Biol*. 2016;95(2):89–99. doi:10.1016/j.ejcb.2015.12.001.
6. Kiani MT, Higgins CA, Almquist BD. The hair follicle: an underutilized source of cells and materials for regenerative medicine. *ACS Biomater Sci Eng*. 2018;4(4):1193–1207. doi:10.1021/acsbomaterials.7b00072.
7. Poblet E, Ortega F, Jiménez F. The arrector pili muscle and the follicular unit of the scalp: a microscopic anatomy study. *Dermatol Surg*. 2002;28(9):800–803. doi:10.1046/j.1524-4725.2002.02038.x.
8. Sperling LC. Continuing medical education Hair anatomy for the clinician. *J Am Acad Dermatol*. 1991;25(1):1–17. doi:10.1016/0190-9622(91)70167-Z.
9. Christoph T, Müller-Röver S, Audring H, Tobin DJ, Hermes B, Cotsarelis G, Rückert R, Paus R. The human hair follicle immune system: cellular composition and immune privilege. *Br J Dermatol*. 2000;142(5):862–873. doi:10.1046/j.1365-2133.2000.03464.x.
10. Whiting DA. Histology of the human hair follicle. In: Blume-Peytavi U, Tosti A, Whiting D, Trüeb R, editors. *Hair growth and disorders*. Berlin, Heidelberg: Springer Berlin Heidelberg; 2008. p. 107–123.
11. Paus R, Cotsarelis G. The biology of hair follicles. *N Engl J Med*. 1999;341(7):491–497. doi:10.1056/NEJM199908123410706.
12. Lademann J, Patzelt A, Richter H, Antoniou C, Sterry W, Knorr F. Determination of the cuticula thickness of human and porcine hairs and their potential influence on the penetration of nanoparticles into the hair follicles. *J Biomed Opt*. 2009;14(2):021014. doi:10.1117/1.3078813.

REFERENCES

13. Paus R. Principles of hair cycle control. *J Dermatol.* 1998;25(12):793–802. doi:10.1111/j.1346-8138.1998.tb02507.x.
14. Schneider MR, Schmidt-Ullrich R, Paus R. The hair follicle as a dynamic miniorgan. *Curr Biol.* 2009;19(3):R132-R142. doi:10.1016/j.cub.2008.12.005.
15. Shimomura Y, Christiano AM. Biology and genetics of hair. *Annu Rev Genomics Hum Genet.* 2010;11(1):109–132. doi:10.1146/annurev-genom-021610-131501.
16. Bertolini M, McElwee K, Gilhar A, Bulfone-Paus S, Paus R. Hair follicle immune privilege and its collapse in alopecia areata. *Exp Dermatol.* 2020;29(8):703–725. doi:10.1111/exd.14155.
17. Paus R, Ito N, Takigawa M, Ito T. The hair follicle and immune privilege. *J Investig Dermatol Symp Proc.* 2003;8(2):188–194. doi:10.1046/j.1087-0024.2003.00807.x.
18. Wensveen FM, Jelenčić V, Polić B. NKG2D: a master regulator of immune cell responsiveness. *Front Immunol.* 2018;9:441. doi:10.3389/fimmu.2018.00441.
19. Benigno M, Anastassopoulos KP, Mostaghimi A, Udall M, Daniel SR, Cappelleri JC, Chander P, Wahl PM, Laphorn J, Kauffman L, et al. A large cross-sectional survey study of the prevalence of alopecia areata in the United States. *Clin Cosmet Investig Dermatol.* 2020;13:259–266. doi:10.2147/CCID.S245649.
20. Aldhouse NVJ, Kitchen H, Knight S, Macey J, Nunes FP, Dutronc Y, Mesinkovska N, Ko JM, King BA, Wyrwich KW. “You lose your hair, what’s the big deal?’ I was so embarrassed, I was so self-conscious, I was so depressed:” a qualitative interview study to understand the psychosocial burden of alopecia areata. *J Patient Rep Outcomes.* 2020;4(1):76. doi:10.1186/s41687-020-00240-7.
21. Divito SJ, Kupper TS. Inhibiting Janus kinases to treat alopecia areata. *Nat Med.* 2014;20(9):989–990. doi:10.1038/nm.3685.
22. Xing L, Dai Z, Jabbari A, Cerise JE, Higgins CA, Gong W, Jong A de, Harel S, DeStefano GM, Rothman L, et al. Alopecia areata is driven by cytotoxic T lymphocytes and is reversed by JAK inhibition. *Nat Med.* 2014;20(9):1043–1049. doi:10.1038/nm.3645.
23. Meah N, Wall D, York K, Bhoirul B, Bokhari L, Sigall DA, Bergfeld WF, Betz RC, Blume-Peytavi U, Callender V, et al. The alopecia areata consensus of experts (ACE) study: Results of an international expert opinion on treatments for alopecia areata. *J Am Acad Dermatol.* 2020;83(1):123–130. doi:10.1016/j.jaad.2020.03.004.
24. Strazzulla LC, Wang EHC, Avila L, Lo Sicco K, Brinster N, Christiano AM, Shapiro J. Alopecia areata: An appraisal of new treatment approaches and overview of current therapies. *J Am Acad Dermatol.* 2018;78(1):15–24. doi:10.1016/j.jaad.2017.04.1142.

REFERENCES

25. Gupta AK, Carviel JL, Foley KA, Shear NH, Piraccini BM, Piguet V, Tosti A. Monotherapy for alopecia areata: A systematic review and network meta-analysis. *Skin Appendage Disord*. 2019;5:331–337. doi:10.1159/000501940.
 26. Craiglow BG, King BA. Killing two birds with one stone: Oral tofacitinib reverses alopecia universalis in a patient with plaque psoriasis. *J Invest Dermatol*. 2014;134(12):2988–2990. doi:10.1038/jid.2014.260.
 27. Ferreira SB, Ferreira RB, Scheinberg MA. Topical tofacitinib in treatment of alopecia areata. *Einstein (Sao Paulo)*. 2020;18:eAI5452. doi:10.31744/einstein_journal/2020ai5452.
 28. Kennedy Crispin M, Ko JM, Craiglow BG, Li S, Shankar G, Urban JR, Chen JC, Cerise JE, Jabbari A, Winge MC, et al. Safety and efficacy of the JAK inhibitor tofacitinib citrate in patients with alopecia areata. *JCI Insight*. 2016;1(15):e89776. doi:10.1172/jci.insight.89776.
 29. Jabbari A, Nguyen N, Cerise JE, Ulerio G, Jong A de, Clynes R, Christiano AM, Mackay-Wiggan J. Treatment of an alopecia areata patient with tofacitinib results in regrowth of hair and changes in serum and skin biomarkers. *Exp Dermatol*. 2016;25(8):642–643. doi:10.1111/exd.13060.
 30. Chiang A, Ortenzio F, Juhasz MLW, Yu V, Mesinkovska NA. Balance of tofacitinib efficacy and disease flare in the treatment of alopecia universalis: A case report and review of the literature. *JAAD Case Rep*. 2018;4(7):733–736. doi:10.1016/j.jdc.2018.04.006.
 31. Gupta AK, Carviel JL, Abramovits W. Efficacy of tofacitinib in treatment of alopecia universalis in two patients. *J Eur Acad Dermatol Venereol*. 2016;30(8):1373–1378. doi:10.1111/jdv.13598.
 32. Anzengruber F, Maul J-T, Kamarachev J, Trüeb RM, French LE, Navarini AA. Transient efficacy of tofacitinib in alopecia areata universalis. *Case Rep Dermatol*. 2016;8:102–106. doi:10.1159/000445182.
 33. Scheinberg M, Lucena Couto Océa RA de, Cruz BA, Ferreira SB. Brazilian experience of the treatment of alopecia universalis with the novel antirheumatic therapy tofacitinib: A case series. *Rheumatol Ther*. 2017;4:503–508. doi:10.1007/s40744-017-0069-z.
 34. Liu LY, Craiglow BG, Dai F, King BA. Tofacitinib for the treatment of severe alopecia areata and variants: A study of 90 patients. *J Am Acad Dermatol*. 2017;76(1):22–28. doi:10.1016/j.jaad.2016.09.007.
 35. Erduran F, Adışen E, Aksakal AB. Excellent response to tofacitinib treatment in a patient with alopecia universalis. *Acta Dermatovenerol Alp Pannonica Adriat*. 2017;26:47–49. doi:10.15570/actaapa.2017.15.
-

REFERENCES

36. Craiglow BG, Liu LY, King BA. Tofacitinib for the treatment of alopecia areata and variants in adolescents. *J Am Acad Dermatol.* 2017;76(1):29–32. doi:10.1016/j.jaad.2016.09.006.
37. Liu LY, King BA. Tofacitinib for the treatment of severe alopecia areata in adults and adolescents. *J Investig Dermatol Symp Proc.* 2018;19(1):S18-S20. doi:10.1016/j.jisp.2017.10.003.
38. Liu LY, Craiglow BG, King BA. Tofacitinib 2% ointment, a topical Janus kinase inhibitor, for the treatment of alopecia areata: A pilot study of 10 patients. *J Am Acad Dermatol.* 2018;78(2):403-404.e1. doi:10.1016/j.jaad.2017.10.043.
39. Jabbari A, Sansaricq F, Cerise J, Chen JC, Bitterman A, Ulerio G, Borbon J, Clynes R, Christiano AM, Mackay-Wiggan J. An open-label pilot study to evaluate the efficacy of tofacitinib in moderate to severe patch-type alopecia areata, totalis, and universalis. *J Invest Dermatol.* 2018;138(7):1539–1545. doi:10.1016/j.jid.2018.01.032.
40. Craiglow BG. Topical tofacitinib solution for the treatment of alopecia areata affecting eyelashes. *JAAD Case Rep.* 2018;4(10):988–989. doi:10.1016/j.jdcr.2018.07.018.
41. Cheng MW, Kehl A, Worswick S, Goh C. Successful treatment of severe alopecia areata with oral or topical tofacitinib. *J Drugs Dermatol.* 2018;17(7):800–803.
42. Bokhari L, Sinclair R. Treatment of alopecia universalis with topical Janus kinase inhibitors - a double blind, placebo, and active controlled pilot study. *Int J Dermatol.* 2018;57(12):1464–1470. doi:10.1111/ijd.14192.
43. Serdaroğlu S, Engin B, Çelik U, Erkan E, Aşkın Ö, Oba Ç, Kutlubay Z. Clinical experiences on alopecia areata treatment with tofacitinib: A study of 63 patients. *Dermatol Ther.* 2019;32(3):e12844. doi:10.1111/dth.12844.
44. Phan K, Sebaratnam DF. JAK inhibitors for alopecia areata: a systematic review and meta-analysis. *J Eur Acad Dermatol Venereol.* 2019;33(5):850–856. doi:10.1111/jdv.15489.
45. Hogan S, Wang S, Ibrahim O, Piliang M, Bergfeld W. Long-term treatment with tofacitinib in severe alopecia areata: an update. *J Clin Aesthet Dermatol.* 2019;12(6):12–14.
46. Ferreira RB, Ferreira SB, Scheinberg MA. An excellent response to tofacitinib in a Brazilian adolescent patient with alopecia areata: A case report and a review of the literature. *Clin Case Rep.* 2019;7(12):2539–2542. doi:10.1002/ccr3.2484.
47. Ismail FF, Sinclair R. JAK inhibition in the treatment of alopecia areata - a promising new dawn? *Expert Rev Clin Pharmacol.* 2020;13(1):43–51. doi:10.1080/17512433.2020.1702878.

REFERENCES

48. Schwartz DM, Kanno Y, Villarino A, Ward M, Gadina M, O'Shea JJ. JAK inhibition as a therapeutic strategy for immune and inflammatory diseases. *Nat Rev Drug Discov.* 2017;16:843–862. doi:10.1038/nrd.2017.201.
49. Hodge JA, Kawabata TT, Krishnaswami S, Clark JD, Telliez J-B, Dowty ME, Menon S, Lamba M, Zwillich S. The mechanism of action of tofacitinib - an oral Janus kinase inhibitor for the treatment of rheumatoid arthritis. *Clin Exp Rheumatol.* 2016;34(2):318–328.
50. U.S. Food and Drug Administration. Prescribing Information XELJANZ (tofacitinib). Reference ID: 4269956. Silver Spring, Maryland: U.S. Food and Drug Administration; 2018 [accessed 2020 Aug 7]. https://www.accessdata.fda.gov/drugsatfda_docs/label/2018/203214s018lbl.pdf
51. FDA Drug Safety Communication. FDA approves Boxed Warning about increased risk of blood clots and death with higher dose of arthritis and ulcerative colitis medicine tofacitinib (Xeljanz, Xeljanz XR). Silver Spring, Maryland: U.S. Food and Drug Administration; 2019 [accessed 2020 Aug 7]. <https://www.fda.gov/drugs/drug-safety-and-availability/fda-approves-boxed-warning-about-increased-risk-blood-clots-and-death-higher-dose-arthritis-and>
52. FDA Drug Safety Communication. Initial safety trial results find increased risk of serious heart-related problems and cancer with arthritis and ulcerative colitis medicine Xeljanz, Xeljanz XR (tofacitinib). Silver Spring, Maryland: U.S. Food and Drug Administration; 2021 [accessed 2021 Feb 12]. <https://www.fda.gov/drugs/drug-safety-and-availability/initial-safety-trial-results-find-increased-risk-serious-heart-related-problems-and-cancer-arthritis>
53. Shreberk-Hassidim R, Ramot Y, Zlotogorski A. Janus kinase inhibitors in dermatology: A systematic review. *J Am Acad Dermatol.* 2017;76(4):745-753.e19. doi:10.1016/j.jaad.2016.12.004.
54. Tegtmeier K, Zhao J, Maloney NJ, Atassi G, Beestrum M, Lio PA. Off-label studies on tofacitinib in dermatology: a review. *J Dermatolog Treat.* 2021;32(4):1–11. doi:10.1080/09546634.2019.1673877.
55. Ibrahim O, Bayart CB, Hogan S, Piliang M, Bergfeld WF. Treatment of alopecia areata with tofacitinib. *JAMA Dermatol.* 2017;153(6):600–602. doi:10.1001/jamadermatol.2017.0001.
56. Siebenand S. JAK-Hemmer: Die Multizytokin- Inhibitoren. 38/2017. Stuttgart: Avoxa – Mediengruppe Deutscher Apotheker GmbH; 2019 [accessed 2021 Feb 12]. Pharmazeutische Zeitung. de. <https://www.pharmazeutische-zeitung.de/ausgabe-382017/die-multizytokin-inhibitoren/>

-
57. Bobo D, Robinson KJ, Islam J, Thurecht KJ, Corrie SR. Nanoparticle-based medicines: A review of FDA-approved materials and clinical trials to date. *Pharmaceutical Research*. 2016;33:2373–2387. doi:10.1007/s11095-016-1958-5.
 58. Ho D-K, Nichols BLB, Edgar KJ, Murgia X, Loretz B, Lehr C-M. Challenges and strategies in drug delivery systems for treatment of pulmonary infections. *Eur J Pharm Biopharm*. 2019;144:110–124. doi:10.1016/j.ejpb.2019.09.002.
 59. Yasar H, Ho D-K, Rossi C de, Herrmann J, Gordon S, Loretz B, Lehr C-M. Starch-Chitosan polyplexes: A versatile carrier system for anti-infectives and gene delivery. *Polymers (Basel)*. 2018;10(3):252. doi:10.3390/polym10030252.
 60. Hansen S, Lehr C-M. Nanoparticles for transcutaneous vaccination. *Microb Biotechnol*. 2012;5(2):156–167. doi:10.1111/j.1751-7915.2011.00284.x.
 61. Pelaz B, Alexiou C, Alvarez-Puebla RA, Alves F, Andrews AM, Ashraf S, Balogh LP, Ballerini L, Bestetti A, Brendel C, et al. Diverse applications of nanomedicine. *ACS Nano*. 2017;11(3):2313–2381. doi:10.1021/acsnano.6b06040.
 62. Kandekar SG, Del Río-Sancho S, Lapteva M, Kalia YN. Selective delivery of adapalene to the human hair follicle under finite dose conditions using polymeric micelle nanocarriers. *Nanoscale*. 2018;10(3):1099–1110. doi:10.1039/c7nr07706h.
 63. Lapteva M, Möller M, Gurny R, Kalia YN. Self-assembled polymeric nanocarriers for the targeted delivery of retinoic acid to the hair follicle. *Nanoscale*. 2015;7(44):18651–18662. doi:10.1039/C5NR04770F.
 64. Mathes C, Melero A, Conrad P, Vogt T, Rigo L, Selzer D, Prado WA, Rossi C de, Garrigues TM, Hansen S, et al. Nanocarriers for optimizing the balance between interfollicular permeation and follicular uptake of topically applied clobetasol to minimize adverse effects. *J Control Release*. 2016;223:207–214. doi:10.1016/j.jconrel.2015.12.010.
 65. Danhier F, Ansorena E, Silva JM, Coco R, Le Breton A, Pr eat V. PLGA-based nanoparticles: an overview of biomedical applications. *Journal of Controlled Release*. 2012;161(2):505–522. doi:10.1016/j.jconrel.2012.01.043.
 66. Weiss B, Schaefer UF, Zapp J, Lamprecht A, Stallmach A, Lehr C-M. Nanoparticles made of fluorescence-labelled Poly(L-lactide-co-glycolide): preparation, stability, and biocompatibility. *J Nanosci Nanotechnol*. 2006;6(9-10):3048–3056. doi:10.1166/jnn.2006.424.
 67. Couvreur P. Nanoparticles in drug delivery: past, present and future. *Adv Drug Deliv Rev*. 2013;65(1):21–23. doi:10.1016/j.addr.2012.04.010.
 68. Couvreur P, Stella B, Reddy LH, Hillaireau H, Dubernet C, Desma le D, Lep tre-Mouelhi S, Rocco F, Dereuddre-Bosquet N, Clayette P, et al. Squalenoyl
-

-
- nanomedicines as potential therapeutics. *Nano Lett.* 2006;6(11):2544–2548. doi:10.1021/nl061942q.
69. Desmaële D, Gref R, Couvreur P. Squalenoylation: a generic platform for nanoparticulate drug delivery. *Journal of Controlled Release.* 2012;161(2):609–618. doi:10.1016/j.jconrel.2011.07.038.
70. Sémiramoth N, Di Meo C, Zouhiri F, Saïd-Hassane F, Valetti S, Gorges R, Nicolas V, Poupaert JH, Chollet-Martin S, Desmaële D, et al. Self-assembled squalenoylated penicillin bioconjugates: an original approach for the treatment of intracellular infections. *ACS Nano.* 2012;6(5):3820–3831. doi:10.1021/nn204928v.
71. Hillaireau H, Dereuddre-Bosquet N, Skanji R, Bekkara-Aounallah F, Caron J, Lepêtre S, Argote S, Bauduin L, Yousfi R, Rogez-Kreuz C, et al. Anti-HIV efficacy and biodistribution of nucleoside reverse transcriptase inhibitors delivered as squalenoylated prodrug nanoassemblies. *Biomaterials.* 2013;34(20):4831–4838. doi:10.1016/j.biomaterials.2013.03.022.
72. Maksimenko A, Mougín J, Mura S, Sliwinski E, Lepeltier E, Bourgaux C, Lepêtre S, Zouhiri F, Desmaële D, Couvreur P. Polyisoprenoyl gemcitabine conjugates self assemble as nanoparticles, useful for cancer therapy. *Cancer Lett.* 2013;334(2):346–353. doi:10.1016/j.canlet.2012.08.023.
73. Buchy E, Valetti S, Mura S, Mougín J, Troufflard C, Couvreur P, Desmaële D. Synthesis and cytotoxic activity of self-assembling squalene conjugates of 3-[(Pyrrol-2-yl)methylidene]-2,3-dihydro-1H-indol-2-one anticancer agents. *European Journal of Organic Chemistry.* 2015;(1):202–212. doi:10.1002/ejoc.201403088.
74. Wei X, Wu J, Zhao G, Galdamez J, Lele SM, Wang X, Liu Y, Soni DM, Purdue PE, Mikuls TR, et al. Development of a Janus kinase inhibitor prodrug for the treatment of rheumatoid arthritis. *Mol Pharm.* 2018;15(8):3456–3467. doi:10.1021/acs.molpharmaceut.8b00433.
75. Ralay-Ranaivo B, Desmaële D, Bianchini EP, Lepeltier E, Bourgaux C, Borgel D, Pouget T, Tranchant JF, Couvreur P, Gref R. Novel self assembling nanoparticles for the oral administration of fondaparinux: synthesis, characterization and in vivo evaluation. *Journal of Controlled Release.* 2014;194:323–331. doi:10.1016/j.jconrel.2014.07.060.
76. Ho D-K, Murgia X, Rossi C de, Christmann R, Hüfner de Mello Martins AG, Koch M, Andreas A, Herrmann J, Müller R, Empting M, et al. Squalenyl hydrogen sulfate nanoparticles for simultaneous delivery of tobramycin and an alkylquinolone quorum sensing inhibitor enable the eradication of *P. aeruginosa* biofilm infections. *Angew Chem Int Ed Engl.* 2020;59(26):10292–10296. doi:10.1002/anie.202001407.
-

-
77. Schroepfer GJ. Sterol biosynthesis. *Annual Review of Biochemistry*. 1981;50:585–621.
 78. Reddy LH, Couvreur P. Squalene: A natural triterpene for use in disease management and therapy. *Adv Drug Deliv Rev*. 2009;61(15):1412–1426. doi:10.1016/j.addr.2009.09.005.
 79. Smith KR, Thiboutot DM. Thematic review series: skin lipids. Sebaceous gland lipids: friend or foe? *J Lipid Res*. 2008;49(2):271–281. doi:10.1194/jlr.R700015-JLR200.
 80. Lademann J, Richter H, Schanzer S, Knorr F, Meinke M, Sterry W, Patzelt A. Penetration and storage of particles in human skin: Perspectives and safety aspects. *Eur J Pharm Biopharm*. 2011;77(3):465–468. doi:10.1016/j.ejpb.2010.10.015.
 81. Lademann J, Richter H, Meinke MC, Lange-Asschenfeldt B, Antoniou C, Mak WC, Renneberg R, Sterry W, Patzelt A. Drug delivery with topically applied nanoparticles: Science fiction or reality. *Skin Pharmacol Physiol*. 2013;26(4-6):227–233. doi:10.1159/000351940.
 82. Patzelt A, Lademann J. Drug delivery to hair follicles. *Expert Opin Drug Deliv*. 2013;10(6):787–797. doi:10.1517/17425247.2013.776038.
 83. Knorr F, Patzelt A, Darvin ME, Lehr C-M, Schäfer U, Gruber AD, Ostrowski A, Lademann J. Penetration of topically applied nanocarriers into the hair follicles of dog and rat dorsal skin and porcine ear skin. *Vet Dermatol*. 2016;27(4):256–e60. doi:10.1111/vde.12325.
 84. Maibach HI, Feldman RJ, Milby TH, Serat WF. Regional variation in percutaneous penetration in man. *Archives of Environmental Health: An International Journal*. 1971;23(3):208–211. doi:10.1080/00039896.1971.10665987.
 85. Vogt A, Mandt N, Lademann J, Schaefer H, Blume-Peytavi U. Follicular targeting—a promising tool in selective dermatotherapy. *J Investig Dermatol Symp Proc*. 2005;10(3):252–255. doi:10.1111/j.1087-0024.2005.10124.x.
 86. Rougier A, Lotte C, Maibach HI. In vivo percutaneous penetration of some organic compounds related to anatomic site in humans: predictive assessment by the stripping method. *J Pharm Sci*. 1987;76(6):451–454. doi:10.1002/jps.2600760608.
 87. Rougier A, Dupuis D, Lotte C, Roguet R, Wester RC, Maibach HI. Regional variation in percutaneous absorption in man: measurement by the stripping method. *Arch Dermatol Res*. 1986;278(6):465–469. doi:10.1007/BF00455165.
 88. Otberg N, Patzelt A, Rasulev U, Hagemester T, Linscheid M, Sinkgraven R, Sterry W, Lademann J. The role of hair follicles in the percutaneous absorption of caffeine. *Br J Clin Pharmacol*. 2008;65(4):488–492. doi:10.1111/j.1365-2125.2007.03065.x.
-

-
89. Lademann J, Knorr F, Richter H, Blume-Peytavi U, Vogt A, Antoniou C, Sterry W, Patzelt A. Hair follicles—an efficient storage and penetration pathway for topically applied substances. Summary of recent results obtained at the Center of Experimental and Applied Cutaneous Physiology, Charité -Universitätsmedizin Berlin, Germany. *Skin Pharmacol Physiol*. 2008;21(3):150–155. doi:10.1159/000131079.
 90. Mohd F, Todo H, Yoshimoto M, Yusuf E, Sugibayashi K. Contribution of the hair follicular pathway to total skin permeation of topically applied and exposed chemicals. *Pharmaceutics*. 2016;8(4):32. doi:10.3390/pharmaceutics8040032.
 91. Lademann J, Richter H, Schaefer UF, Blume-Peytavi U, Teichmann A, Otberg N, Sterry W. Hair follicles - a long-term reservoir for drug delivery. *Skin Pharmacol Physiol*. 2006;19(4):232–236. doi:10.1159/000093119.
 92. Otberg N, Richter H, Schaefer H, Blume-Peytavi U, Sterry W, Lademann J. Variations of hair follicle size and distribution in different body sites. *J Invest Dermatol*. 2004;122(1):14–19. doi:10.1046/j.0022-202X.2003.22110.x.
 93. Patzelt A, Knorr F, Blume-Peytavi U, Sterry W, Lademann J. Hair follicles, their disorders and their opportunities. *Drug Discovery Today: Disease Mechanisms*. 2008;5(2):e173-e181. doi:10.1016/j.ddmec.2008.04.006.
 94. Lademann J, Otberg N, Richter H, Weigmann H-J, Lindemann U, Schaefer H, Sterry W. Investigation of follicular penetration of topically applied substances. *Skin Pharmacol Appl Skin Physiol*. 2001;14:17–22. doi:10.1159/000056385.
 95. Lademann J, Otberg N, Richter H, Jacobi U, Schaefer H, Blume-Peytavi U, Sterry W. Follikulare Penetration. Ein entscheidender Penetrationsweg von topisch applizierten Substanzen. *Hautarzt*. 2003;54(4):321–323. de. doi:10.1007/s00105-003-0513-6.
 96. Lademann J, Otberg N, Jacobi U, Hoffman RM, Blume-Peytavi U. Follicular penetration and targeting. *J Invest Dermatol Symp Proc*. 2005;10(3):301–303. doi:10.1111/j.1087-0024.2005.10121.x.
 97. Otberg N, Richter H, Knüttel A, Schaefer H, Sterry W, Lademann J. Laser spectroscopic methods for the characterization of open and closed follicles. *Laser Phys. Lett*. 2003;1(1):46–49. doi:10.1002/lapl.200310011.
 98. Toll R, Jacobi U, Richter H, Lademann J, Schaefer H, Blume-Peytavi U. Penetration profile of microspheres in follicular targeting of terminal hair follicles. *J Invest Dermatol*. 2004;123(1):168–176. doi:10.1111/j.0022-202X.2004.22717.x.
 99. Roberts MS, Mohammed Y, Pastore MN, Namjoshi S, Yousef S, Alinaghi A, Haridass IN, Abd E, Leite-Silva VR, Benson H, et al. Topical and cutaneous delivery using nanosystems. *J Control Release*. 2017;247:86–105. doi:10.1016/j.jconrel.2016.12.022.
-

REFERENCES

100. Bouwstra JA, Honeywell-Nguyen LP, Gooris GS, Ponec M. Structure of the skin barrier and its modulation by vesicular formulations. *Progress in Lipid Research*. 2003;42(1):1–36. doi:10.1016/s0163-7827(02)00028-0.
 101. Lademann J, Weigmann H-J, Rickmeyer C, Barthelmes H, Schaefer H, Mueller G, Sterry W. Penetration of titanium dioxide microparticles in a sunscreen formulation into the horny layer and the follicular orifice. *Skin Pharmacol Physiol*. 1999;12:247–256. doi:10.1159/000066249.
 102. Lademann J, Richter H, Teichmann A, Otberg N, Blume-Peytavi U, Luengo J, Weiss B, Schaefer UF, Lehr C-M, Wepf R, et al. Nanoparticles—an efficient carrier for drug delivery into the hair follicles. *Eur J Pharm Biopharm*. 2007;66(2):159–164. doi:10.1016/j.ejpb.2006.10.019.
 103. Li BS, Cary JH, Maibach HI. Should we instruct patients to rub topical agents into skin? The evidence. *J Dermatolog Treat*. 2019;30(4):328–332. doi:10.1080/09546634.2018.1527997.
 104. Knorr F, Lademann J, Patzelt A, Sterry W, Blume-Peytavi U, Vogt A. Follicular transport route—research progress and future perspectives. *Eur J Pharm Biopharm*. 2009;71(2):173–180. doi:10.1016/j.ejpb.2008.11.001.
 105. Radtke M, Patzelt A, Knorr F, Lademann J, Netz RR. Ratchet effect for nanoparticle transport in hair follicles. *Eur J Pharm Biopharm*. 2017;116:125–130. doi:10.1016/j.ejpb.2016.10.005.
 106. Patzelt A, Richter H, Knorr F, Schäfer U, Lehr C-M, Dähne L, Sterry W, Lademann J. Selective follicular targeting by modification of the particle sizes. *J Control Release*. 2011;150(1):45–48. doi:10.1016/j.jconrel.2010.11.015.
 107. Melero A, Ferreira Ourique A, Guterres SS, Pohlmann AR, Lehr C-M, Beck RCR, Schaefer UF. Nanoencapsulation in lipid-core nanocapsules controls mometasone furoate skin permeability rate and its penetration to the deeper skin layers. *Skin Pharmacol Physiol*. 2014;27(4):217. doi:10.1159/000354921.
 108. Mittal A, Schulze K, Ebensen T, Weißmann S, Hansen S, Lehr CM, Guzmán CA. Efficient nanoparticle-mediated needle-free transcutaneous vaccination via hair follicles requires adjuvantation. *Nanomedicine*. 2015;11(1):147–154. doi:10.1016/j.nano.2014.08.009.
 109. Mittal A, Raber AS, Schaefer UF, Weissmann S, Ebensen T, Schulze K, Guzman CA, Lehr C-M, Hansen S. Non-invasive delivery of nanoparticles to hair follicles: a perspective for transcutaneous immunization. *Vaccine*. 2013;31(34):3442–3451. doi:10.1016/j.vaccine.2012.12.048.
 110. Patzelt A, Richter H, Buetttemeyer R, Huber HJR, Blume-Peytavi U, Sterry W, Lademann J. Differential stripping demonstrates a significant reduction of the hair
-

-
- follicle reservoir in vitro compared to in vivo. *Eur J Pharm Biopharm.* 2008;70(1):234–238. doi:10.1016/j.ejpb.2008.02.024.
111. Lademann J, Richter H, Meinke M, Sterry W, Patzelt A. Which skin model is the most appropriate for the investigation of topically applied substances into the hair follicles? *Skin Pharmacol Physiol.* 2010;23(1):47–52. doi:10.1159/000257263.
112. Jacobi U, Kaiser M, Toll R, Mangelsdorf S, Audring H, Otberg N, Sterry W, Lademann J. Porcine ear skin: an in vitro model for human skin. *Skin Res Technol.* 2007;13(1):19–24. doi:10.1111/j.1600-0846.2006.00179.x.
113. Teichmann A, Jacobi U, Ossadnik M, Richter H, Koch S, Sterry W, Lademann J. Differential Stripping: Determination of the amount of topically applied substances penetrated into the hair follicles. *Journal of Investigative Dermatology.* 2005;125(2):264–269. doi:10.1111/j.0022-202X.2005.23779.x.
114. Weigmann H-J, Lademann J, Meffert H, Schaefer H, Sterry W. Determination of the horny layer profile by tape stripping in combination with optical spectroscopy in the visible range as a prerequisite to quantify percutaneous absorption. *Skin Pharmacol Physiol.* 1999;12:34–45. doi:10.1159/000029844.
115. Shah VP, Flynn GL, Yacobi A, Maibach HI, Bon C, Fleischer NM, Franz TJ, Kaplan SA, Kawamoto J, Lesko LJ, et al. Bioequivalence of topical dermatological dosage forms—methods of evaluation of bioequivalence. *Pharm Res.* 1998;15(2):167–171. doi:10.1023/a:1011941929495.
116. Melero A, Hahn T, Schaefer UF, Schneider M. In vitro human skin segmentation and drug concentration-skin depth profiles. *Methods Mol Biol.* 2011;763:33–50. doi:10.1007/978-1-61779-191-8_2.
117. Wagner H, Kostka KH, Lehr CM, Schaefer UF. Drug distribution in human skin using two different in vitro test systems: comparison with in vivo data. *Pharm Res.* 2000;17(12):1475–1481. doi:10.1023/a:1007648807195.
118. Marks R, Dawber RP. Skin surface biopsy: an improved technique for the examination of the horny layer. *Br J Dermatol.* 1971;84(2):117–123. doi:10.1111/j.1365-2133.1971.tb06853.x.
119. Raber AS, Mittal A, Schäfer J, Bakowsky U, Reichrath J, Vogt T, Schaefer UF, Hansen S, Lehr C-M. Quantification of nanoparticle uptake into hair follicles in pig ear and human forearm. *J Control Release.* 2014;179:25–32. doi:10.1016/j.jconrel.2014.01.018.
120. Knorr F, Patzelt A, Richter H, Schanzer S, Sterry W, Lademann J. Approach towards developing a novel procedure to selectively quantify topically applied substances in the hair follicles of the model tissue porcine ear skin. *Exp Dermatol.* 2013;22(6):417–418. doi:10.1111/exd.12113.
-

-
121. Hofmeier KS, Surber C. Nanomedicine in Dermatology: Nanotechnology in Prevention, Diagnosis, and Therapy. In: Müller B, van de Voorde MH, editors. *Nanoscience and nanotechnology for human health*. Weinheim: Wiley-VCH Verlag GmbH & Co. KGaA; 2017. p. 329–356.
 122. Christmann R, Thomas C, Jager N, Raber AS, Loretz B, Schaefer UF, Tschernig T, Vogt T, Lehr C-M. Nanoparticle targeting to scalp hair follicles: New perspectives for a topical therapy for alopecia areata. *J Invest Dermatol*. 2020;140(1):243-246.e5. doi:10.1016/j.jid.2019.05.028.
 123. Committee for Medicinal Products for Human Use. Assessment report: Xeljanz; INN-tofacitinib. London, UK: European Medicines Agency; 2013 [accessed 2020 Sep 15]. https://www.ema.europa.eu/en/documents/assessment-report/xeljanz-epar-public-assessment-report_en-0.pdf
 124. Wu X, Zeng X, Wang L, Hang T, Song M. Identification of related substances in tofacitinib citrate by LC-MS techniques for synthetic process optimization. *J Pharm Biomed Anal*. 2017;143:17–25. doi:10.1016/j.jpba.2017.05.012.
 125. Younis US, Vallorz E, Addison KJ, Ledford JG, Myrdal PB. Preformulation and evaluation of tofacitinib as a therapeutic treatment for asthma. *AAPS PharmSciTech*. 2019;20(5):167. doi:10.1208/s12249-019-1377-0.
 126. Ho D-K, Christmann R, Murgia X, Rossi C de, Frisch S, Koch M, Schaefer UF, Loretz B, Desmaele D, Couvreur P, et al. Synthesis and biopharmaceutical characterization of amphiphilic squalenyl derivative based versatile drug delivery platform. *Front. Chem*. 2020;8:584242. doi:10.3389/fchem.2020.584242.
 127. Christmann R, Ho D-K, Wilzopolski J, Lee S, Koch M, Loretz B, Vogt T, Bäumer W, Schaefer UF, Lehr C-M. Tofacitinib loaded squalenyl nanoparticles for targeted follicular delivery in inflammatory skin diseases. *Pharmaceutics*. 2020;12(12):1131. doi:10.3390/pharmaceutics12121131.
 128. Fukuyama T, Ehling S, Cook E, Bäumer W. Topically administered Janus-kinase inhibitors tofacitinib and oclacitinib display impressive antipruritic and anti-inflammatory responses in a model of allergic dermatitis. *J Pharmacol Exp Ther*. 2015;354(3):394–405. doi:10.1124/jpet.115.223784.
 129. Bäumer W, Seegers U, Braun M, Tschernig T, Kietzmann M. TARC and RANTES, but not CTACK, are induced in two models of allergic contact dermatitis. Effects of cilomilast and diflorasone diacetate on T-cell-attracting chemokines. *Br J Dermatol*. 2004;151(4):823–830. doi:10.1111/j.1365-2133.2004.06220.x.
 130. Scientific Committee on Consumer Safety SCCS. SCCS Notes of Guidance for the Testing of Cosmetic Ingredients and their Safety Evaluation 10th revision. 2018
-

[accessed 2020 Jul 8]

https://ec.europa.eu/health/sites/health/files/scientific_committees/consumer_safety/docs/sccs_o_224.pdf

131. Verheijen M, Lienhard M, Schrooders Y, Clayton O, Nudischer R, Boerno S, Timmermann B, Selevsek N, Schlapbach R, Gmuender H, et al. DMSO induces drastic changes in human cellular processes and epigenetic landscape in vitro. *Sci Rep.* 2019;9(1):4641. doi:10.1038/s41598-019-40660-0.
132. Williams AC, Barry BW. Penetration enhancers. *Adv Drug Deliv Rev.* 2012;64:128–137. doi:10.1016/j.addr.2012.09.032.
133. Lademann J, Knorr F, Richter H, Jung S, Meinke MC, Rühl E, Alexiev U, Calderon M, Patzelt A. Hair follicles as a target structure for nanoparticles. *J. Innov. Opt. Health Sci.* 2015;08(04):1530004. doi:10.1142/S1793545815300049.
134. Laufer-Britva R, Keren A, Paus R, Gilhar A. Apremilast and tofacitinib exert differential effects in the humanized mouse model of alopecia areata. *Br J Dermatol.* 2020;182(1):227–229. doi:10.1111/bjd.18264.
135. Gilhar A, Keren A, Paus R. A new humanized mouse model for alopecia areata. *J Investig Dermatol Symp Proc.* 2013;16(1):S37-38. doi:10.1038/jidsymp.2013.11.

6. SCIENTIFIC OUTPUT

6.1. AWARD

2018 Research Award of Freunde des Universitätsklinikums des Saarlandes (UKS):

- ❖ **Dr. Theiss Science Award** (with Dr. Carla Thomas)

Title: In-vitro Organkultur humaner Haarfollikel zur Erforschung nanomedizinischer Konzepte zur topischen Therapie bei Alopecia Areata.

6.2. PUBLICATIONS

- ❖ **R. Christmann**, C. Thomas, N. Jager, A.S. Raber, B. Loretz, U.F. Schaefer, T. Tschernig, T. Vogt, C.-M. Lehr. Nanoparticle targeting to scalp hair follicles: new perspectives for a topical therapy of Alopecia Areata. *Journal of Investigative Dermatology* (2020)
- ❖ D.-K. Ho*, **R. Christmann***, X. Murgia, C. De Rossi, S. Frisch, M. Koch, U.F. Schaefer, B. Loretz, D. Desmaele, P. Couvreur, C.-M. Lehr. Synthesis and biopharmaceutical characterization of amphiphilic squalenyl derivatives based versatile drug delivery platform. *Frontiers in Chemistry* (2020)
**These authors have contributed equally to this work and share first authorship*
- ❖ **R. Christmann**, D.-K. Ho, J. Wilzopolski, S. Lee, M. Koch, B. Loretz, T. Vogt, W. Bäumer, U.F. Schaefer, C.-M. Lehr. Tofacitinib loaded squalenyl nanoparticles for targeted follicular delivery in inflammatory skin diseases. *Pharmaceutics* (2020)
- ❖ **R. Christmann**, A.S. Raber, U.F. Schaefer, A. Melero, B. Loretz. Chapter 53 Tape Stripping: Technique and Applications in *Percutaneous absorption - Drug - Cosmetics - Mechanism - Methodology* 5th edition by N. Dragicevic, H.I. Maibach. (in print)
- ❖ D.-K. Ho, X. Murgia, C. De Rossi, **R. Christmann**, A.G. Hufner de Mello Martins, M. Koch, A. Andreas, J. Herrmann, R. Müller, M. Empting, R.W. Hartmann, D. Desmaele, B. Loretz, P. Couvreur, C.-M. Lehr. Squalenyl hydrogen sulfate nanoparticles for simultaneous delivery of tobramycin and an alkylquinolone quorum sensing inhibitor enable the eradication of *P. aeruginosa* biofilm infections. *Angewandte Chemie* (2020)
- ❖ C. Schütz, D.-K. Ho, M.M. Hamed, A.S. Abdelsamie, T. Röhrig, C. Herr, A.M. Kany, K. Rox, S. Schmelz, L. Siebenbürger, M. Wirth, C. Börger, S. Yahiaoui, R. Bals, A. Scrima, W. Blankenfeldt, J.C. Horstmann, **R. Christmann**, X. Murgia, M. Koch, A. Berwanger, B. Loretz, A.K.H. Hirsch, R.W. Hartmann, C.-M. Lehr, M. Empting. A New PqsR inverse agonist potentiates tobramycin efficacy to eradicate *pseudomonas aeruginosa* biofilms. *Advanced science* (2021)

6.3. ORAL PRESENTATIONS

- ❖ **R. Christmann**, C. Thomas, N. Jager, A.S. Raber, B. Loretz, U.F. Schaefer, T. Tschernig, T. Vogt, C-M. Lehr. *Smart follicular drug delivery in the context of Alopecia Areata – a human in vivo study*
 - Barrier Function of Mammalian Skin, Gordon Research Seminar & Conference 2019, Waterville Valley, NH, US
- ❖ **R. Christmann**, C. Thomas, A.S. Raber, B. Loretz, U.F. Schaefer, T. Tschernig, T. Vogt, C-M. Lehr. *Quantitative determination of nanoparticle deposition in a single hair follicle in human forearm and scalp – an in-vivo study*
 - Controlled Release Society (CRS) World Meeting 2019, Valencia, Spain
- ❖ **R. Christmann**, C. Thomas, N. Jager, A.S. Raber, B. Loretz, U.F. Schaefer, T. Tschernig, T. Vogt, C-M. Lehr. *Nanoparticle targeting to scalp hair follicles - new perspectives for a topical therapy of Alopecia Areata. Journal of Investigative Dermatology*
 - Helmholtz Institute for Pharmaceutical Research Saarland (HIPS), Papers Mai 2019, Saarbrücken
- ❖ **R. Christmann**, C. Thomas. *In-vitro Organkultur humaner Haarfollikel zur Erforschung nanomedizinischer Konzepte zur topischen Therapie bei Alopecia Areata.*
 - Preisverleihung der Forschungspreise der Freunde des UKS, 2018, Homburg

6.4. POSTER PRESENTATIONS

- ❖ **R. Christmann**, C. Thomas, N. Jager, A.S. Raber, B. Loretz, U.F. Schaefer, T. Tschernig, T. Vogt, C.-M. Lehr. *Smart Follicular Drug Delivery in the Context of Alopecia Areata – a human in vivo study*
 - Barrier Function of Mammalian Skin, Gordon Research Seminar & Conference 2019, Waterville Valley, NH, US
 - ❖ **R. Christmann**, C. Thomas, N. Jager, A.S. Raber, B. Loretz, U.F. Schaefer, T. Tschernig, T. Vogt, C.-M. Lehr. *Quantitative Determination of Nanoparticles deposited in a single Hair Follicle – A human in vivo Study in the context of Alopecia Areata*
 - HIPS Symposium 2019, Saarbrücken
 - ❖ **R. Christmann**, C. Thomas, A.S. Raber, B. Loretz, U. Schaefer, T. Tschernig, T. Vogt, C.-M. Lehr. *Follicular delivery to human scalp hair follicle – feasible in the treatment of Alopecia Areata? – An in vivo study*
 - Controlled Release Society (CRS) Local Chapter Meeting 2019, Leipzig
-

- ❖ **R. Christmann**, C. Thomas, A.S. Raber, B. Loretz, U.F. Schaefer, T. Vogt, C.-M. Lehr.
Quantification of Nanoparticle Uptake into Human Terminal Hair Follicles in the Context of Alopecia Areata.
 - 1st Controlled Release Asia (CRA) Meeting 2018, Singapore
 - Globalization of Pharmaceutics Education Network (GPEN) Meeting 2018, Singapore
- ❖ **R. Christmann**, C. Thomas, A.S. Raber, B. Loretz, U.F. Schaefer, T. Vogt, C.-M. Lehr.
Quantification of Nanoparticle Penetration into Human Scalp Hair Follicle
 - Controlled Release Society (CRS) Local Chapter Meeting 2018, Halle

7. ACKNOWLEDGEMENTS

Mein Dank gilt allen, die mich bei der Erstellung dieser Arbeit tatkräftig unterstützt und dies für mich ermöglicht haben.

Besonders danken möchte ich meinen beiden Doktorvätern Prof. Dr. Claus-Michael Lehr und Prof. Dr. Thomas Vogt sowie meinen Betreuern Prof. Dr. Uli Schäfer und Dr. Brigitta Loretz: Von Herzen danke ich Euch für die Überlassung dieses Projektes, der hervorragenden Betreuung und Unterstützung, der Förderung und Forderung meiner wissenschaftlichen sowie persönlichen Weiterentwicklung, die unzähligen konstruktiven und hilfreichen Gespräche und für Eure ansteckende Leidenschaft für die Forschung.

Danken möchte ich darüber hinaus...

- ... Dr. Carla Thomas und Dr. Nadine Jung für die hervorragende interdisziplinäre Zusammenarbeit bei unseren Projekten.
- ... Dr. Duy-Khiet Ho für die grandiose Zusammenarbeit, seine ansteckende Begeisterung für die Forschung, seine Unterstützung, seinen Glauben an mich und seine Freundschaft.
- ... Olga Hartwig, für ihre Hilfe und Unterstützung bei der Mikroskopie, darüber hinaus für ihre Freundschaft und Unterstützung in jeder Lebenslage.
- ... Dr. Anne Raber für die Einführung in die Differential Stripping Methode und ihre hilfreichen Ratschläge.
- ... Dr. Sangeun Lee für ihre Hilfe bei chemischen Fragestellungen und die tolle Zusammenarbeit.
- ... meinen Kooperationspartnern, Prof. Dr. Thomas Tschernig und seinem Team, Prof. Dr. Wolfgang Bäumer und Dr. Jenny Wilzopolski, Dr. Marcus Koch, sowie all meinen Co-Autoren für die erstklassige und ausgezeichnete Zusammenarbeit.
- ... Prof. Dr. Markus Meyer für die Übernahme meiner wissenschaftlichen Begleitung.
- ... dem DDEL-Office Team (Karin Groß, Sarah Müller und Annette Herkströter), unseren Technikern (Jana Westhues, Petra König, Pascal Paul, Annette Boese und Dr. Chiara de Rossi) und der IT-Abteilung (Michael Roth, Mark Caspari) für ihre immerwährende Unterstützung und Hilfe.
- ... meinen Büro-Mitbewohnern Benedikt Huck, Olga Hartwig, Jana Westhues und Dr. Eilien Heinrich für unsere Freundschaft und diese unvergessliche Zeit.
- ... Dr. Kathryn and Dr. Douglas Miller für ihre großartige Unterstützung beim Language-Check.
- ... all meinen wundervollen Kolleginnen und Kollegen der DDEL- und BION-Gruppe, der Arbeitsgruppe Pharmazeutische Technologie der UdS und allen anderen (im HIPS-Gebäude und außerhalb), die mir in dieser Zeit mit Rat und Tat zur Seite standen: Danke für die großartige Arbeitsatmosphäre, die schönen Erlebnisse, den wissenschaftlichen Austausch, die Unterstützung, Ratschläge und vor allem die Freundschaften.

Mein Dank aus tiefstem Herzen geht an meine Familie, für ihre unermüdliche Unterstützung bei all meinen Vorhaben und ihre Liebe.
